HEAT STERILIZABLE AND IMPACT RESISTANT Ni-Cd BATTERY DEVELOPMENT

Jet Propulsion Laboratory
Contract No. 951972, Modification No. 6

Report for Seventh Quarter
1 January to 31 March, 1969

TEXAS INSTRUMENTS
INCORPORATED

HEAT STERILIZABLE AND IMPACT RESISTANT Ni-Cd BATTERY DEVELOPMENT

Jet Propulsion Laboratory
Contract No. 951972, Modification No. 6

Report for Seventh Quarter
1 January to 31 March, 1969

by

P.V. Popat: Project Manager
Principal Contributors:
R.L. Crawford: Electrochemistry
J.M. Gondusky: Impact Resistant Cells
E.J. Rubin: Battery Engineering

TEXAS INSTRUMENTS INCORPORATED
Research and Development Laboratories
Attleboro, Massachusetts

This work was performed for the Jet Propulsion Laboratory, California Institute of Technology, sponsored by the National Aeronautics and Space Administration under Contract NAS-7-100; Task Order No. RD-26.

I N D E X

NOTICE

This report was prepared as an account of government-sponsored work. Neither the United States, nor the National Aeronautics and Space Administration (NASA), nor any person acting on behalf of NASA:

(a) makes warranty of representation, expressed or implied with respect to the accuracy, completeness, or usefulness of the information contained in this report, or that the use of any information, apparatus, method, or process disclosed in this report may not infringe privately owned rights;

(b) assumes any liabilities with respect to the use of , or for damages resulting from the use of any information, apparatus, method or process disclosed in this report.

As used above, "person acting on behalf of NASA" includes any employees or contractor of NASA, or employee of such contractor to the extent that such employees or contractor of NASA, or employee of such contractor, prepares, disseminates, or provides access to any information pursuant to his employment with such contractor.

Request for copies of this report should be referred to:

National Aeronautics and Space Administration
Office of Scientific and Technical Information
Attention: AFSS-A

ABSTRACT

The objective of this program is the development of heat-sterilizable as well as heat-sterilizable and impact resistant, hermetically sealed, Ni-Cd cells suitable for rigorous space requirements. Significant progress has been made in the following areas:

I. Electrochemistry of Heat-Sterilizable Cells:
Heat-sterilized, prismatic, 17-plate, 4AH cells with FT2140 separator (factorial design experiment) have satisfactorily completed 146 charge-deep discharge cycles without capacity loss or malfunction. Similar 18-plate cells have also satisfactorily completed 90 charge-deep discharge cycles after sterilization. The post-sterilization increase in the end of charge voltage is found to be associated primarily with the positive (nickel) electrode and not with the negative electrode as previously suspected. This is encouraging because the slightly higher (~30mv) end of charge voltage is not an indication of hydrogen evolution reaction. Pre-treatments of the separator with (a) chromic acid (b) surfactants or (c) RAI proprietary process show no permanent beneficial effect with post-sterilized cells. Further work to improve the characteristic of heat-sterilizable cells is underway.

II. Battery Engineering:
A basic design and fabrication procedure for a crimped polymeric seal has been established, several prototypes fabricated and leak-tested. The leakage rates prior to and after heat sterilization are approximately 1 to 2 x 10^{-8} and 2 to 5 x 10^{-6} Std. cc. He/sec./atm. respectively. Further development of hermetic seal capable of heat sterilization is in progress.

Basic cell design parameters for 25AH, prismatic and cylindrical cells have been established. Prototype cells of each design have been fabricated and tested. Cells are generally performing as predicted. A test program for electrochemical and physical characterization of these cells prior to and after heat-sterilization has been established and implemented.

In order to increase the energy density of heat-sterilizable cells, a series of heavily loaded positive and negative plates have been manufactured and tested under flooded cell conditions. Positive plates with 0.045" thickness deliver approximately 11AH per cubic inch under these test conditions. This work is progressing satisfactorily.

III. Impact Testing of Cells and Components:
To facilitate the development and testing of shock resistant

Ni-Cd cells, a high-impact test facility has been established at Brown University in Providence. It has capability of accelerating a 50lb carriage mass to 125 ft./sec. Subsequent impact is controlled to produce a shock environment of 4000g for 1 millisec. Preliminary testing of Ni-Cd cells under this environment has begun. The cell components will be tested during the next quarter.

A structural model of the electrodes has been developed to predict their mechanical properties and will be verified experimentally.

1.0 Introduction

This is the seventh quarterly report on the heat-sterilizable, as well as heat-sterilizable and impact resistant Ni-Cd battery research and development under Jet Propulsion Laboratory Contract No. 951972 Modification No. 6. The program is sponsored under NASA Contract NAS-7-100, Task Order No. RD-26. The object of this contract is to perform research development and engineering work leading to the design, development, engineering, manufacture and testing of hermetically sealed, rechargeable Nickel-Cadmium cells capable of heat-sterilization as well as heat-sterilization and impact landing for space missions.

Since the last quarterly report, several modifications have been made in the technical portion of the work statement. The several tasks under the modified work statement may be grouped under the following three broad headings:

1. Electrochemistry of heat sterilizable cells. This will include basic research and development work on the positive and negative plates and separator as well as design, assembly and testing of complete cells leading to batteries capable of satisfactory operation after undergoing heat-sterilization.

2. Battery Engineering: This will include full size cell design development, optimization, production and testing of heat-sterilizable as well as heat-sterilizable and impact resistant cells. Initially two designs (a) cylindrical and (b) rectangular (prismatic) of 25 AH

nominal capacity will be developed and evaluated. Hermetic seal design, assembly and testing to withstand the heat-sterilization as well as impact testing will be part of the battery engineering program.

3. Impact Testing of Cells and Components: Both static and dynamic testing of seals, cases, plates, and complete cells will be performed up to approximately 4000g in order to develop cell capable of hard impact landing missions.

The work performed during the seventh quarter is reported in above three separate sections.

2.0 Electrochemical Investigations of Heat Sterilization Cells and Components:

2.1 Prismatic, 4AH, 17-Plate Factorial Cells: Table I-1 gives the factors and levels selected for the factorial experimental cells. These cells which began cycling in August, 1968 have now undergone 146 post-sterilization cycles. The results for cycles 110, 129 and 146 given in Table I-2 show that 7 out of 8 cells made with type FT2140 separator are still cycling. The end of charge voltage is below 1.5V for all cells and the capacity is stable. Cycling will continue.

2.2 Prismatic, 4AH, 18-Plate Cells:

Typical data from cycles from 32 to 90 in Table I-3 show that these post-sterilized cells continue to deliver high capacity (over 80% of theoretical capacity of the positive plate). The uniform behavior noted in the first 30 cycles is still in evidence. The high end of

charge voltage (1.503V) on cycle 90 may be due to measurement error. The capacity after 90 cycles is above 4AH. Cycling will continue.

TABLE I-1

Designation	Description	Factors Low Level (0)	Factors High Levels (1)
A	Nature of Separator	#14019 poly-propylene	#FT2140 poly-propylene
B	Concentration (w/o) of KOH	30	34
C	Amount of KOH (o/o pore fill)	70	80
D	Heat Treatment	Unsterilized	Sterilized

2.3 Studies of Factors Affecting Electrolyte Distribution:

This is the continuation of the studies reported in the preceding quarterly report on the electrolyte distribution and the separator wetting characteristics aimed at improving the cell characteristics, particularly the reproducibility.

2.3.1 Effect of Surfactant Addition and Separator Pretreatment on Cell Operational Behavior:

Four groups of 18-plate Ni-Cd cells have been constructed for the purpose of examining the effect of (a) the chromic acid FT2140 separator pretreatment, (b) the addition of 500 ppm of two surfactant types, (1) FC-128 (2) FC-176, (3M Co.) on cell performance, in comparison with a control, during cycling before and after heat steri-

TABLE I-2

Ni-Cd Rectangular Cells; Factorial Design Experiment

ELECTROCHEMICAL PERFORMANCE DATA

FOR FACTOR DESCRIPTION AND LEVELS SEE TABLE I-1

Cell No.	Factors				Cycle No.	Charge Data						Discharge Data; 1.0V Cut Off				
	A	B	C	D		Amp.	Hrs.	AH Input	ECV Volts	ECP PSIA	ECR mΩ	Amp	AH Output	EDP PSIA	EDR mΩ	Eff. %
17	1	0	0	1	110	400	17	6.8	1.465	--	17.79	2.0	3.218	--	32.60	64.9
19	1	0	0	1	110	400	17	6.8	1.461	--	13.74	2.0	3.484	--	19.85	70.2
21	1	0	1	1	110	400	17	6.8	1.469	--	10.44	2.0	3.734	--	12.30	75.3
23	1	0	1	1	110	400	17	6.8	1.476	--	11.00	2.0	4.000	--	11.78	80.6
25	1	1	0	1	110	400	17	6.8	1.464	--	14.90	2.0	3.718	--	40.41	75.0
27	1	1	0	1	110											
29	1	1	1	1	110	400	17	6.8	1.461	--	9.36	2.0	3.884	--	11.61	78.3
31	1	1	1	1	110	400	17	6.8	1.478	--	34.59	2.0	4.084	--	32.58	82.3

* Cell 27 not charged

TABLE I-2(cont.)

Ni-Cd Rectangular Cells; Factorial Design Experiment (17-Plate)

ELECTROCHEMICAL PERFORMANCE DATA

FOR FACTOR DESCRIPTION AND LEVELS SEE TABLE I-1

Cell No.	Factors				Cycle No.	Charge Data						Discharge Data; 1.0V Cut Off				
	A	B	C	D		Amp.	Hrs.	AH Input	ECV Volts	ECP PSIA	ECR mΩ	Amp	AH Output	EDP PSIA	EDR mΩ	Eff. %
17	1	0	0	1	129	.400	17	6.8	1.451	--	19.02	2.0	3.184	--	35.18	64.2
19	1	0	0	1	129	.400	17	6.8	1.443	--	15.93	2.0	3.100	--	35.87	62.5
21	1	0	1	1	129	.400	17	6.8	1.462	--	11.09	2.0	3.666	--	11.75	73.9
23	1	0	1	1	129	.400	17	6.8	1.486	--	11.44	2.0	4.252	--	16.02	85.7
25	1	1	0	1	129	.400	17	6.8	1.440	--	15.88	2.0	3.218	--	37.77	64.9
27	1	1	0	1	129											
29	1	1	1	1	129	.400	17	6.8	1.463	--	10.14	2.0	3.866	--	11.14	77.9
31	1	1	1	1	129	.400	17	6.8	1.471	--	20.14	2.0	4.352	--	31.30	87.7

TABLE I - 2 (cont'd.)

Ni-Cd Rectangular Cells; Factorial Design Experiment

ELECTROCHEMICAL PERFORMANCE DATA

FOR FACTOR DESCRIPTION AND LEVELS SEE TABLE I - 1

Cell No.	Factors				Cycle No.	Charge Data						Discharge Data; 1.0V Cut Off				
	A	B	C	D		Amp.	Hrs.	AH Input	ECV Volts	ECP PSIA	ECR mΩ	Amp	AH Output	EDP PSIA	EDR mΩ	Eff. %
17	1	0	0	1	146	400	17	6.8	1.473	---	19.42	2.0	3.084	---	36.09	62.2
19	1	0	0	1	146	400	17	6.8	1.452	---	18.90	2.0	3.118	---	41.45	62.9
21	1	0	1	1	146	400	17	6.8	1.473	---	11.13	2.0	3.700	---	11.24	74.6
23	1	0	1	1	146	400	17	6.8	1.488	---	11.94	2.0	4.166	---	14.94	84.0
25	1	1	0	1	146	400	17	6.8	1.474	---	16.08	2.0	3.266	---	42.10	65.8
27	1	1	0	1	146											
29	1	1	1	1	146	400	17	6.8	1.472	---	10.48	2.0	3.952	---	11.07	79.7
31	1	1	1	1	146	400	17	6.8	1.475	---	25.28	2.0	4.384	---	37.72	88.4

TABLE I-3

Ni-Cd, RECTANGULAR, 18-PLATE CELLS, 30% KOH, 80% PORE FILL, FT2140 SEPARATOR

POST-STERILIZATION DATA

C.R. = C/12.5 C.L. = 137% D.R. = C/2.5 REPLICATE: 4 CELLS

Cycle #	E.C.V	(v)	O.C.V.	(v)	Cell Voltage at Various D. of D. 25%		50%		75%		E.C.R.(m)		E.D.R.(m)		Cap.	(AH)	Eff.(%)
	Av.		Av.		Av.		Av.		Av.		Av.		Av.		Av.		Av.
32	1.453	0.003	1.400	0.001	1.270	0.011	1.259	0.011	1.244	0.011	14.25	4.22	14.21	3.89	4.054	0.066	81.7 1.3
38	1.463	0.008	1.419	0.004	1.277	0.002	1.265	0.004	1.253	0.004	13.01	0.79	15.42	2.54	4.163	0.082	83.9 1.7
44	1.476	0.003	1.413	0.004	1.272	0.009	1.262	0.010	1.248	0.010	13.64	3.54	15.45	5.15	4.055	0.177	81.8 3.6
49	1.468	0.004	1.398	0.005	1.274	0.009	1.263	0.011	1.246	0.010	13.58	3.80	14.76	5.36	4.042	0.134	81.5 2.7
53	1.472	0.004	1.400	0.005	1.267	0.015	1.257	0.015	1.242	0.014	14.20	5.41	16.30	7.25	3.905	0.201	78.7 4.1
60	1.478	0.004	1.408	0.004	1.270	0.007	1.258	0.007	1.246	0.007	13.19	2.89	16.29	4.43	4.063	0.154	81.9 3.1
70	1.476	0.006	1.415	0.004	1.277	0.006	1.262	0.008	1.244	0.008	12.59	1.78	18.79	4.37	4.088	0.194	82.4 3.9
71	1.468	0.005	1.406	0.004							12.17	1.65	15.84	4.47	4.042	0.234	81.5 4.7
80	1.471	0.004	1.399	0.005							12.65	3.22	16.33	5.73	4.008	0.169	80.8 3.4
90	1.503	0.007	1.430	0.004							13.02	3.42	22.06	10.59	4.092	0.191	82.5 3.8

lization. Five replicates of each cell were fabricated and tested. Following sterilization, one of the control and one of the FC-128 cells failed to accept charge, probably due to the development of an internal short. During this period, the cells were subjected to twelve pre-sterilization cycles, 12.5 hour charge rate to 137% charge input level, discharge at the 2.5 hour rate to the 1.0V cut-off. Representative data after various cycles is shown in Table I-4. The average parameter values for the five cells, and the standard deviations are given. The discharge voltage data is shown at 25%, 50% and 75% depth of discharge, based upon the average capacity delivered in the first cycle. This data shows that, prior to sterilization, those cells employing pre-treated FT2140 as separator yield the highest delivered capacity, above 75% of theoretical formation capacity after eight cycles. It is to be noted that such efficiency is significantly greater than has been achieved in the pre-sterilization stage with polypropylene separators up to this time. Furthermore, it is to be noted that these cells exhibit the lowest end-of-charge, and end-of-discharge resistances, with the least amount of scatter. Although the "pre-treated" cells yielded the greatest capacity, it is to be noted that those cells containing the FC-128 surfactant showed the least amount of scatter in the efficiency data. Following sterilization, the four groups of cells were cycled according to the same charge-discharge routine. The post-sterilization data for the first four cycles is

TABLE I-4

EFFECT OF SURFACTANT ADDITION AND SEPARATOR PRETREATMENT ON CELL OPERATIONAL BEHAVIOR

Ni-Cd, 18-Plate Cells. FT2140 Separator. 30% KOH. 30% Pore Fill Level
C.R. = C/12.5 C.L. = 137% D.R. = C/2.5

PRE-STERILIZATION DATA

Cell Group	Cycle #	E.C.V. (v)		O.C.V. (v)		Cell Voltage at Various D. of D. (v) 25%		50%		75%		E.C.R.(mΩ)		E.D.R.(mΩ)		Cap.(AH)		Effcy (%)	
		Av.	σ	Ave.	σ	Av.	σ	Av.	σ	Av.	σ	Av.	σ	Av.	σ	Av.	σ	Av.	σ
Control	2	1.416	0.002	1.385	0.001	1.257	0.002	1.244	0.003			12.21	0.71	11.72	0.73	3.140	0.156	63.3	3.1
Pretreat	"	1.414	0.002	1.384	0.001	1.270	0.001	1.257	0.002			10.08	0.25	10.50	0.35	3.580	0.086	72.2	1.7
FC-128	"	1.410	0.001	1.381	0.001	1.269	0.002	1.254	0.001			10.19	0.68	11.92	0.97	3.317	0.082	66.9	1.7
FC-176	"	1.414	0.003	1.384	0.001	1.267	0.004	1.252	0.004			10.85	0.40	11.12	0.35	3.354	0.175	67.6	3.5
Control	5	1.421	0.004	1.379	0.002	1.259	0.004	1.229	0.009	1.188	0.037	11.17	1.06	11.86	1.10	2.640	0.235	53.2	4.7
Pretreat	"	1.425	0.002	1.383	0.002	1.270	0.002	1.250	0.003	1.223	0.007	9.69	0.38	10.34	0.22	3.364	0.173	67.8	3.5
FC-128	"	1.418	0.002	1.379	0.001	1.267	0.002	1.242	0.002	1.167	0.040	10.16	0.66	10.67	0.85	2.831	0.069	57.1	1.4
FC-176	"	1.422	0.004	1.380	0.001	1.265	0.004	1.241	0.005	1.192	0.022	10.24	0.33	11.34	0.45	2.827	0.153	57.0	3.1
Control	7	1.431	0.005	1.379	0.003	1.256	0.004	1.231	0.010	1.175	0.051	12.72	0.98	12.42	1.36	2.958	0.276	59.6	5.6
Pretreat	"	1.436	0.003	1.383	0.003	1.268	0.001	1.255	0.002	1.242	0.003	9.30	0.37	9.79	0.26	3.627	0.210	73.1	4.2
FC-128	"	1.435	0.001	1.382	0.001	1.268	0.002	1.252	0.002	1.232	0.003	10.24	0.85	11.70	1.17	3.167	0.061	63.9	1.2
FC-176	"	1.436	0.002	1.381	0.003	1.262	0.004	1.246	0.006	1.226	0.012	10.26	1.16	10.66	1.10	3.104	0.221	62.6	4.5
Control	9	1.425	0.006	1.379	0.003	1.261	0.006	1.238	0.010	1.187	0.049	11.90	1.40	13.98	1.76	2.843	0.281	57.3	5.7
Pretreat	"	1.432	0.002	1.387	0.002	1.275	0.001	1.259	0.002	1.241	0.003	9.67	0.30	10.48	0.29	3.811	0.124	76.8	2.5
FC-128	"	1.423	0.002	1.380	0.002	1.272	0.002	1.248	0.002	1.222	0.003	10.38	1.03	10.98	1.13	3.109	0.073	62.7	1.5
FC-176	"	1.428	0.004	1.382	0.002	1.270	0.005	1.247	0.005	1.221	0.011	10.76	0.99	11.18	0.95	3.138	0.283	63.3	5.7
Control	11	1.425	0.006	1.374	0.003	1.259	0.007	1.236	0.011	1.197	0.027	12.20	1.64	12.77	2.09	2.864	0.291	57.7	5.9
Pretreat	"	1.431	0.002	1.382	0.001	1.272	0.003	1.255	0.004	1.231	0.006	9.65	0.38	9.69	0.28	3.794	0.176	76.5	3.5
FC-128	"	1.422	0.002	1.376	0.001	1.270	0.002	1.246	0.003	1.207	0.007	10.64	1.12	11.33	1.17	3.146	0.089	63.4	1.8
FC-176	"	1.428	0.004	1.377	0.002	1.266	0.004	1.242	0.007	1.210	0.011	10.27	0.87	10.64	0.96	3.237	0.307	65.3	6.2

shown in Table I-5. The high end-of-charge and open-circuit voltages are again in evidence. The efficiency for all four groups of cells increases noticeably after sterilization. Post-sterilization data from cycles 5, 10, 15, 20 and 25 are shown in Table I-6. All of the cells in the control and pre-treated group leaked on cycles immediately after sterilization. The leaks disappeared after changing the "O" rings on the vent seals, but some loss of electrolyte resulted in low capacity in these cells. Eighteen plate sterilized cells normally yield 4.0 AH, while these two groups are yielding 3.0 to 3.4 AH.

Consequently, the data on cells with surfactant addition should be compared to the previously made 18-plate cells described in item 2.2. Of these three cells being tested, one exhibits high resistance 31.29 m versus 11.09 m and 10.08 m (ECR). Since the high resistance directly effects the cell voltage at various fractions of discharge, the data for cells with surfactant addition should be compared to the data for the two remaining cells (last line of Table I-7. Comparison of this data shows that cells with the addition of FC128 are not significantly different from cells without the addition of surfactant while the cells with FC176 exhibit variable, lower capacity (3.817 ± .295 AH versus 4.018 ± .200 AH). No further work is planned with these surfactants or treatment.

2.3.2 Other Treatments of Separator Material:

Samples of FT2140 polypropylene separator were sent to (1) RAI Research

TABLE I-5

EFFECT OF SURFACTANT ADDITION AND SEPARATOR PRETREATMENT ON CELL OPERATIONAL BEHAVIOR

Ni-Cd, 18-Plate Cells. FT2140 Separator. 30% KOH. 80% Pore Fill Level
C.R. = C/12.5 C.L. = 137% D.R. = C/2.5

POST-STERILIZATION DATA

Cell Group	Cycle #	E.C.V. (v)		O.C.V. (v)		Cell Voltage at Various D. of D. (v) 25%		50%		75%		E.C.R. (mΩ)		E.D.R. (mΩ)		Cap. (AH)		Effcy. (%)	
		Av.	σ	Av.	σ	Av.	σ	Av.	σ	Av.	σ	Av.	σ	Av.	σ	Av.	σ	Av.	σ
Control	1	1.505	0.002	1.415	0.001	1.247	0.002	1.242	0.002	1.228	0.005	11.50	0.70	11.76	0.93	3.680	0.257	74.2	5.2
Pretreat	"	1.503	0.001	1.415	0.001	1.254	0.005	1.246	0.003	1.235	0.006	9.53	0.25	10.31	0.29	3.472	0.237	70.0	4.8
FC-128	"	1.497	0.002	1.413	0.001	1.252	0.001	1.247	0.000	1.238	0.001	10.30	0.45	10.32	0.51	4.051	0.065	81.7	1.3
FC-176	"	1.504	0.003	1.413	0.002	1.255	0.006	1.245	0.004	1.235	0.008	10.30	0.55	11.21	0.66	3.688	0.275	74.4	5.5
Control	2	1.486	0.004	1.414	0.001	1.250	0.001	1.243	0.002	1.220	0.008	11.50	0.79	13.06	0.79	3.738	0.271	75.4	5.5
Pretreat	"	1.493	0.005	1.418	0.002	1.252	0.003	1.246	0.004	1.223	0.009	10.96	0.30	10.42	0.57	3.560	0.246	71.8	5.0
FC-128	"	1.486	0.003	1.414	0.001	1.255	0.001	1.252	0.001	1.239	0.002	10.46	0.42	11.10	0.58	4.067	0.082	82.0	1.6
FC-176	"	1.501	0.005	1.419	0.003	1.252	0.001	1.247	0.004	1.229	0.012	12.00	0.94	10.79	0.94	3.907	0.308	78.8	6.2
Control	3	1.473	0.004	1.405	0.003	1.256	0.001	1.247	0.002	1.221	0.011	11.81	0.63	13.51	1.12	3.517	0.282	70.9	5.7
Pretreat	"	1.474	0.004	1.404	0.003	1.256	0.003	1.246	0.006	1.219	0.013	10.73	0.89	10.43	0.36	3.620	0.247	73.0	5.0
FC-128	"	1.476	0.003	1.407	0.002	1.259	0.000	1.243	0.002	1.243	0.002	10.56	0.34	10.35	0.57	3.858	0.126	77.8	2.5
FC-176	"	1.489	0.005	1.409	0.005	1.256	0.001	1.248	0.005	1.230	0.013	11.49	0.84	10.82	1.06	4.107	0.342	82.8	6.9
Control	4	1.470	0.004	1.389	0.019	1.259	0.002	1.249	0.004	1.217	0.013	11.96	1.38	11.44	0.54	3.288	0.308	66.3	6.2
Pretreat	"	1.472	0.006	1.407	0.004	1.262	0.001	1.256	0.004	1.226	0.013	10.85	0.42	10.02	0.47	3.251	0.240	65.5	4.8
FC-128	"	1.482	0.004	1.416	0.001	1.263	0.001	1.261	0.000	1.247	0.002	10.97	0.34	12.69	0.80	4.013	0.117	80.9	2.4
FC-176	"	1.488	0.004	1.413	0.004	1.260	0.002	1.256	0.003	1.237	0.012	12.14	0.92	10.87	0.84	3.758	0.314	75.8	6.3

TABLE I-6

EFFECT OF SURFACTANT ADDITION AND SEPARATOR PRETREATMENT ON CELL OPERATIONAL BEHAVIOR
POST-STERILIZATION DATA

Ni-Cd, 18-Plate Cells. FT2140 Separator. 30% KOH. 80% Pore Fill Level
C.R. = C/12.5 C.L. = 137% D.R. = C/2.5

Cycle	Group	ECV(v)		OCV(v)		Cell Voltage at Various D. of D. (v) 25%		50%		75%		ECR(mΩ)		EDR(mΩ)		Cap.(AH)		Effcy(%)	
		Av.	S	Av.	S	Av.	S	Av.	S	Av.	S	Av.	S	Av.	S	Av.	S	Av.	S
5	Control	1.452	.003	1.399	.003	1.264	.001	1.249	.004	1.218	.013	11.95	0.63	11.80	1.06	3.183	.302	64.2	6.1
5	Pretreat	1.447	.007	1.395	.003	1.267	.003	1.258	.005	1.225	.012	10.58	0.51	10.60	0.56	3.364	.232	67.8	4.7
5	FC128	1.451	.004	1.399	.002	1.269	.001	1.264	.001	1.252	.002	11.16	0.63	11.64	0.68	4.208	.130	84.8	2.6
5	FC176	1.458	.003	1.400	.004	1.267	.002	1.260	.004	1.240	.011	11.63	0.87	11.73	1.49	3.737	.283	75.3	5.7
10	Control	1.462	.004	1.390	.002	1.264	.001	1.254	.002	1.224	.009	12.26	0.94	11.50	0.72	3.075	.250	62.0	5.1
10	Pretreat	1.460	.005	1.387	.003	1.269	.003	1.260	.007	1.233	.018	10.79	1.03	10.66	0.82	3.160	.335	63.7	6.8
10	FC128	1.465	.003	1.393	.002	1.271	.002	1.265	.002	1.243	.005	10.77	0.73	10.67	0.63	3.713	.175	74.9	3.5
10	FC176	1.466	.002	1.392	.003	1.269	.003	1.262	.004	1.245	.010	11.19	1.22	11.88	1.45	3.644	.311	73.5	6.3
15	Control	1.478	.005	1.407	.003	1.266	.001	1.257	.002	1.229	.007	11.84	0.34	14.39	0.60	3.234	.215	65.2	4.3
15	Pretreat	1.480	.004	1.404	.003	1.270	.003	1.263	.005	1.238	.015	10.97	0.58	11.96	1.40	3.398	.365	68.5	7.4
15	FC128	1.478	.003	1.407	.001	1.271	.002	1.267	.002	1.255	.003	11.22	0.91	11.40	0.82	3.867	.166	78.0	3.3
15	FC176	1.481	.003	1.407	.003	1.269	.003	1.263	.004	1.246	.009	11.63	1.55	13.47	2.61	3.810	.315	76.8	6.3
20	Control	1.467	.003	1.386	.002	1.267	.002	1.253	.002	1.231	.007	11.59	0.78	13.65	0.73	3.208	.171	64.7	3.4
20	Pretreat	1.466	.003	1.387	.003	1.271	.006	1.261	.009	1.239	.016	11.10	2.06	10.28	1.77	3.381	.335	68.2	6.7
20	FC128	1.472	.003	1.395	.002	1.271	.003	1.267	.002	1.260	.002	10.42	0.78	10.91	0.73	3.871	.177	78.0	3.6
20	FC176	1.470	.001	1.391	.003	1.267	.003	1.260	.003	1.244	.010	12.76	3.76	12.17	3.66	3.804	.314	76.7	6.3
25	Control	1.472	.002	1.410	.000	1.265	.002	1.255	.002	1.229	.004	13.74	1.56	13.61	1.99	3.159	.138	63.7	2.8
25	Pretreat	1.480	.003	1.416	.002	1.271	.005	1.261	.007	1.240	.014	11.60	1.53	10.93	0.93	3.430	.328	69.2	6.6
25	FC128	1.472	.002	1.416	.002	1.275	.001	1.269	.002	1.252	.004	11.10	0.72	13.84	1.15	4.051	.155	81.7	3.1
25	FC176	1.478	.001	1.417	.003	1.268	.009	1.260	.009	1.244	.011	13.33	4.42	13.24	3.86	3.817	.295	77.0	5.9

TABLE I-7

COMPARISON OF CELLS WITH AND WITHOUT SURFACTANT ADDITION

POST-STERILIZATION DATA

Ni-Cd, 18-Plate Cells. FT2140 Separator. 30% KOH. 80% Pore Fill Level
C.R. = C/12.5 C.L. - 137% D.R. = C/2.5

Cycle #	Group	n	ECV(v)		OCV(v)		Cell Voltage at Various D. of D. (v) 25%		50%		75%		ECR(mΩ)		EDR(mΩ)		Cap.(AH)		Effcy(%)	
			Av.	S	Av.	S	Av.	S	Av.	S	Av.	S	Av.	S	Av.	S	Av.	S	Av.	S
25	"B"	3	1.487	.002	1.411	.002	1.264	.012	1.254	.012	1.238	.012	17.75	9.57	16.67	6.61	4.085	.125	82.4	2.5
25	FC128	4	1.472	.002	1.416	.002	1.275	.001	1.269	.002	1.252	.004	11.10	0.72	13.84	1.15	4.051	.155	81.7	3.1
25	FC176	4	1.478	.001	1.417	.003	1.268	.009	1.260	.009	1.244	.011	13.33	4.42	13.24	3.86	3.817	.295	77.0	5.9
25	*	2	1.487	.002	1.411	.001	1.273	.005	1.263	.005	1.246	.006	10.99	0.20	11.99	0.48	4.018	.200	81.0	4.0

* Group "B" cells without the cell with high resistance.

Corporation, New York, (2) Southwest Research Institute, (SRI) San Antonio, Texas, to be given their respective proprietary treatments to improve the surface wetting properties. In Table I-8 are shown some pertinent physical properties of the as-received and treated materials. The FT2140 polypropylene treated by the South West Research Institute presents a drastic change in appearance from the original material. Even the least severe treatment results in a 10% shrinkage in the cross-fibre direction, a marked increase in the thickness and in the mass per unit area. Although this treatment enhances the KOH electrolyte pick-up, only the most severe treatment effects an increase in the absorption rate. Even in this case, the increase is not too significant. On the other hand, the RAI treated FT2140 exhibits greatly enhance wettability properties, without any marked change on the other physical properties of the material. No further work is indicated or planned with SRI treated material.

Two rectangular,18-plate cells, incorporating RAI-treated FT2140 separator have been prepared and cycled 11 times. The data tabulated in Table I-9 show only one significant effect of the RAI treatment. The pressure developed during overcharge is greater than in the control cell. This is understandable since the treatment reduces the effective porosity of the material, resulting in greater resistance to oxygen diffusion from the positive to the negative plate and its recombination rate during overcharge. Other effects of the RAI-

TABLE I-8

PHYSICAL PROPERTIES OF AS-RECEIVED AND TREATED FT2140 POLYPROPYLENE SEPARATOR

Sample	Mass/Unit Area ($gm/in.^2$)	Thickness (in.)	Shrinkage	KOH Pick-up (gm KOH/gm Sep)	Time(min) to Attain a Height of: 0.5 cm	1.0 cm	2.5 cm
As-Received	0.044	0.0075		-	200	400	>400
RAI Treatment	0.047	0.0090	None	2.54	0.2	0.5	1.7
SWRI Treatment* 1	0.102	0.023	~10%	4.79	100	340	>24 hrs
" " 2	0.096	0.022	"	3.46	160	700	>24 hrs
" " 3	0.073	0.018	"	3.61	650	1290	>24 hrs

* Southwest Research Institute - Treatment 1 - Most severe
" 2 - Intermediate severity
" 3 - Least severe

TABLE I - 9

Effect of RAI Treated Separator

PRE-STERILIZATION

Ni-Cd 18-Plates FT2140 Separator 30% KOH 80% Pore Fill

C.R. = C/12.5 C.L. = 137% D.R. = C/2.5

Separator	Cell #	Cycle #	ECV volts	ECR mΩ	EDR mΩ	ECP psia	EDP psia	ECC A.H.	EFF. %
RAI	1	1	1.427	10.96	12.31	65.7	34.7	3.066	61.8
RAI	2	1	1.426	10.79	12.12			3.084	62.2
Control	1	1	1.445	10.51	12.46	23.7	<14.7	3.384	68.2
Control	2	1	1.443	10.53	12.17			3.300	66.5
RAI	1	6	1.442	11.02	10.58	134.7	<14.7	2.800	56.5
RAI	2	6	1.445	10.71	10.42			2.918	58.8
Control	1	6	1.438	11.41	11.37	46.7	<14.7	2.818	56.8
Control	2	6	1.436	11.04	11.13			2.100	42.3
RAI	1	11	1.476	11.11	11.65	154.7	40.7	3.800	76.6
RAI	2	11	1.482	10.82	11.22			4.100	82.7
Control	1	11	1.463	11.71	13.26	86.7	<14.7	3.800	76.6
Control	2	11	1.474	11.69	12.23			3.952	79.7

treatment e.g. on ECV, ECR, EDR and capacity are all minor. Since no permanent, improved cell performance results from RAI-treatment, no further work is planned with this treated separator.

2.4 Effect of Sterilization Time on Cell Performance:

In order to study the effect of varying sterilization times on the relevant cell operational parameters, eight rectangular, 18-plate cells were fabricated. Each cell employed 18 plates, untreated FT2140 separator and 30% KOH at the 80% pore fill level. Seven of the cells were heat-sterilized at 135°C for 1, 2, 4, 8, 16, 32 and 64 hours. Each cell together with the eighth unsterilized control cell, was subjected to the normal cycling routine, charge at the 12.5 hourly rate to 137% level - discharge at the 2.5 hourly rate to the 1.0V cut-off. As can be seen from the 2nd cycle data, shown in Figure I-1 the time during which the cells are subjected to sterilization has a marked effect on the cell voltages, both at end-of-charge and on open circuit, and on the efficiency. There is no analogous effect observed with the cell resistance data. This type of variation persisted throughout the eleven tests performed. This data indicates that sterilization in the cell environment effects a permanent change in the electrochemical characteristics of one or both of the electrodes.

2.4.1 Single Electrode Potential Studies in the Cell Environment:

In order to investigate the source and causes of the high end-of-charge voltage exhibited by all cells following heat-sterilization,

FIG. I -/1

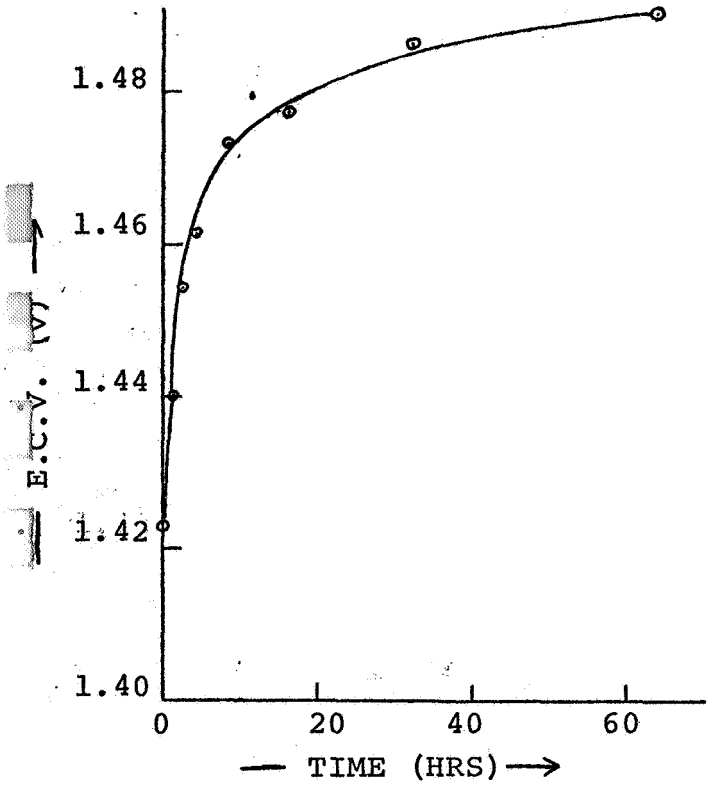
E.C.V. (V)
1.48
1.46
1.44
1.42
1.40
0
20
40
60
TIME (HRS)

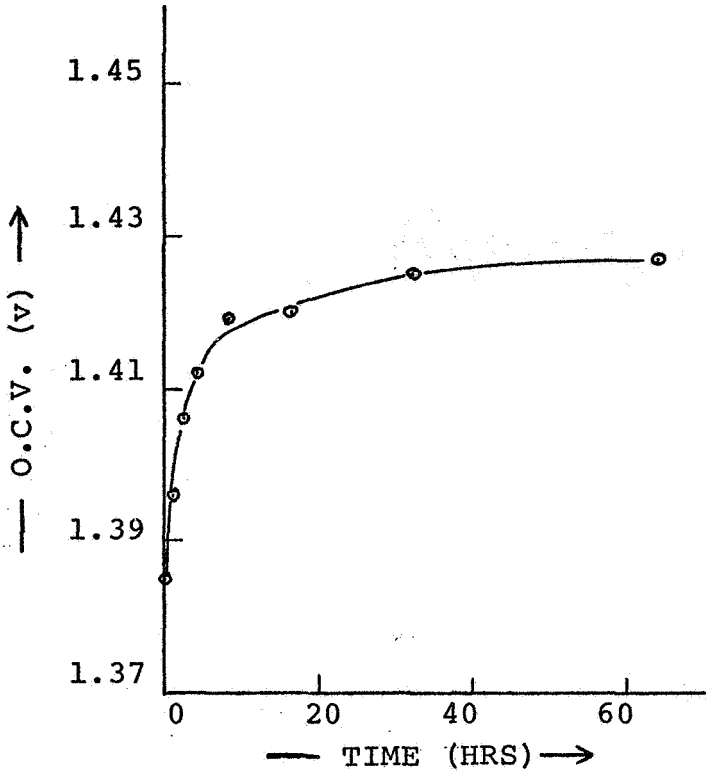
O.C.V. (v)
1.45
1.43
1.41
1.39
1.37
0
20
40
60
TIME (HRS)

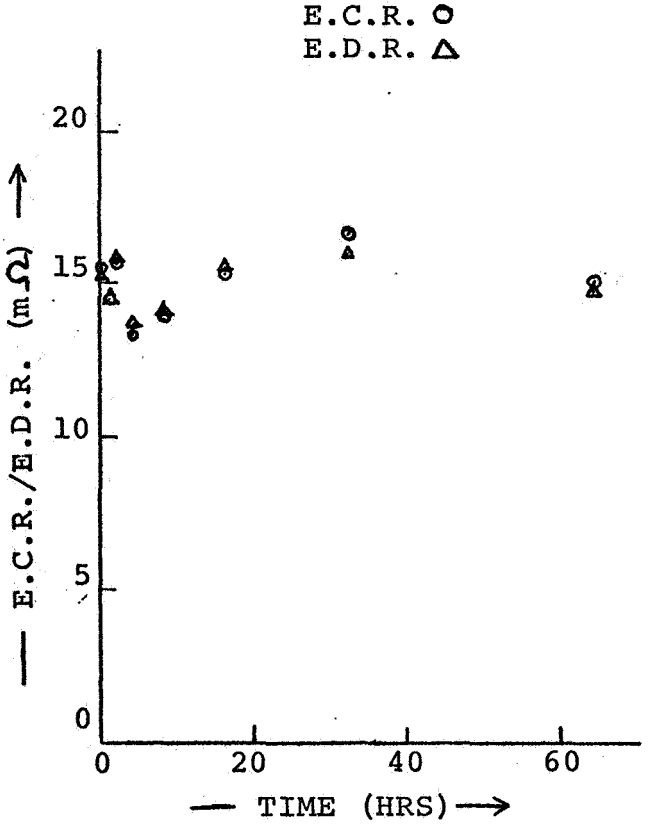
E.C.R. O
E.D.R. Δ
E.C.R./E.D.R. (mΩ)
20
15
10
5
0
0
20
40
60
TIME (HRS)

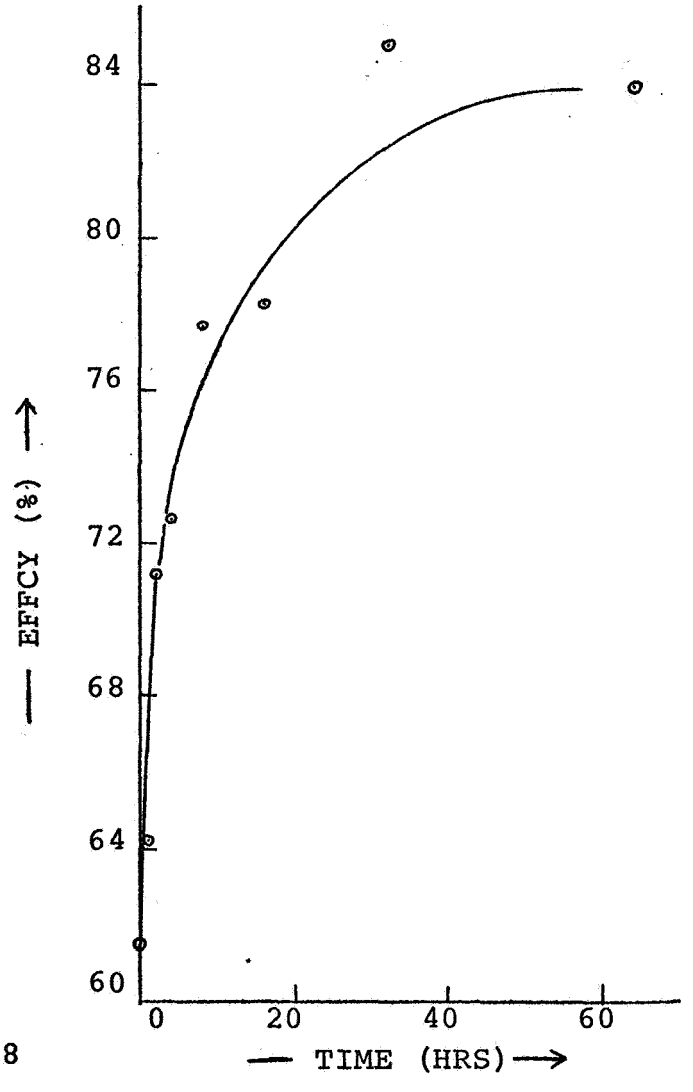
EFFCY (%)
84
80
76
72
68
64
60
0
20
40
60
TIME (HRS)

It was considered of prime importance to design and test an externally located reference electrode, capable of being inserted into a cell in order to monitor the separate potentials of the positive and negative electrodes. Such an electrode has been designed. Prototypes have been constructed and shown to work admirably.

A diagram of the Lucite electrode assembly is shown in Figure I-2. The electrode proper consists of the Hg/HgO/KOH system set-up in the wider section of the Lucite container, as shown. External contact to the mercury is made by means of the platinum wire cemented into the cap. (shown separated in the diagram). The narrow, cylindrical base section of the assembly is packed with separator material (Pellon-nylon or FT2140 - Polypropylene), pre-soaked with cell electrolyte, 30% KOH. This section, acting as a salt-bridge, extends into the threaded part of the Lucite body, and protrudes slightly at the base. The cap is finally cemented into the main body. A KOH-resistant O-ring fits into a groove, located just above the threaded section. The entire reference electrode system is screwed into a threaded hole, tapped into the top plate of the cell. When tightened, the lower section presses firmly against the cell separator protruding from between the alternate electrode plates forming the cell pack. The electrode assembly, as described, is capable of being used to monitor the positive and negative electrode potentials simultaneously, and is capable of withstanding the high pressures, (up to 80 psig),

FIG. I-2

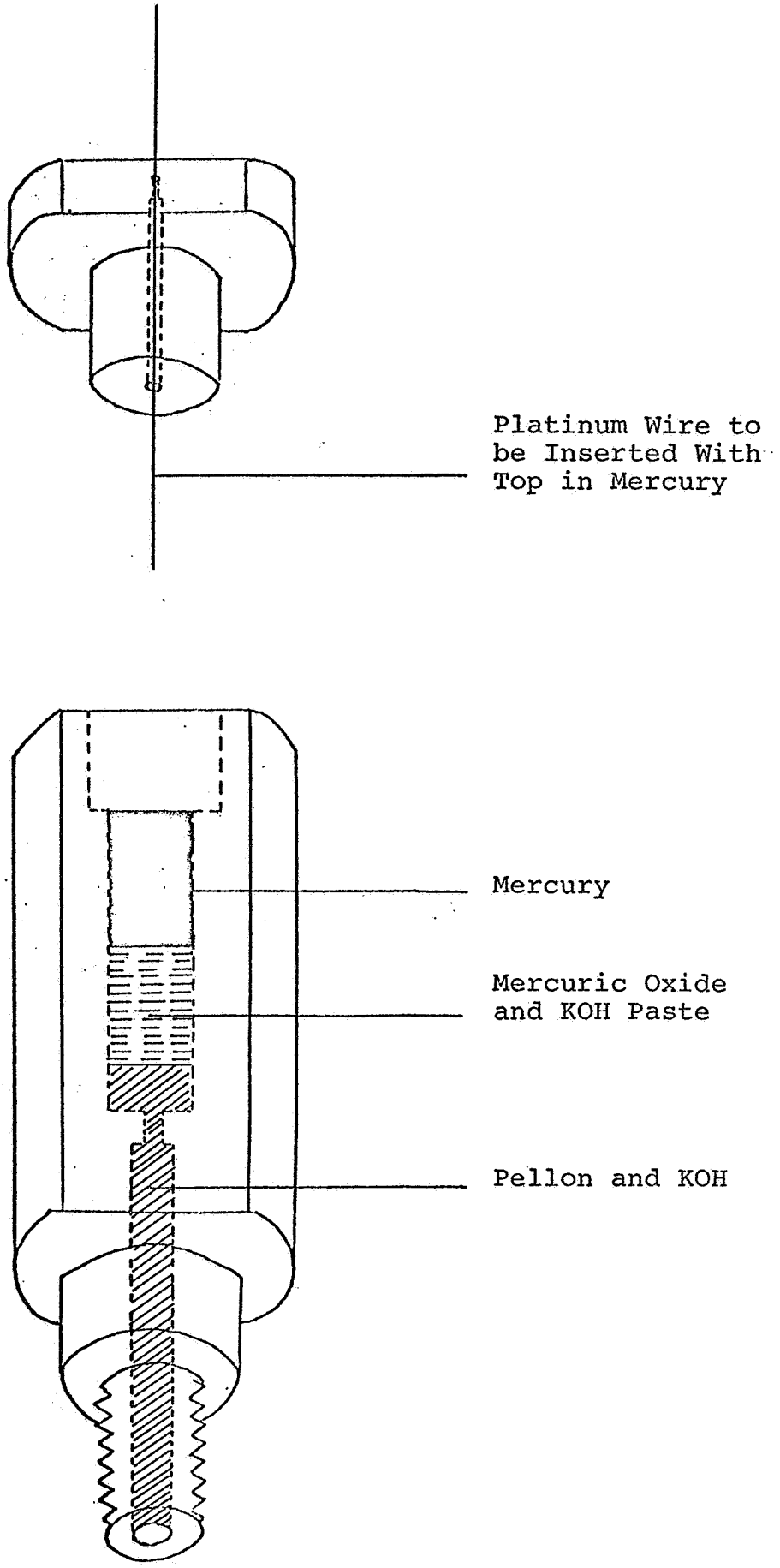
Platinum Wire to be Inserted With Top in Mercury
Mercury
Mercuric Oxide and KOH Paste
Pellon and KOH

commonly developed on over charge, without disrupting or leaking. In Fig.I-3 are shown some typical positive and negative electrode potentials and cell voltage-time curves, monitored during a normal charge-discharge routine, i.e. charge at the 12.5 hour rate to 137% level, discharge at the 2.5 hour rate. The full lines are for an unsterilized cell, the dashed lines are for a post-sterilized cell. The reference electrode is at ground potential. The positive reference, and negative reference potential differences are fed to the recorder via two separate, operational amplifiers, voltage follower circuits, with separate power supplies. The cell voltage is monitored directly. This data indicates that the high end-of-charge voltage is a result of changes associated with both electrodes. However, the major contribution appears to result from the positive electrode. Sterilization appears to have little or no effect on the electrode potentials during discharge. As can be seen, in the case of the unsterilized cell, the cell appears to be negative-limited on discharge. Following sterilization, however, the negative electrode exhibits greater capacity. In fact, both positive and negative electrodes appear to have approximately the same capacity.

These studies were extended in a new series of experiments as follows. The cells were taken through two complete charge-discharge cycles. Before the first charge each cell was subjected to a discharge current to determine the extent to which the cell was discharged. When it was observed that a given electrode potential had reversed, it

Fig. I-3

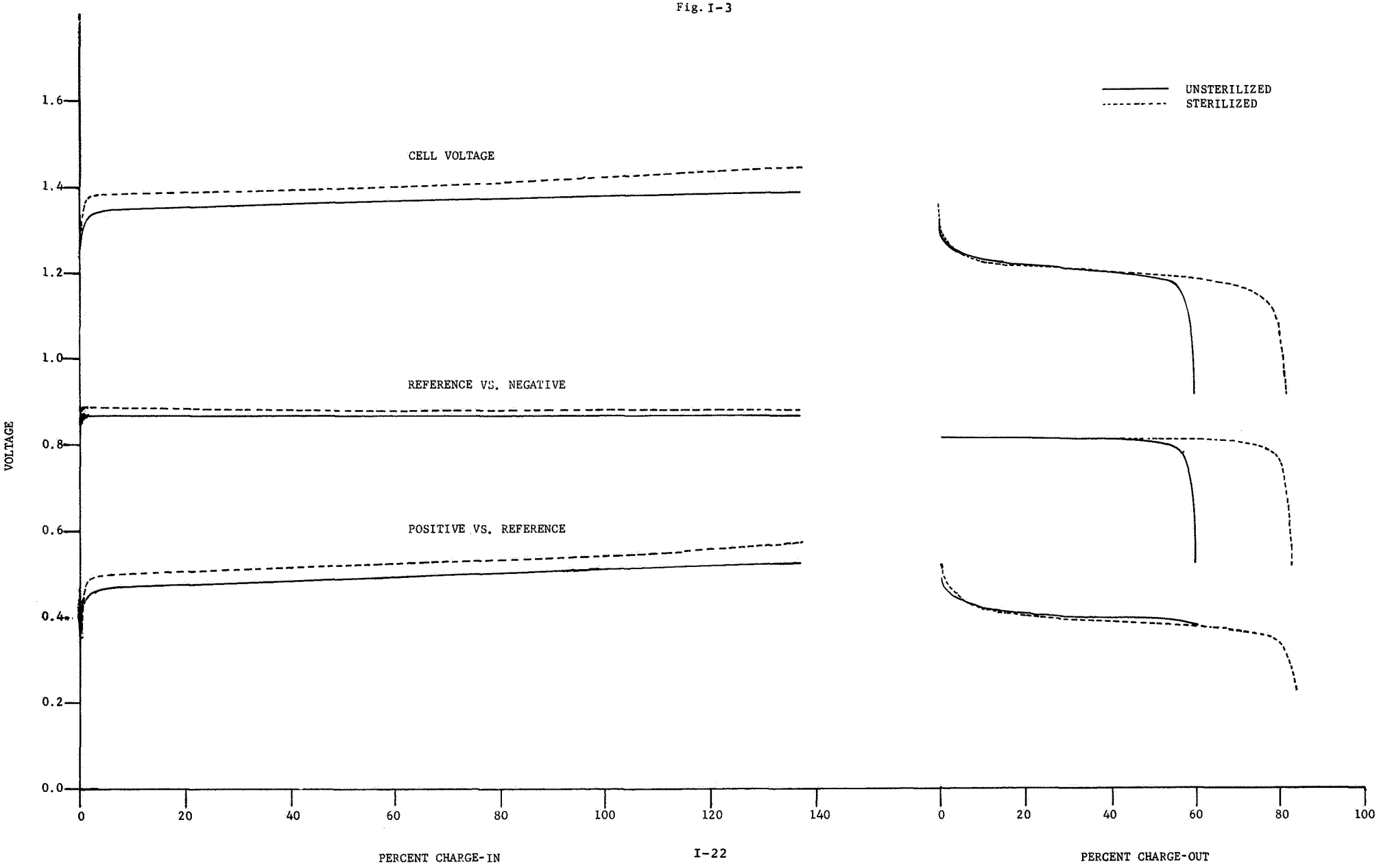
UNSTERILIZED
STERILIZED
CELL VOLTAGE
REFERENCE VS. NEGATIVE
POSITIVE VS. REFERENCE
VOLTAGE
1.6
1.4
1.2
1.0
0.8
0.6
0.4
0.2
0.0
0
20
40
60
80
100
120
140
PERCENT CHARGE-IN
PERCENT CHARGE-OUT

was assumed that the electrode was completely discharged. However, in some cases after the discharge current was interrupted, the electrode potentials did not remain reversed. The first charge was carried out with the cells vented. All gas evolved on over-charge was collected and the amount measured. It was assumed that all evolved gas was oxygen. The amount collected would, therefore, be equivalent to the amount of excess charge given to the negative electrode over the positive, the excess being 107 AH of cadmium per mole oxygen collected. This charge adjust was required to make the cells positive limiting upon discharge. Next, each cell was discharged after a 2 hr. stand, with the exception of the first cell discharged after only 1/2 hr. stand. The delivered capacity was calculated on the basis of the 1v cell voltage cut-off point. Both positive and negative electrode potentials vs. Hg/HgO as well as cell terminal voltages were monitored during discharge.

Individual electrode potentials were also monitored on the second charge and discharge processes. The results of the two cycles are presented in Tables I-10, I-11 and I-12.

The results of these experiments are summarized as follows:

(1) There appears to be no correlation between the amount of charge adjust added to the negative electrode on charge, and the delivered capacity. On both discharge cycles the capacities for all cells were high and little or no correlation between capacity and sterilization time was observed. These facts indicate cells

TABLE I - 10

Charge Parameters, 18-Plate, Rectangular Ni-Cd Cells
FT2140 Separator, 30% KOH, 80% Pore Fill

C.R. = C/12.5 C.L. = 137%

# of Cell	Time Hrs. Ster.	Cell Volt. at 50% Theo. Cap.	Cell Volt. at 100% Theo. Cap.	Max. Cell Volt. Attained on Over-charge	Volts E.C.V.	Volts O.C.V.	C.L. (%)	Charge Adjust (A.H.)
1	0	1.400	1.423	1.463	1.450	1.386*	160	0.679
2	1	1.400	1.424	1.469	1.469	1.342	137	0.975
3	2	1.400	1.423	1.464	1.464	1.368	137	1.21
4	4	cell	shorted	-----	-----	-----	---	----
5	8	1.410	1.445	1.476	1.476	1.376	137	1.05
6	16	1.403	1.437	1.482	1.482	1.387	137	0.715
7	32	1.402	1.437	1.484	1.484	1.392	137	0.562
8	64	1.406	1.437	1.492	1.492	1.394	137	0.286

* Stand time ½ hour all others 2 hours

TABLE I - 11

Discharge Parameters, 18-Plate, Rectangular Ni-Cd Cells

FT2140 Separator, 30% KOH, 80% Pore Fill. Discharge Rate C/2.5

# of Cell	Time Hrs. Ster.	Voltages at 65% Discharge (1st Cycle Only)			Voltage at 1 Volt (Cut-off (1st Cyc. On.)		A.H. Delivered at 1v Cut-off	
		Term.	Pos. vs. Hg/HgO	Neg. vs. Hg/HgO	Pos. vs. Hg/HgO	Neg. vs. Hg/HgO	1st Cycle	2nd Cycle
1	0	1.237	0.406	-0.833	0.368	-0.636	4.54	4.12
2	1	1.240	0.417	-0.831	0.301	-0.732	4.44	4.28
3	2	1.221	0.393	-0.839	0.236	-0.777	4.46	----
4	4	-----	-----	------	-----	------	----	----
5	8	1.245	0.404	-0.845	0.248	-0.775	4.36	4.34
6	16	1.236	0.393	-0.847	0.271	-0.760	4.62	4.42
7	32	1.238	0.399	-0.845	0.352	-0.664	4.49	4.38
8	64	1.241	0.396	-0.846	0.335	-0.668	4.45	4.26

TABLE I - 12

Charge Parameters with Hg/HgO Reference Electrode

18-Plate Rectangular Ni-Cd Cells, FT2140 Separator, 30% KOH, 80% Pore Fill

C.R. = C/12.5 C.L. = 137%

Cell	Hrs. Ster.	VOLTAGE AT: 50% Theo. Cap. Term.	50% Theo. Cap. Pos.	50% Theo. Cap. Neg.	100% Theo. Cap. Term.	100% Theo. Cap. Pos.	100% Theo. Cap. Neg.	E.C.V.* Term.	E.C.V.* Pos.	E.C.V.* Neg.	O.C.V. Term.	O.C.V. Pos.	O.C.V. Neg.
1	0	1.400	0.503	0.900	1.414	.520	0.897	1.440	0.537	0.895	1.374	0.503	0.866
2	1	1.403	0.506	0.898	1.432	.530	0.900	1.459	0.557	0.894	1.387	0.506	0.872
3	2	cell shorted											
4	4	cell shorted											
5	8	1.415	0.506	0.903	1.478	0.563	0.910	1.472	0.570	0.900	1.398	0.519	0.870
6	16	1.420	0.506	0.906	1.454	0.535	0.910	1.472	0.560	0.904	1.400**	0.511**	0.879**
7	32	1.417	0.496	0.915	1.460	0.533	0.985	1.468	0.566	0.901	1.378	0.498	0.880
8	64	1.419	0.498	0.914	1.450	0.523	0.917	1.480	0.562	.906	1.380	0.494	0.880

* Note: Max. voltages on overcharge were greater than ECV for cells 5 through 8, as follows:

CELL	TERM.	POS.	NEG.
5	1.490	0.578	0.915
6	1.481	0.565	0.913
7	1.494	0.579	0.926
8	1.490	0.570	0.920

** Cell not held full two hrs. before OCV taken

were positive limited, but direct confirmation of this could not be made without destroying the charge adjust.

(2) On the first charge, cell voltages at the end of charge increased with sterilization as was observed previously. The open circuit voltages after two hour stand also increased. The increase in E.C.V. with sterilization was not as prominent on the second charge cycle in which the positive and negative potentials were recorded vs. the Hg/HgO reference electrode. (Table I-12). However, an increase did occur over the first three cells (0, 1, 8 hrs. sterilization) and the increase was about the same as observed for 8 to 16 hours. sterilization in the previous charge, (Table 1-10).

The positive electrode can account for virtually all of the observed increase in E.C.V. at the cell terminals. Furthermore, the increase in E.C.V. appears to be associated with a change in oxygen over-voltage at the positive electrode. The difference in voltage between the 50% charge point of a given cell, and the maximum voltage attained on over charge is an indication of the oxygen over-voltage for that particular cell. It can be seen that this difference in potential accounts for the 30 mv. increase in E.C.V. with sterilization.

2.5 Characterization of Sterilized Plates in Flooded Cells:

The study of the end-of-charge voltage problem in sealed cells is complicated by possible interactions among plates, separator and

electrolyte. It would be desirable to observe this high voltage separately at each electrode. Accordingly it was planned to remove electrodes from unsterilized and sterilized cells and observe their behavior in flooded cells containing fresh electrolyte, no separator and using a reference electrode.

The flooded cells containing a Hg/HgO reference electrode were prepared. Provisions for measurement of electrode potentials during the complete charge-discharge cycle was made as outlined in the January report. Four cells were selected to supply the sample electrodes, two sterilized and two unterilized. These cells were 18-plate, 30% KOH, 80% pore fill cells used in the initial evaluation of 18-plate cells. The unsterilized cells had undergone five cycles; the sterilized cells had undergone five presterilization cycles and five post-sterilization cycles.

The cells were cut open, the test plates removed from near the middle of the pack, placed immediately into 30% KOH in the flooded cells and charging begun. The charge rate and charge level were selected to correspond to the cycling condition of: CR = C/12.5, CL = 137%, D.R. = C.2.5 where C is the formation capacity of the positive plate.

The first test consisted of 3 negative plates (1 plate for each flooded cell) removed from one unsterilized cell. Each counter electrode consisted of three as received positive plates in each flooded

cell. The second test consisted of 3 negatives from a sterilized cell. Since the results did not differ significantly within each group of three plates, the third test was made utilizing two sterilized and one unsterilized positive plates from the remaining two cells.

The results (see Table I-14) show that the positive electrode after sterilization exhibits higher end of charge voltage (.031 volts greater) than prior to sterilization, while the potential of the neta-tive at the same charge input remains unchanged. Sterilization also results in a slight decrease in flooded capacity (6-7% relative) for both the positive and negative plates. A small amount of shedding of material was observed from the sterilized positive plate. Thus it has been demonstrated that the high end of charge voltage may be observed in flooded cells enabling us to more easily investigate this phenomena.

TABLE I-14

BEHAVIOR OF UNSTERILIZED & STERILIZED PLATES

IN FLOODED CELLS

Electrode Material	E.C.V.[1] (137%) Unster.	Ster.		Effcy.[2] (%) Unster.	Ster.	
Neg. Plate	-0.903	-0.903		132	124	
Neg. Plate	-0.906	-0.909		135	126	
Neg. Plate	-0.909	-0.906		129	121	
Mean	-0.906	-0.906	0.000	132	124	8
Pos. Plate	0.512	0.544		91	86	
		0.542			84	
Mean	0.512	0.543	0.031	91	85	6

(1) Voltage versus Hg/HgO Reference

(2) Charge delivered/formation capacity of positive

II 25 Ampere Hour Cell Design, Construction and Evaluation

The engineering phase has been sub-divided into three major areas of effort, viz.,

A. Seal Development

1. Crimped/swaged polymeric seal
2. Modification of existing ceramic-to-metal seals to conform to the requirements of the 25 AH heat-sterilizable cells.

B. Cell Design and Test

1. Cylindrical design - 25 AH
2. Prismatic design - 25 AH

C. Physical and Electrochemical Evaluation of Impact Test Specimens

D. Fabrication of Heavily Loaded Plates

A. Seal Development

This area of effort was essentially devoted to the design, fabrication of crimped polymeric seals although ceramic-to-metal and glass-to-metal seals were designed and are used as back up during the development of this seal. The crimped/swaged polymeric seal is constructed using a center conductor which is insulated from a thick outer metal sleeve by chemically resistant, high dielectric, polymeric materials. KEL-F has been successfully used. The outer metal sleeve is threaded along its inside diameter with a thread which matches the thread on the outside diameter of the polymeric insulator. The seal is produced by drawing or crimping the three piece assembly.

In order to optimize the seal design in terms of hermeticity, and electrical and thermal conductivity, several seal configurations will be tested. To date, six sizes with

center conductor diameters ranging from 0.060 to 0.250 inches, and sleeve diameters ranging from 0.250 to 0.750 inches, have been selected. Initially several seals were fabricated by assembling the components then drawing the assemblies through various dies. These first samples consisted of a 1/4 inch outside diameter sleeve with a 5/32P - 32 BSW thread, a matching insulator and a 1/16" diameter conductor pin. The seal was completed by drawing the assemblies through various dies as noted in TABLE II-1. The seals were then leak detected on an NCR 925 mass spectrometer.

The seven polymeric compression seal samples were subjected to heat sterilization at 135°C for 72 hours, then releak tested on an NCR 925 mass spectrometer. Comparative data are shown in TABLE II-1.

TABLE II-1

Sample No	Leak Rate (Std. cc He/sec./atm.) As Assembled	After 72 hours @ 135°C	Assembly Method
1a	25 (gross leaker)	160μ*	drawn through 0.246" die
1b	2.0×10^{-8}	2μ*	drawn through 0.246" die
1c	1.5×10^{-8}	1.8×10^{-6}	drawn through 0.246" die
1d	0.7×10^{-8}	5μ*	drawn through 0.246" die
2	0.4×10^{-8}	5μ*	drawn through a tapered die (.250"/.236")
3	1.0×10^{-8}	3.8×10^{-6}	drawn through a 0.246" die
4	0.8×10^{-8}	6.0×10^{-6}	drawn through 3 dies progressively (.246", .242", .238")

* during the pumping down operation this minimum pressure was achieved, after which the safety switches on the mass spectrometer leak detector were automatically tripped, indicating a large leak.

All samples tested show an increase in leak rate after being subjected to heat sterilization. Three of the six acceptable seals tested became gross leakers and were considered failures. X-ray examination of the seals indicated axial distortion produced by the extrusion (or swaging) method of seal manufacture. This evidence underscores the favorability of the radial crimping technique which should not produce this effect.

Due to the nature of the thread form and the machinability of the KEL-F material the match between internal and external threads on these initial samples is also suspected to be imperfect. Three of the seven samples were encapsulated and sectioned to allow further investigation.

Microscopic examination of the seals indicated that the thread form of the plastic insulator was less than ideal. This allowed a helical leak path to develop which was aggravated by the expansion and contraction during the heat sterilization process. Since the machinability of the plastic insulator is poor especially when fabricating small components, and since large conductors are required to withstand large current drains from the 25 ampere-hour cells. The next group of seals to be fabricated will have center conductors of 0.093", 0.125" and 0.187".

In addition to the difficulties previously discussed, cell top assembly methods (i.e. attachment of seal to cell top) also favor use of an "in situ" radial crimping method as opposed to the drawing method. Therefore, the radial crimping has been selected as the better fabrication method. Crimping dies to assemble the seals were

designed and fabricated. Completion of the first group of seals is expected during the first part of April. Welding electrodes and crimping dies have been designed and manufactured.

Back-up seal designs for cylindrical cells incorporating glass or ceramic-to-metal seals have been drawn and vendors have been contacted. Ceramic-to-metal seals for prismatic cells have been purchased.

After fabrication the seals will be tested according to the schedule listed in TABLE II-2.

TABLE II-2
Test Plan for Seals

1. Test 20 samples of each of the configuration to determine absolute leak rate.
2. Heat sterilize 15 samples of each type from A.
3. Leak test samples after heat sterilization.
4. Submit 3 samples of each type from 1. - non heat sterilized for destructive tensile strength test.
5. Submit 3 samples of each type from 3. - heat sterilized for destructive tensile strength.
6. Submit 9 samples of each configuration from 3. - heat sterilized - for impact testing at the following levels:
   3 samples @ 4000g
   3 samples @ 3300g
   3 samples @ 2700g
7. Produce metallurgical section of 3 samples of each configuration:
   2 heat sterilized samples from 3.
   1 non heat sterilized sample from 1.

B. Cell Design

1. Prismatic Cell Design - The basic design for the prismatic cells has been established. Plate loadings and dimensions have been determined but may be altered if information gathered during testing indicates changes are required. Emphasis in design has been given to the following areas:

   a. Electrode edges - to minimize edge wires and loose active material, electrodes will be die cut or sheared to size on a power metal shear. Also the plate corners will be rounded to further reduce chance of separator penetration caused by sharp edges. To further minimize the chance of bare wires or loose material, the edges of the electrodes are coined (compressed). The die for coining plate has been designed, built and is being tested.

   b. Tab attachment - Engineering effort on this item was focused on two areas, viz., 1) tab attachment to the plate and 2) tab attachment to the terminal. The tab size was determined based on minimizing electrical resistance and maximizing ease of attachment to the plate and terminal connection. The resistance of the tab itself is in the order of 1×10^{-5} ohms and contributes very little to the total cell resistance. Some difficulty was initially encountered in welding tabs of this size (0.5 inches wide) to the plate. The plate structure (i.e. plaque and active material) burned and sputtered under the heat generated by the electrical resistance welding. A tab attachment now includes the removal of sintered

nickel and the resistance welding of the tabs to the screen itself. Initially, the welding of the tabs into collectors resulted in excess heat flowing into the plates discoloring them and melting the separator in spite of the use of rather intricate water cooled chills. A redesign of the comb and the use of resistance welding has minimized this difficulty. A sample of the weldment achieved using resistance welding is being evaluated for its stability under oxidizing conditions in KOH. Cross section samples of these weldments were prepared. Microscopic inspection of these weldments indicated that each tab had melted during the welding operation resulting in a metallurgical bond. A typical cross section is shown in Figure II-A.

The cell design was evaluated by constructing and testing several engineering prototypes. To date six prismatic cells have been built and four have been tested. Test consoles which allow for constant current discharge as high as 30 amperes as well as being compatible with our present data acquisition system are presently under construction. Fixed resistors are being used to discharge the following cells.

Cell P-1 is a cell of 30 Ah design with a polyamide separator. Cell P-2 was similarly constructed with the exception that a polypropylene separator was used and electrode tabs were attached by direct welding to the substrate. Cells P-3 and P-4, heat sterilizable cells, with glass seals were manufactured, placed on test and

Figure A

MICRO SECTION OF WELD JOINT

Typical of Joints Made on Taylor-Winfield
30 KVA Resistance Welding Machine

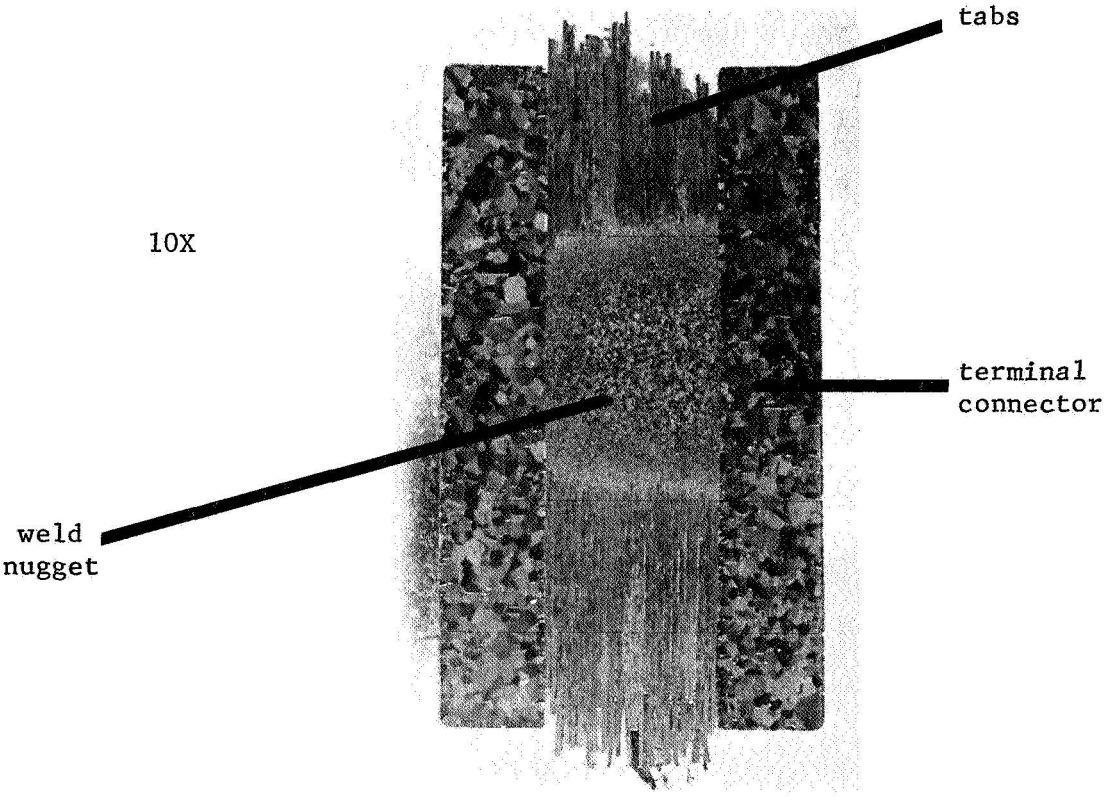

subsequently heat sterilized. Cells P-5 and P-6, non heat sterilizable cells with polyamide separator were also placed on test to act as control cells. The behavior of these cells to date is discussed.

Cell P-1 (TABLE II-3) - The electrochemical behavior of the cell is described in TABLE II-3. The end-of-charge voltage (ECV), the discharge voltage at 50% depth of discharge (V @ 50% DOD), end-of-charge (ECR) and end-of-discharge resistances (EDR), the end-of-charge (ECP) and the end-of-discharge pressures (EDP) and the cell capacity (ECC) are presented. The capacity data gathered to date at the 10 ampere discharge rate can only be considered approximate since fixed loads were used in place of constant current discharging. The variations in internal impedence and resultant voltage differences observed for these cells affect the average discharge current used in estimating cell capacity. These inaccuracies in cell capacity will be eliminated when the high constant current capacity stations under construction are completed. From cycles #6, #9, #14 and #18 the capacity of the cell can be determined to be 30 to 32 ampere hours at the three amp discharge rate and 28 ampere hours at the ten ampere discharge rate. This size cell was designed to deliver 25 ampere hours after heat sterilization is performed on polypropylene containing cells. The end-of-charge voltage of this cell constantly rose during cycles #1 thru #15 when it reached 1.54 volts. The end-of-charge and end-of-discharge pressure also rose during these cycles. These data suggest the evolution of hydrogen gas during charging. Additional data which will be obtained from this cell include determining a charge voltage profile and charge

RECTANGULAR CELL - 25Ah Cell No. P-1

TABLE II-3

Cycle No.	Discharge Current (amps)	ECV (volt)	OCV (volt)	V @ 50% DOD (volts)	ECR (mΩ)	EDR (mΩ)	ECP (psia)	EDP (psia)	ECC (Ah)
1	10	1.414	1.365	1.203	9.7	10.2	33	19	34.4
2	10	1.421	1.376	1.245	4.1	4.4	33	18	31.9
3	10	1.431	1.373	1.248	3.2	4.4	35	18	34.0
4	*3	1.437	1.376	1.271	4.0	4.3	39	18	31.2
5	*3	1.449	1.393	1.270	4.6	4.7	41	19	31.4
6	*3	1.480	1.380	1.269	4.5	4.8	58	27	31.5
7	10	1.459	1.371	1.249	4.6	4.9	53	29	31.3
8	10	1.489	1.376	1.244	4.5	5.1	95	53	31.3
9	*3	1.481	1.396	1.261	5.1	5.2	79	23	29.3
10	10	1.489	1.373	1.243	---	---	113+	15	27.8
11	10	1.495	1.377	1.244	4.8	5.2	115+	63	30.4
12	--	-----	-----	-----	---	---	----	---	----
13	10	1.513	1.410	1.237	4.6	5.0	115+	69	29.4
14	*10	1.520	1.382	1.251	5.0	8.0	115+	108	28.5
15	*10	1.541	1.387	1.248	4.7	5.6	115+	115+	31.2
16	10	1.530	1.383	1.248	4.8	5.5	115+	115+	31.0
17	10	1.520	1.379	1.248	4.9	5.2	115+	115+	31.5
18	*3	1.520	1.372	1.272	5.0	5.2	115+	98	32.3
19	10	-----	1.352	1.198	---	9.5	----	----	29.9

NOTES:

1. Polyamide separator (2505KI)
2. 80% Fill Level - 100cc (30% KOH)
3. 13 Negative Plates
4. 12 Positive Plates
5. Tabs - 1/2" wide nickel on each plate TIG welded to terminal comb
6. Weight - 1124 grams
7. Charging current is 3 amperes for 16 hours
8. Discharge to 1.00 volts
9. * indicates constant current discharge

pressure profile. Cells P-5 and P-6 which are essentially identical to P-1 have been submitted for testing but as yet (March 30) have not been cycled.

Cell P-2 (TABLE II-4) - This cell is similar in construction to P-1 excepting the separator which is polypropylene. Compared to P-1, this cell has a normal charge voltage (i.e. below 1.5 volts) in the range of 1.43 volts for the end-of-charge. The cell pressure is somewhat high but is acceptable, considering that the polypropylene separator is used. The cell, in general, is operating as designed. This fact is encouraging since P-1 is apparently negative limited on charge.

These cells (P-1, P-2) will continue cycling as reference cells and will not be heat sterilized. Other cells presently being manufactured will be heat sterilized and tested for proper design in terms of electrochemical behavior and mechanical integrity.

Cell P-3 and P-4 (TABLE II-5) - Both cells are similar in design and construction of P-2 with the exception of the seals, which are glass-to-metal with a protective epoxy coating. The cells were cycled five times prior to sterilization. Compared to P-1 these cells have similar and acceptable voltage characteristics, higher resistance values due to the glass seal design and higher end-of-charge pressures. Again the capacity data are scattered due to the fixed resistance method of discharging. Nonetheless, these cells will be heat sterilized and the cycling continued.

RECTANGULAR CELL - 25Ah Cell No. P-2

TABLE II-4

Cycle No.	Discharge Current (amp)	ECV (volt)	OCV (volt)	V @ 50% DOD (volts)	ECR (mΩ)	EDR (mΩ)	ECP (psia)	EDP (psia)	ECC (Ah)
1	*3	1.416	1.373	1.262	4.6	5.3	45	15	30.8
2	*3	1.430	1.374	1.264	4.5	5.5	49	15	31.4
3	*3	1.425	1.371	1.265	4.9	5.2	53	15	30.8
4	10	1.419	1.368	1.238	5.0	5.5	67	19	29.9
5	10	1.430	1.370	1.229	5.2	6.1	95	19	30.7
6	*3	1.426	1.387	1.257	5.7	6.4	85	15	28.7
7	*10	1.429	1.367	1.245	---	---	85	15	27.7
8	10	1.428	1.371	1.243	5.1	5.6	89	19	29.8
9	10	1.420	1.383	1.245	5.4	8.0	90	19	27.0
10	10	1.429	1.392	1.239	5.6	5.9	95	15	29.5
11	*10	1.428	1.375	1.252	5.7	7.3	89	15	27.7
12	10	1.445	1.378	1.250	4.9	6.0	93	15	30.9
13	10	1.430	1.371	1.248	5.1	5.8	93	15	30.8
14	10	1.428	1.371	1.249	5.2	5.6	93	15	30.7
15	*3	1.424	1.365	1.270	5.2	5.4	93	15	29.3
16	*10	-----	1.336	1.232	---	8.0	15	15	26.3

NOTES:

1. Polypropylene Separator (FT2140)
2. 80% Fill Level - 99cc (30% KOH)
3. 12 Positive Plates
4. 13 Negative Plates
5. Tabs - 1/2" wide nickel on each plate TIG welded to terminal comb
6. Weight - 1126 grams
7. Charging current is 3 amperes for 16 hours
8. Discharge to 1.00 volts
9. * indicates constant current discharge

RECTANGULAR CELL - 25Ah Cell No. P-3, P-4

TABLE II-5

Cycle No.	Cell No	Discharge Current (amp)	ECV (volt)	OCV (volt)	V @ 50% DOD (volts)	ECR (mΩ)	EDR (mΩ)	ECP (psia)	EDP (psia)	ECC (Ah)
1	P-3	10	1.429	1.379	1.237	11.6	12.7	100+	23	28.7
	P-4	10	1.454	1.385	1.220	13.4	16.4	100+	53	28.9
2	P-3	10	1.448	1.374	1.238	11.2	13.8	100+	51	25.1
	P-4	10	1.440	1.375	1.221	13.8	17.0	100+	58	28.6
3	P-3	10	1.436	1.368	1.236	11.6	14.0	100+	67	28.0
	P-4	10	1.442	1.373	1.219	14.7	15.8	100+	71	27.4
4	P-3	10	1.437	1.367	1.237	11.8	12.9	100+	73	27.6
	P-4	*3	1.436	1.364	1.255	14.2	14.7	100+	25	24.7
5	P-3	*3	1.428	1.361	1.236	11.2	12.3	100+	29	26.0
	P-4	*10	-----	1.325	1.205	----	8.5	----	15	23.6

NOTES:

1. Polypropylene separator (FT2140)
2. 80% fill level - 99cc (30% KOH)
3. 12 Positive plates
4. 13 Negative plates
5. Tabs - 1/2" wide nickel, resistance welded to plate substrate and terminal connector
6. Weight: P-3 = 1110 grams, P-4 = 1148 grams
7. Charging current is 3 amperes for 16 hours
8. Discharge to 1.00 volts
9. * indicates constant current discharge

Prismatic Cell Summary

In general the prismatic cells are operating as designed with two exceptions:

1. the cell pressures are higher than expected, which may indicate improper fill, over or under compression or contamination from another source (e.g. separator) which affects the oxygen recombination process and
2. the high end-of-charge voltage observed for P-1 is indicative of hydrogen gas evolution and may be a result of too small a negative-to-positive ratio.

These topics form the base for continued testing on prismatic cells.

Sufficient data has been generated to date to allow for design and fabrication of prismatic cells for delivery at the end of April. Except for delivery of the ceramic-to-metal seal headers this phase of the program is on schedule.

2. Cylindrical Cells - The cells contain four negative and three positive plates rolled in a "jelly roll" or "Swiss roll" to form a right circular cylinder. The advantages of this design include: (1) the use of fewer and larger electrodes which minimizes "edges" and their characteristic problem of loose wires and/or burrs; (2) the spiral design of the cell core in combination with Texas Instruments' plate (supporting substrate is on one side of the plate and is kept on the outside of "jelly rolls") which maintains a compressive force on the active material and therefore reduces the tendency for active material spalling; (3) a high >1.5 negative to positive material ratio without the use of heavily loaded plates since four negative plates and three positive plates provide at least 1.3 geometric ratio; and (4) no need for restraining plates.

A total of eight cells have been fabricated. Of these, four heat sterilizable and non-heat sterilizable have been tested to date. Cells C-0, C-3 and C-4 contain polyamide separator and cells C-1 and C-2 contain polypropylene separator. All cells tested to date (March 28) contain 1/4" tabs (1 per plate). This tab arrangement is only an expedient to allow cell testing and evaluation of electrode materials prior to the final design.

Cell C-0 (TABLE II-6) - This cell has polyamide separator and is filled to 75% of the free pore volume as determined empirically. The charging voltage and pressure characteristics are within acceptable limits and stable with no tendency to rise or fall

CYLINDRICAL CELL - 25Ah Cell No. C-0

TABLE II-6

ycle p.	Discharge Current (amp)	ECV (volt)	OCV (volt)	V @ 50% DOD (volts)	ECR (mΩ)	EDR (mΩ)	ECP (psia)	EDP (psia)	ECC (Ah)
2	10	1.417	1.360	1.201	9.8	10.8	20	15	35.1
4	10	1.406	1.357	1.185	10.0	11.8	23	15	32.8
5	*3	1.411	1.354	1.250	9.8	10.6	23	17	33.3
6	10	1.418	1.352	1.203	9.4	10.7	27	18	31.7
8	*3	1.432	1.387	1.265	4.1	4.4	37	15	31.9
9	*3	1.404	1.356	1.250	9.7	10.0	39	18	29.9
10	*3	1.418	1.362	1.253	9.6	10.8	37	17	32.0
2	10	1.423	1.360	1.206	9.6	11.3	39	20	35.3
14	10	1.406	1.352	1.203	9.9	10.4	20	21	32.6
6	10	1.396	1.346	1.191	9.8	10.5	51	19	25.9
8	10	1.402	1.363	1.247	10.0	11.0	41	15	28.3
20	10	1.412	1.356	1.195	10.6	11.7	43	17	31.7
2	10	1.418	1.377	1.185	11.2	12.6	43	16	28.8
24	*3	1.427	1.365	-----	10.1	11.3	37	15	30.7
6	*3	1.427	1.367	1.259	10.5	10.6	40	15	31.5

NOTES:

1. Polyamide separator (2505KI)
2. 75% fill level - 110cc (30% KOH)
3. Four negative plates
4. Three positive plates
5. Tabs - 1/4" wide nickel resistance welded to plate and current collector.
6. Weight - 1144 grams
7. Charging current is 3 amperes for 16 hours
8. Discharge to 1.00 volts
9. * indicates constant current discharge

as a function of cycling. The voltage during the 10 ampere discharge is approximately 50 millivolts lower than desired and can be attributed to IR loss caused by the higher resistance of these cells associated with the tabbing arrangement. The capacity appeared to be decreasing as a function of cycling. However upon continued cycling it appears these capacity variations are only fluctuations as opposed to trends. The capacity data of cycles #5, #8-#10, #24, #26 (3 ampere constant current discharges) indicate little if any changes in cell capacity. Additional cycling data will be obtained from this cell.

Cells C-1 and C-2 (TABLE II-7) - The cells are similar in construction to C-0 with the exception that polypropylene separator is used and the cell is filled to 80% of the free pore volume. The behavior of these cells is not unlike that of cell C-0. Charge voltage and pressure are acceptable and stable with the discharge voltage lower than desired again due to high internal resistances. The data of cycles #2, #3 and #11 indicate an essentially stable capacity. Cycling will continue.

Cells C-3 and C-4 (TABLE II-8) - These cells are similar to cell C-0 in both construction and electrochemical behavior. These cells do exhibit a somewhat lower capacity than expected. Cycling will continue.

Cells C-5 and C-8 were manufactured to the latest design, using two 1/2" wide tabs per electrode and the same terminal connector weld joint as developed for prismatic cells. Test data are not available on these four cells due to a delay in setting up

CYLINDRICAL CELL - 25Ah Cell No. C-1, C-2

TABLE II-7

Cycle No.	Cell No	Discharge Current (amp)	ECV (volt)	OCV (volt)	V @ 50% DOD (volts)	ECR (mΩ)	EDR (mΩ)	ECP (psia)	EDP (psia)	ECC (Ah)
2	C-1	*3	1.396	1.356	1.248	8.8	8.8	15	15	28.1
	C-2	*3	1.391	1.352	1.245	9.1	9.1	15	18	27.5
3	C-1	*3	1.410	1.362	1.252	8.7	9.6	15	15	30.6
	C-2	*3	1.409	1.362	1.252	9.0	9.7	31	19	30.7
4	C-1	10	1.403	1.356	1.208	8.9	9.3	15	15	31.7
	C-2	10	1.402	1.357	1.200	9.1	9.4	39	21	30.4
6	C-1	10	1.405	1.358	1.214	8.8	10.2	15	15	36.5
	C-2	10	1.405	1.358	1.203	9.0	10.4	53	21	32.7
8	C-1	10	1.384	1.341	1.210	9.7	10.1	63	15	29.2
	C-2	10	1.383	1.340	1.189	10.0	10.4	71	24	26.5
10	C-1	10	1.418	1.358	1.212	9.5	9.0	45	15	35.6
	C-2	10	1.419	1.358	1.205	9.8	9.3	57	23	33.1
11	C-1	*3	1.405	1.376	1.247	9.5	9.9	50	15	28.6
	C-2	*3	1.404	1.376	1.247	9.9	10.3	63	15	28.5
12	C-1	10	1.410	1.352	1.196	9.2	8.8	50	15	27.8
	C-2	10	1.409	1.351	1.184	5.1	9.2	61	15	27.8
14	C-1	10	1.402	1.362	1.192	9.5	21.0	57	15	26.2
	C-2	10	-----	-----	-----	---	----	--	--	----
16	C-1	*10	1.417	1.366	-----	9.1	19.7	55	15	----
	C-2	*10	-----	-----	-----	---	----	--	--	----
18	C-1	10	-----	1.367	1.243	---	9.0	--	--	30.0
	C-2	10	-----	1.338	1.242	---	8.5	--	--	27.4

NOTES:

1. Polyamide separator
2. 80% fill level - 117cc (30% KOH)
3. Four negative plates
4. Three positive plates
5. Tabs - 1/4" wide nickel, resistance welded to plate and current collector
6. Weight: C-1 = 1146 grams, C-2 = 1138 grams
7. Charging current is 3 amperes for 16 hours
8. Discharge to 1.00 volts
9. * Indicates constant current discharge

CYLINDRICAL CELL - 25Ah Cell No. C-3, C-4

TABLE II-8

Cycle No.	Cell No	Discharge Current (amp)	ECV (volt)	OCV (volt)	V @ 50% DOD (volts)	ECR (mΩ)	EDR (mΩ)	ECP (psia)	EDP (psia)	ECC (Ah)
1	C-3	*3	1.392	1.351	1.246	9.8	10.1	15	15	28.8
	C-4	*3	1.391	1.351	1.242	9.9	10.4	20	15	28.8
2	C-3	*3	1.399	1.354	1.244	10.0	10.8	15	15	27.8
	C-4	*3	1.398	1.352	1.243	10.4	11.3	15	15	27.5
3	C-3	*3	1.395	1.350	1.239	10.3	10.5	15	15	25.5
	C-4	*3	1.395	1.350	1.238	10.7	10.7	25	15	25.2
4	C-3	10	1.403	1.354	1.193	10.0	11.4	15	15	31.3
	C-4	10	1.408	1.356	1.193	10.5	11.7	15	15	31.7
6	C-3	10	1.348	1.349	1.182	10.3	10.6	25	15	26.1
	C-4	10	1.399	1.350	1.182	10.7	10.7	34	15	26.2
8	C-3	10	1.389	1.341	1.169	10.4	11.1	28	15	22.6
	C-4	10	1.391	1.342	1.169	10.7	11.2	33	15	22.8
10	C-3	*3	1.395	1.360	1.231	11.1	11.7	43	15	22.2
	C-4	*3	1.395	1.358	1.231	11.0	11.5	35	15	21.4
12	C-3	10	1.401	1.352	1.178	11.1	11.3	40	15	25.2
	C-4	10	1.398	1.350	1.171	11.5	11.9	37	15	24.2
14	C-3	10	1.415	1.375	1.161	12.6	12.4	35	15	23.6
	C-4	10	1.410	1.371	1.162	12.4	11.9	40	15	21.3
16	C-3	*3	1.416	1.362	-----	11.7	12.0	40	15	23.1
	C-4	*3	1.417	1.359	-----	12.6	14.4	36	15	22.1

NOTES:

1. Polypropylene separator (FT2140)
2. 80% fill level - 113cc (30% KOH)
3. Four negative plates
4. Three positive plates
5. Tabs - 1/4" wide nickel, resistance welded to plate and current collector
6. Weight: C-3 = 1158 grams, C-4 = 1153 grams
7. Charging current is 3 amperes for 16 hours
8. Discharge to 1.00 volts
9. * indicates constant current discharge

and debugging the new test consoles with high constant current capability.

Cells C-5 and C-6 were manufactured using polypropylene separator and glass seals. After several characterization cycles these cells will be heat sterilized and testing resumed.

Cells C-7 and C-8 contain polyamide separator and will be used as standard cells and cycled.

Cylindrical Cell Summary

Cells have been built using both nylon and polypropylene separators. In general, the cells are functioning as designed. There are indications of capacity variations during cycling for cells containing both types of separators and this is believed to be an effect of cell geometry and/or electrolyte level. Since cells containing both types of separators exhibit this characteristic and since the negative to positive ratio in cylindrical cells is high (165:100) the decreasing capacity presently exhibited is not considered a chemistry effect. The cell geometry and its effect on electrolyte distribution is most suspect. Cells containing polypropylene separator have not yet been sterilized.

The electrochemical and physical parameters of the cells are generally similar but differ somewhat from the prismatic cells. ECV is lower and resistance is higher for cylindricals. The lowered ECV can be caused by a rapid oxygen recombination and/or heat generated by the higher internal impedence.

The higher resistance exhibited by the cylindrical cells is believed to be caused by the tab size and arrangement used for these initial samples. Other cells are being fabricated using different tab arrangements designed to reduce this effect. The cylindrical cells tested to date had an out-of-round core which is subjected to non-uniform compression within the cell. This was corrected by altering the design of the spindle used for core manufacture.

Therefore progress to date includes design and use of a revised mandrel which allows the cell core to be rolled cylindrically (.030" TIR) as opposed to the out-of-round shape obtained previously. Also, tab size and position were designed such that positive and negative tabs can be resistance welded in a similar manner as in prismatic cells. The only delay envisioned in this phase is the manufacture of acceptable seals (crimped polymeric seals are planned).

C. Impact Test Support

Activity this quarter dealt with compiling and preparing for analysis pre-impact, impact and post-impact testing of cylindrical cells. In addition, prismatic cells were subjected to the impact levels at cell orientations previously discussed. These data are also being reduced for analysis. The data summarized to date are shown in TABLE II-9. As yet these data have not been correlated with the x-rays and other information generated during the impact test. Several of these cells are undergoing continued cycling after impact. It is planned to have all these data fully analyzed by the end of the next quarter. The test plan being followed is outlined in TABLE II-10.

Cell No	Cell Capacity (AH) Before Impact	After Impact	diff.	EOCR (mΩ) Before Impact	After Impact	diff.	EODR (mΩ) Before Impact	After Impact	diff.	Cell Orientation	g Calc	g Meas.
P/N 0055 00 - Long Sub-C												
5	2.551	-----	-2.551	7.4	----	-----	7.8	*12.5	+ 4.7	+y	4070	3600
9	2.491	2.320	-0.171	7.6	12.5	+ 4.9	8.2	*10.5	+ 2.3	--	----	----
12	2.510	2.340	-0.170	8.0	7.3	- 0.7	8.5	7.7	- 1.2	z	2520	2000
14	2.560	0.931	-1.629	7.3	9.5	+ 2.2	7.6	15.7	+ 8.1	-y	3130	----
17	2.630	2.240	-0.390	7.8	7.0	- 0.6	8.2	7.4	- 0.8	x	2360	2000
18	2.600	2.240	-0.360	7.9	7.4	- 0.5	8.5	7.8	- 0.7	z	3340	2400
19	2.570	2.471	-0.099	8.2	10.0	+ 1.8	9.2	16.7	+ 7.5	-y	4100	3400
20	2.680	2.431	-0.249	6.1	11.2	+ 5.1	7.1	18.8	+11.7	-y	2300	2500
21	2.671	2.080	-0.591	7.6	9.1	+ 1.5	9.2	9.6	+ 0.4	x	4220	3400
22	2.720	2.220	-0.500	8.6	7.5	- 1.1	9.8	7.9	- 1.9	z	4210	3400
23	2.450	2.012	-0.438	7.9	6.1	- 1.8	9.3	6.4	- 2.9	x	3320	3000
P/N 0038 00 - Short Sub-C with Spindle												
24	0.722	0.621	-0.101	6.8	6.0	- 0.8	7.0	6.5	- 0.5	-y	4210	3500
28	0.716	0.589	-0.127	13.0	14.8	+ 1.8	13.2	*15.5	+ 2.3	--	----	----
30	0.709	0.621	-0.088	12.0	7.3	- 4.7	12.0	8.1	- 3.9	-y	3190	2500
31	0.732	0.684	-0.048	12.3	11.6	- 0.7	12.5	*10.7	- 1.8	--	----	----
37	0.706	0.656	-0.050	13.2	14.3	+ 1.1	13.3	*12.0	- 1.3	+y	4220	4700
41	0.684	-----	-0.684	11.1	12.2	+ 1.1	11.5	10.1	- 1.4	x	4420	3750
44	0.703	0.678	-0.025	13.2	12.0	- 1.2	13.4	12.3	- 1.1	x	2510	1900
45	0.719	0.671	-0.048	12.0	11.3	+ 1.3	12.5	11.2	- 1.3	x	4300	3600
46	0.713	0.681	-0.032	12.7	11.3	+ 0.6	12.6	11.4	- 1.2	x	3300	3750
47	0.725	0.608	-0.117	14.2	5.9	- 8.5	14.6	6.6	- 8.0	-y	2370	----
P/N 0062 00 - Short Sub-C w/O Spindle												
51	1.225	0.751	-1.474	12.3	19.0	+ 6.7	13.3	21.9	+ 8.6	x	2580	1800
55	1.175	1.126	-0.049	12.5	20.7	+ 8.2	13.8	*20.0	+ 6.2	+y	4180	3200
57	1.276	1.150	-0.126	11.8	7.0	- 4.8	13.5	7.2	- 6.3	-y	3210	2500
58	1.160	1.100	-0.060	12.3	17.6	+ 5.3	14.1	*17.5	+ 3.4	--	----	----
61	1.240	1.110	-0.130	12.1	6.9	- 5.2	13.8	7.3	- 6.5	-y	4170	----
62	1.255	1.140	-0.115	12.9	7.0	- 5.9	14.7	7.5	- 7.2	-y	2340	2000
65	1.240	1.075	-0.165	12.8	19.0	+ 6.2	13.7	*17.0	+ 3.3	+y	3170	3200
67	1.140	0.713	-0.427	10.0	21.9	-11.9	10.9	24.3	+13.4	x	3360	2500

x axis: ⊥ to longitudinal axis and directed at a tab.
y axis: longitudinal axis, algebraic signs are conventional.
z axis: ⊥ to longitudinal axis, ⊥ to x axis.

* Resistohmeter used.

TABLE II-10

Impact Test Plan

1. Preimpact Testing
   - A. Physical
     1. Determine cell weight
     2. Determine cell dimensions
     3. X-ray cells prior to impact (2 observations 90° apart)
   - B. Electrochemical
     1. Charge cells for 16 hrs. at the c/10 rate
     2. Measure cell end-of-charge voltage
     3. Measure cell end-of-charge resistance
     4. Discharge cells at the c/2 rate to 1.00 volts to determine cell capacity
     5. Determine cell discharge voltage profile
     6. Determine cell end-of-discharge resistance
     7. Repeat for 3 cycles
     8. Charge cells prior to impact

II. Impact Testing
   - A. Select load level
   - B. Select cell orientation (cell axes - 3 for cylindrical - 4 for prismatic
   - C. Measure impact force with accelerometer
   - D. Monitor cell voltage during impact

III. Postimpact Testing
   - A. Discharge cells at the c/2 rate to 1.00 volts to determine cell capacity
   - B. Determine cell discharge voltage profile
   - C. Measure cell end-of-discharge
   - D. X-ray cells (2 observations 90° apart)
   - E. Determine cell weight
   - F. Determine cell dimensions
   - G. Charge cells for 16 hours at the c/10 rate
   - H. Measure cell end-of-charge voltage
   - I. Measure cell end-of-charge resistance
   - J. Discharge cells at c/2 rate to 1.00 volts to determine cell capacity.

D. Heavily Loaded Electrodes

1. Plaque Manufacture - In this run, sinter weight as well as gauge were controlled in order to maintain favorable porosity and pore size distribution. It was expected that by maintaining a favorable pore size distribution, and experimenting with the pore structure produced, a higher electrochemical loading might be obtained.

   TABLE II-11 identifies the plaque produced and the physical attributes obtained.

   Analysis of Results of Plaque Production - In the production of plaque, sufficient material is applied to the screen to produce a certain gauge at a given temperature, while still maintaining constant porosity and pore size.

   If insufficient material is applied, the correct gauge cannot be achieved. If excess material is applied it is possible to achieve the desired gauge, however, total porosity decreases due to compaction of the unsintered plaque material. The plaque produced for these experiments is considered the optimum with respect to the gauge, sinter weight and porosity interrelationship. These data are presented in Figure II-B.

2. Positive Plate Manufacture - Of the plaque identified in TABLE II-11, those lots which are asterisked were selected for impregnation.

   The long holding tabs used on the plates restricted

TABLE II-11

Identification and Physical Attributes of High Gauge Plaque

	Stack #	Gauge inches	Porosity (%)	Sinter wt g/in^2	(1)Volume Utilization (%)	(2)Electrical Resistance (mΩ)
*	170901-1	.0264	84.0	.509	88.2	10.2
*	901-2	.0301	83.6	.606	88.8	8.8
	901-3A	.0327	83.6	.673	89.7	8.9
*	901-3	.0345	83.6	.703	88.4	8.2
*	901-4	.0405	83.3	.852	89.7	7.3
	901-4A	.0447	82.4	.968	87.5	6.7
*	901-7	.0453	83.1	.952	85.3	6.9
	901-6	.0475	81.3	1.093	84.7	6.0
	901-5	.0477	81.8	1.062	85.1	6.5
*	901-4B	.0485	81.6	1.116	87.8	6.1
*	160901-1	.0266	85.3	.499	91.9	11.3
*	901-2	.0307	84.5	.602	91.1	9.1
*	902-1	.0351	84.6	.691	91.4	9.2
*	902-2	.0402	84.0	.824	92.4	8.3
	902-3	.0426	83.4	.905	91.2	7.4
*	902-4	.0490	82.4	1.108	90.8	6.5
	185902-5	.0256	81.4	.563	86.7	7.3
*	902-6	.0268	81.5	.591	87.2	7.5
*	902-7	.0299	80.7	.690	87.2	6.8
*	902-8	.0340	81.2	.784	88.5	6.5
*	902-9	.0368	80.7	.869	87.5	5.7
*	198902-10	.0250	79.6	.590	85.0	6.5
*	902-11	.0296	79.6	.730	84.5	6.1
*	902-12	.0320	79.2	.785	85.4	5.8
*	902-13	.0362	79.2	.905	86.1	5.1
*	902-14	.0398	78.9	.998	84.5	4.6
*	902-15	.0433	78.4	1.121	85.2	4.2

1. Measure of the plaque shrinkage.

2. Across the length of a 3" x 1" strip

Figure II-B

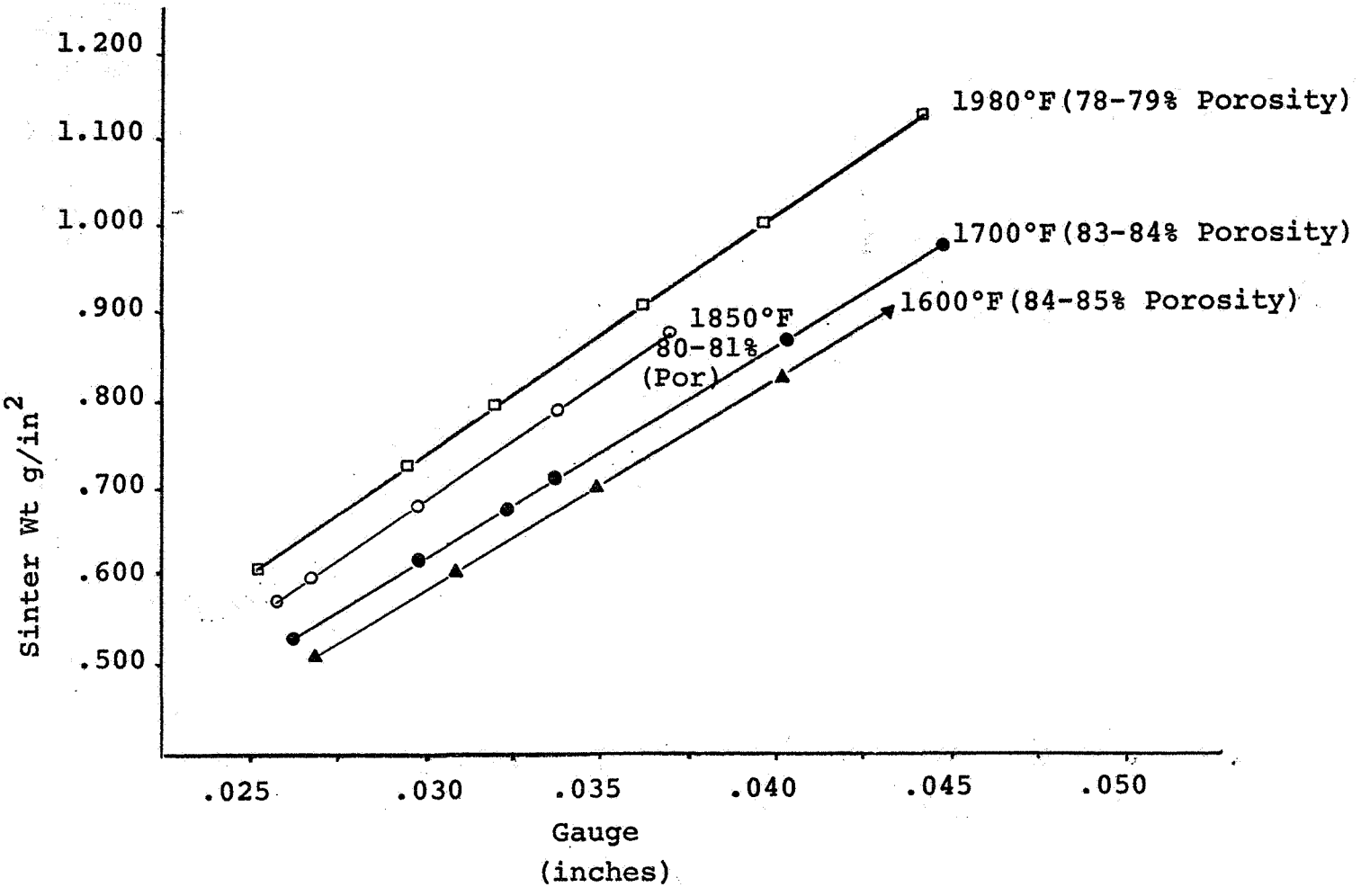

Relationship of Sinter Weight to
Gauge for a Given Porosity

the growth and movement of the plates during impregnation and conversion, resulting in distorted and buckled plates. Many were damaged to such an extent that they were discarded. Due to the malformed condition of the plates from the first positive impregnation run, no formation was performed on these plates. Only analytical data and certain physical attributes were determined and are presented in TABLE II-12.

Using identical plaque material, the impregnation was repeated, this time using shorter holding tabs. Impregnation parameters remained the same except that metal ion concentration was reduced. No problems were experienced, no plate distortion occurred. All plates were available for analysis and subsequent formation. The plates from positive impregnation II were formed, in groups of three. Each three plate group represented a particular plaque type and gauge and a certain impregnation routine. To determine the capacity of the formed plates, the following test cycle was chosen:

Charge - 3 hour rate for 6 hours (100% overcharge)
Discharge - c/2 rate to the knee of the discharge

Flooded capacity data is tabulated in TABLE II-13.

With very few exceptions the electrochemical efficiency of the plates exceeded 90%.

Plates exceeding .035" in gauge warped during formation and cracked under restraint.

Analysis of Positive Impregnation Results - An analysis of the impregnation data, shows a direct relationship

TABLE II-12

Analytical Data High Capacity Positive Impregnation Experiment I

Plate Identification		Act Mat g/in^2	Theor AH/in^2	Theor AH/in^3	Theor AH/g	% Corrosion	Initial Gauge
170	901-3	..968	.281	8.25	.171	37	.0345
		1.263	.366	11.8	.195	43	.0345
	901-4	1.124	.326	8.3	.175	37	.0405
		1.293	.376	9.9	.188	41	.0405
		1.448	.420	11.3	.197	43	.0405
	901-7	1.382	.401	8.9	.183	40	.0453
		1.593	.462	10.0	.195	44	.0453
		1.740	.505	11.5	.202	47	.0453
	901-4B	1.486	.431	9.7	.183	40	.0485
		1.664	.482	10.25	.192	44	.0485
		1.847	.535	11.4	.204	47	.0485
160	902-1	1.028	.298	9.6	.180	40	.0351
	902-2	1.227	.355	8.9	.182	38	.0402
		1.379	.400	10.25	.191	40	.0402
		1.566	.455	12.3	.203	46	.0402
	902-4	1.544	.448	9.35	.184	39	.0490
		1.730	.502	10.5	.195	41	.0490
		1.913	.556	12.0	.203	46	.0490
185	902-6	.747	.217	8.1	.159	33	.0268
		..845	.245	9.1	.168	33	.0268
		.924	.267	9.9	.178	36	.0268
	902-7	.807	.234	7.8	.154	28	.0299
		.926	.269	8.95	.160	31	.0299
		1.020	.295	10.2	.174	34	.0299
	902-8	.936	.271	7.95	.168	31	.0340
		1.053	.305	9.25	.172	34	.0340
		1.159	.333	10.0	.176	34	.0340
	902-6	1.041	.302	8.1	.162	31	.0368
		1.175	.341	9.0	.170	34	.0368
		1.301	.378	10.2	.181	34	.0368
198	902-10	..642	.186	7.5	.143	26	.0250
		.736	.213	8.6	.153	28	.0250
		..820	.238	9.2	.164	30	.0250
	902-11	.769	.223	7.7	.149	26	.0296
		.878	.255	8.8	.160	28	.0296
		.978	.284	9.8	.171	32	.0296
	902-12	.848	.247	7.7	.150	28	.0320
		.964	.279	8.8	.152	31	.0320
		1.054	.305	9.25	.167	31	.0320
	902-13	.939	.254	7.1	.139	27	.0362
		1.048	.304	8.7	.159	30	.0362
		1.164	.338	9.8	.167	31	.0362
	902-14	1.005	.292	7.6	.148	27	.0398
		1.135	.329	8.3	.158	28	.0398
		1.249	.362	9.3	.168	30	.0398
	902-15	1.102	.320	7.6	.150	28	.0433
		1.237	.360	8.4	.159	28	.0433
		1.366	.396	9.4	.168	33	.0433

TABLE II-13

Analytical Data High Capacity Impregnation Experiment II

Plate Identification		Theor AH/in^2	Theor AH/in^3	Theor AH/g	% Corrosion	Initial Gauge	Flooded Cap AH/in^2	% Effic.	Flooded Cap AH/in^3
170	901-1	.206	7.9	.165	36	.0264	.195	95	7.5
		.228	8.8	.177	40		.217	95	8.4
		.243	9.3	.182	44		.229	94	8.7
	901-2	.241	8.4	.169	40	.0301	.232	96	8.1
		.273	9.4	.185	45		.260	95	8.9
		.284	9.8	.188	46		.280	98	9.6
	901-3	.285	9.2	.179	44	.0345	.269	94	8.7
		.326	10.7	.191	48		.322	99	10.6
		.353	11.6	.199	53		.316	90	10.4
	901-4	.342	9.0	.185	45	.0405	.340	99	8.9
		.385	10.1	.197	50		.370	96	9.7
		.406	10.6	.202	53		.390	96	10.2
	901-7	.398	9.1	.187	46	.0453	.399	100	9.1
		.456	10.4	.202	53		.439	96	10.0
		.472	10.7	.204	54		.468	99	10.6
	901-4B	.425	9.1	.188	42	.0485	.409	96	8.7
		.486	10.4	.200	52		.448	92	9.6
		.507	10.8	.202	53		.480	95	10.3
160	901-1	.215	8.3	.176	47	.0266	.211	98	8.1
		.241	9.4	.187	50		.233	97	9.1
		.253	9.9	.192	52		.255	100	9.9
	901-2	.272	9.7	.186	48	.0307	.252	93	9.0
		.307	11.0	.198	52		.276	90	10.9
		.320	11.4	.202	56		.285	89	10.1
	902-1	.316	9.7	.190	47	.0351	.277	88	8.5
		.358	11.0	.202	54		.322	90	10.9
		.377	11.6	.204	56		.350	93	10.8
	902-2	.359	9.6	.189	45	.0402	.284	79	7.6
		.408	10.9	.202	52		.350	86	9.4
		.431	11.5	.208	55		.358	83	9.5
	902-4	.444	8.8	.188	44	.0409	.418	94	8.3
		.500	10.2	.200	49		.434	87	8.9
		.523	10.7	.202	52		.490	94	10.1
185	902-6	.211	7.6	.159	34	.0268	.197	94	7.1
		.232	8.4	.167	36		.213	92	7.7
		.251	9.2	.176	40		.250	99	9.1
	902-7	.239	7.9	.162	38	.0299	.236	99	7.8
		.265	8.7	.172	42		.246	93	8.1
		.289	9.5	.179	43		.264	88	8.4
	902-8	.269	7.7	.163	35	.0340	.256	95	7.3
		.308	8.8	.176	40		.284	92	8.1
		.326	9.3	.183	43		.323	99	9.2
	902-9	.306	8.1	.168	38	.0368	.285	93	7.5
		.341	9.0	.180	45		.330	97	8.7
		.361	9.5	.202	46		.344	95	9.0
198	902-10	.175	6.9	.142	30	.0250	.173	99	6.8
		.198	7.6	.152	33		.192	97	7.4
		.211	8.1	.159	34		.204	97	7.9

To be continued

TABLE II-13

(continuation)

Plate Identification	Theor AH/in^2	Theor AH/in^3	Theor AH/g	% Corrosion	Initial Gauge	Flooded Cap AH/in^2	% Effic.	Flooded Cap AH/in^3
198 902-11	.209	6.8	.147	33	.0296	.205	98	6.7
	.234	7.7	.156	33		.232	99	7.6
	.259	8.5	.167	36		.240	93	7.9
902-12	.249	7.5	.156	33	.0320	.240	96	7.2
	.276	8.3	.164	34		.252	91	7.6
	.301	9.2	.174	40		.289	96	8.8
902-13	.273	7.3	.152	32	.0362	.269	99	7.2
	.308	8.3	.165	37		.288	92	7.6
	.337	9.0	.176	41		.314	93	8.4
902-14	.296	7.3	.154	32	.0398	.274	92	6.7
	.332	8.3	.163	34		.320	96	8.0
	.363	8.9	.174	38		.333	92	8.2
902-15	.333	7.6	.157	34	.0433	.308	93	7.1
	.374	8.5	.168	36		.340	91	7.7
	.394	8.8	.171	37		.367	93	8.2

of gauge to weight of active material introduced into the pore structure by impregnation and conversion.

Since the relationship is a linear function, it is a useful mechanism for anticipating the chemical loading during impregnation or for determining the process parameter changes required to produce a certain plate loading and/or for determining the plaque attributes required to achieve a certain plate loading.

The relationship of active material to gauge for various types of plaque material is illustrated in Figures II-C, II-D, II-E and II-F.

The same relationship exists with respect to flooded delivered capacity vs gauge.

From the data accumulated, the following facts are evident concerning corrosion of the plaque during the impregnation process.

1. More corrosion occurs with low temperature sintered plaque.
2. Corrosion increases with the number of impregnation cycles.
3. The higher the gauge the more corrosion.

Figure II-F exhibits corrosion of plaque produced at various sintering temperatures, during 3, 4 and 5 cycles of positive impregnation.

Figure II- C

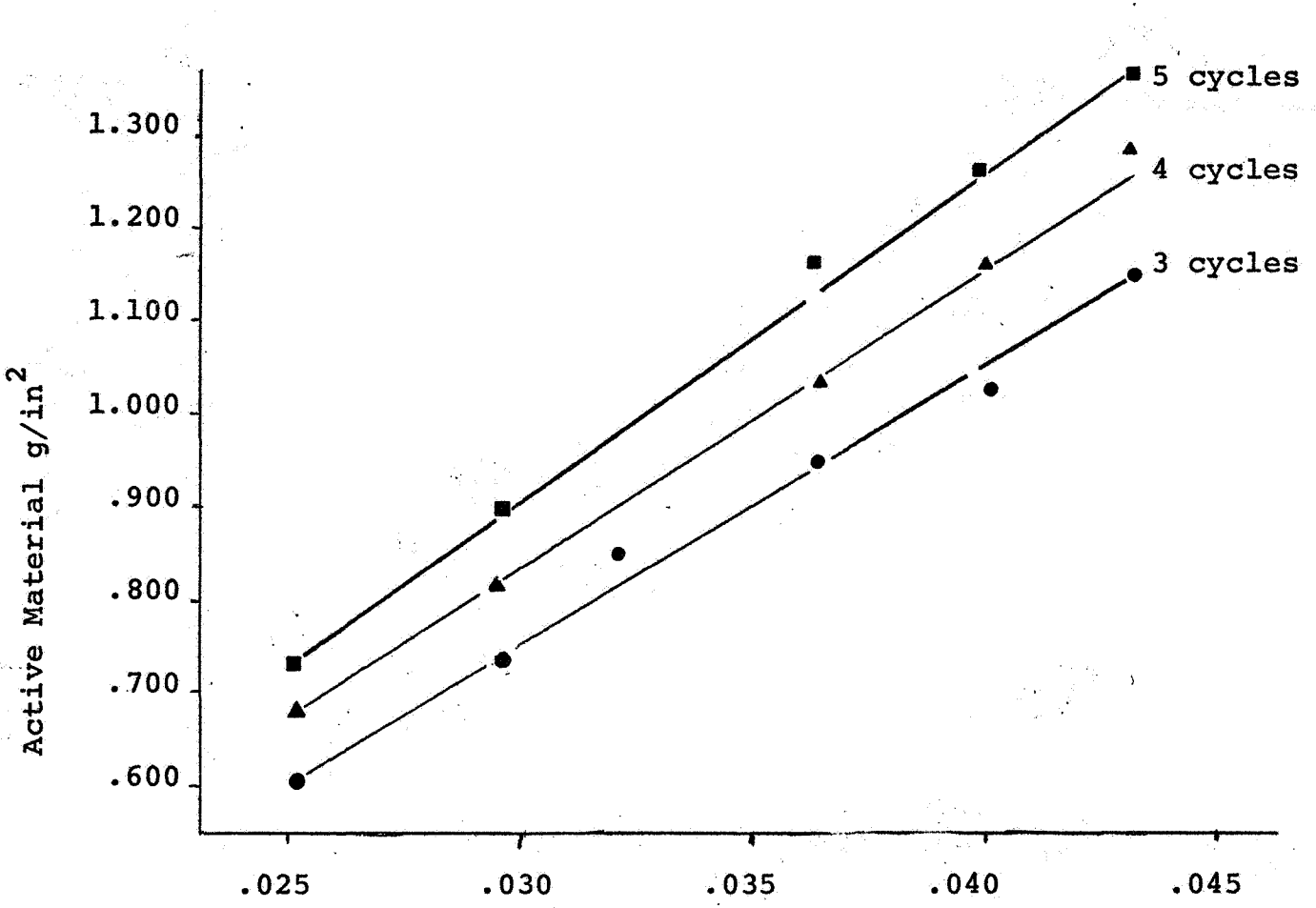

1980°F Sinter (78-79% Porosity)

Positive Impregnation

Figure II-D

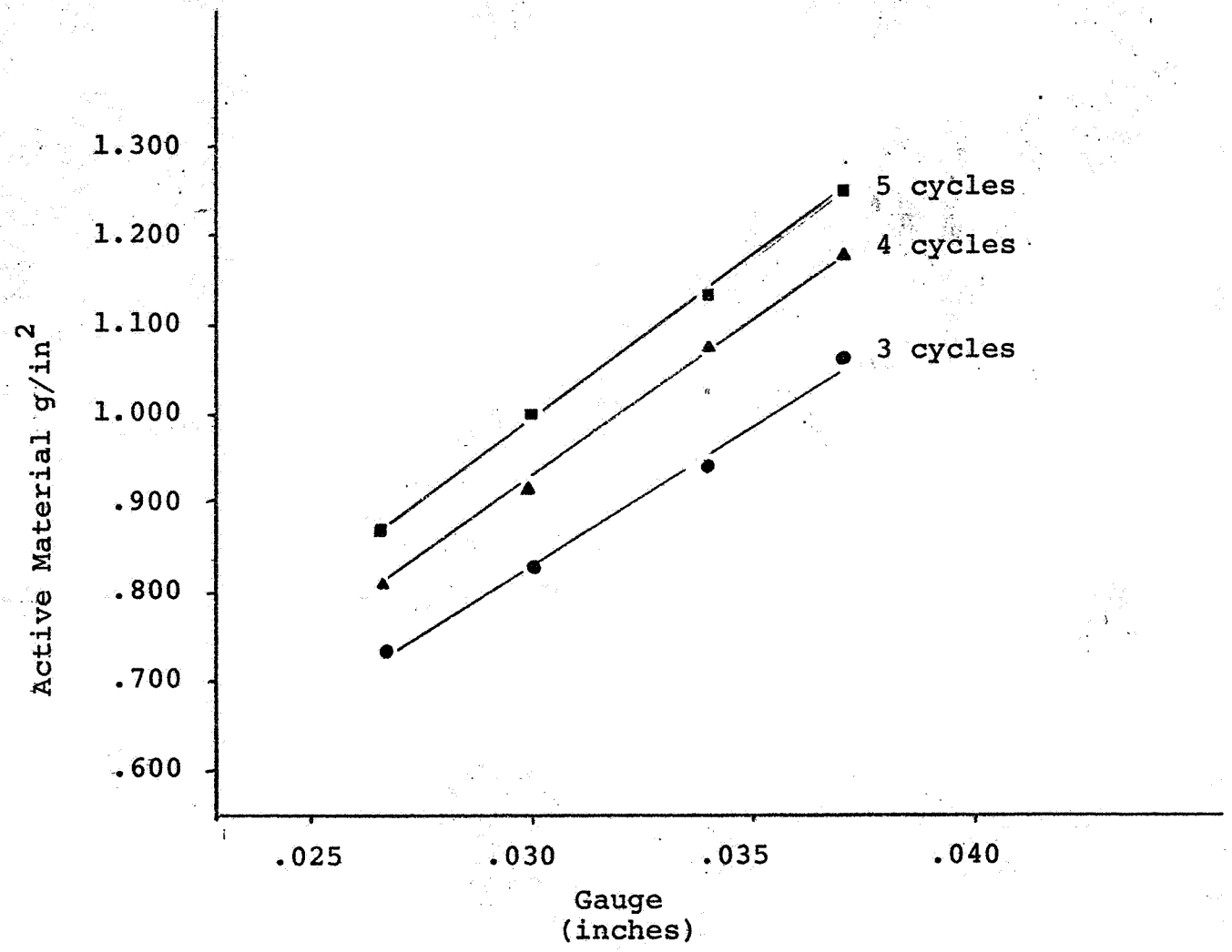

1850°F Sinter (80-81% Porosity)

Positive Impregnation

Figure II-E

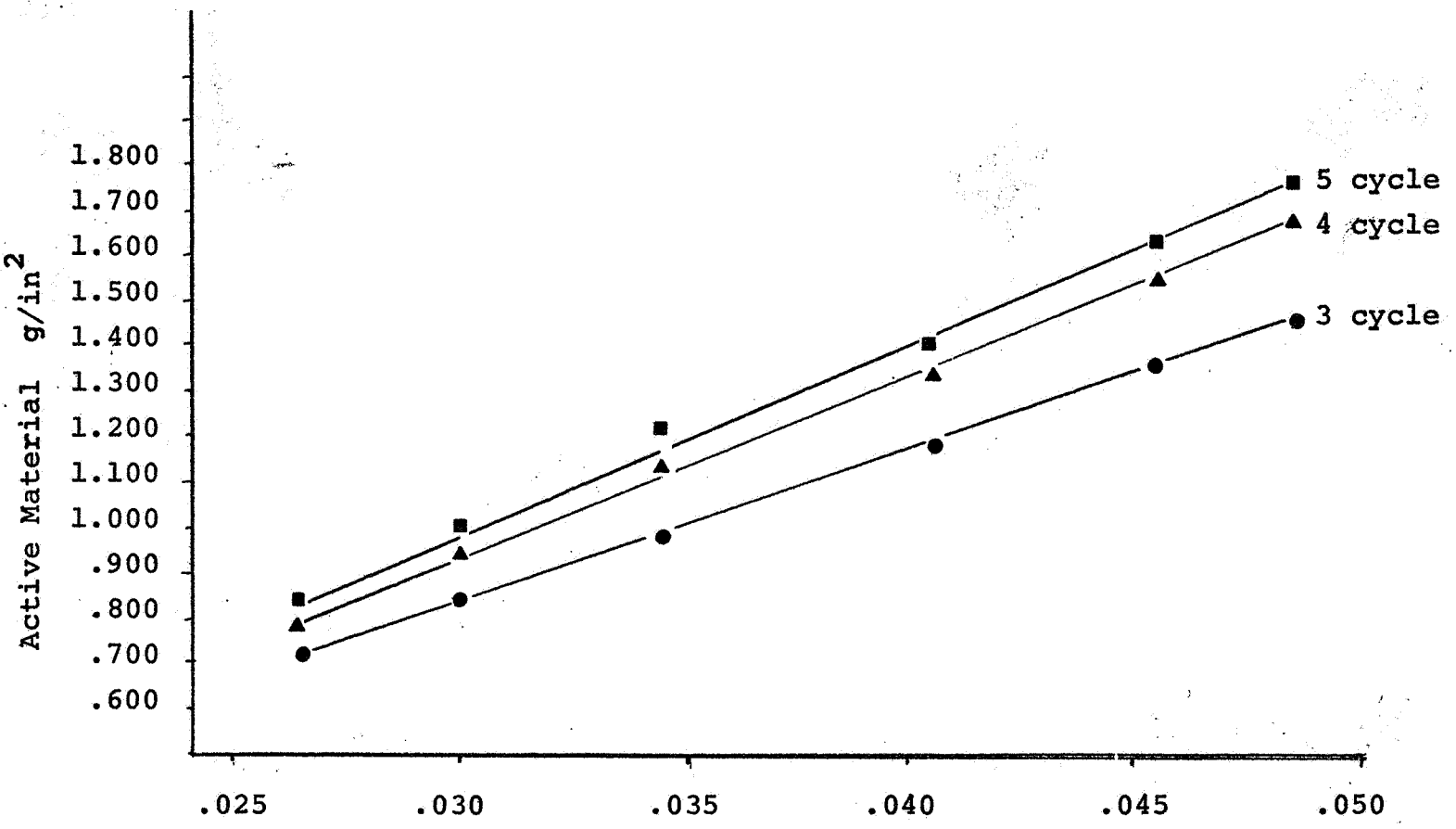

1700°F Sinter (83-84% Porosity)

Positive Impregnation

Figure II-F

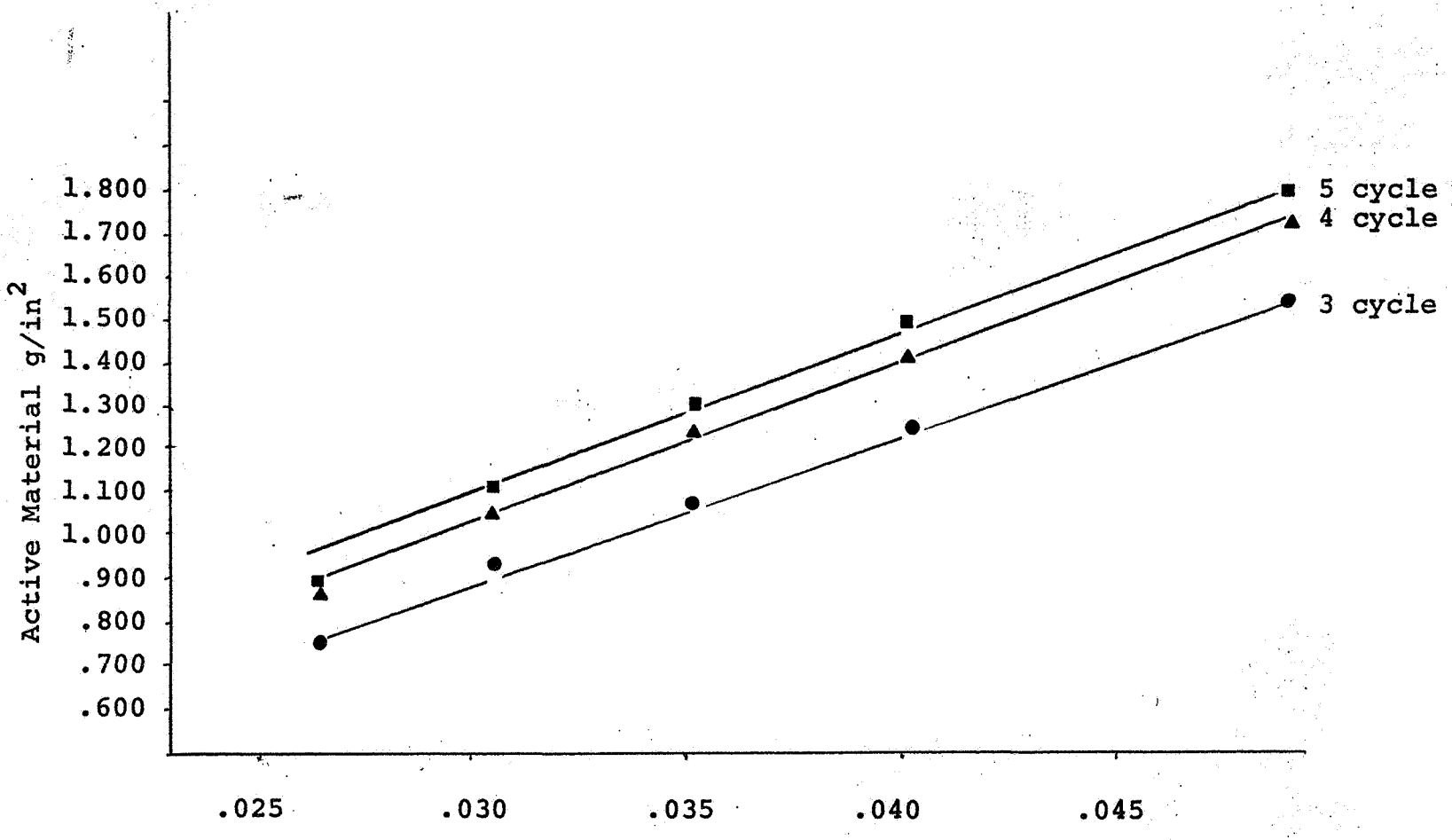

1600°F Sinter (84-85% Porosity)

Positive Impregnation

3. Negative Plate Manufacture - In order to provide matching negative plate for the high capacity positive previously impregnated, high capacity negative plates were impregnated. The plaque used for this impregnation was identical to that used for the high capacity positive. Three sample plates from each plaque lot were removed from the impregnation and analyzed prior to formation. The appearance of all the plates after impregnation was excellent. No distortion, shedding or cracking was apparent.

TABLE II-14 lists the analytical data for the high capacity negative impregnation load.

The plates from the negative impregnation were formed in groups of three. Each group represented a given plaque type, plaque gauge and impregnation routine. Plate capacities were determined in the flooded condition based on the following cycle:

Charge: c/3 rate for 6 hours (100% overcharge)
Discharge: c/2 rate to the knee of the discharge

where c is the capacity of the plates based on chemical analysis. These data are presented in TABLE II-14

Analysis of Negative Impregnation Results - Unlike the positive impregnation, the negative data does not exhibit the straight line relationship between gauge and active material pickup. The straight line relationship shown in Figure II-G exists up to a gauge of .035". At gauges greater than .035" there is a tapering off of active material pick up.

This phenomenon might be attributed to any or a combination of the following:

TABLE II-14

High Capacity Negative Theoretical and Flooded Capacity Data

Plate Ident.	No. of Impreg Cycles	Theor Cap AH/in^2	Flooded Cap AH/in^2	% Efficiency	Init. Gauge
1700 901-1	4	.384	.235	61	.0264
	5	.407	.256	63	
	6	.443	.261	59	
901-2	4	.430	.276	64	.0301
	5	.457	.284	62	
	6	.492	.290	59	
901-3	4	.464	.247	53	.0340
	5	.500	.278	56	
	6	.601	.304	51	
901-4	4	.484	.275	57	.0405
	5	.532	.291	55	
	6	.594	.318	53	
901-7	4	.511	.287	56	.0453
	5	.567	.292	52	
	6	.604	.327	54	
901-4B	4	.555	.287	52	.0485
	5	.606	.293	48	
1600 901-1	4	.409	.256	63	.0266
	5	.429	.274	64	
	6	.470	.282	60	
901-2	4	.448	.281	63	.0307
	5	.484	.290	60	
	6	.531	.313	59	
902-1	4	.458	.249	54	.0351
	5	.507	.268	53	
	6	.565	.291	52	
902-2	4	.499	.253	51	.0402
	5	.533	.268	50	
	6	.596	.299	50	
902-4	4	.580	.284	49	.0490
	5	.626	.300	48	
	6	.638	.326	51	
1850 902-6	4	.381	.235	62	.0268
	5	.403	.239	59	
	6	.455	.264	58	
902-7	4	.417	.245	59	.0299
	5	.441	.248	56	
	6	.492	.278	57	
902-8	4	.451	.258	57	.0340
	5	.480	.263	55	
	6	.528	.287	54	
902-9	4	.484	.268	55	.0368
	5	.518	.275	53	
	6	.552	.290	53	
1980 902-10	4	.337	.211	63	.0250
	5	.371	.212	57	
	6	.396	.238	60	
902-11	4	.396	.235	59	.0296
	5	.420	.263	63	
	6	.459	.272	59	
902-12	4	.427	.251	59	.0320
	5	.454	.265	58	
	6	.497	.268	54	
902-13	4	.443	.244	55	.0362
	5	.477	.302	63	
	6	.523	.310	59	
902-14	4	.472	.287	61	.0398
	5	.504	.302	60	
	6	.545	.328	60	
902-15	4	.485	.260	54	.0433
	5	.530	.274	52	
	6	.579	.308	53	

Figure II-G

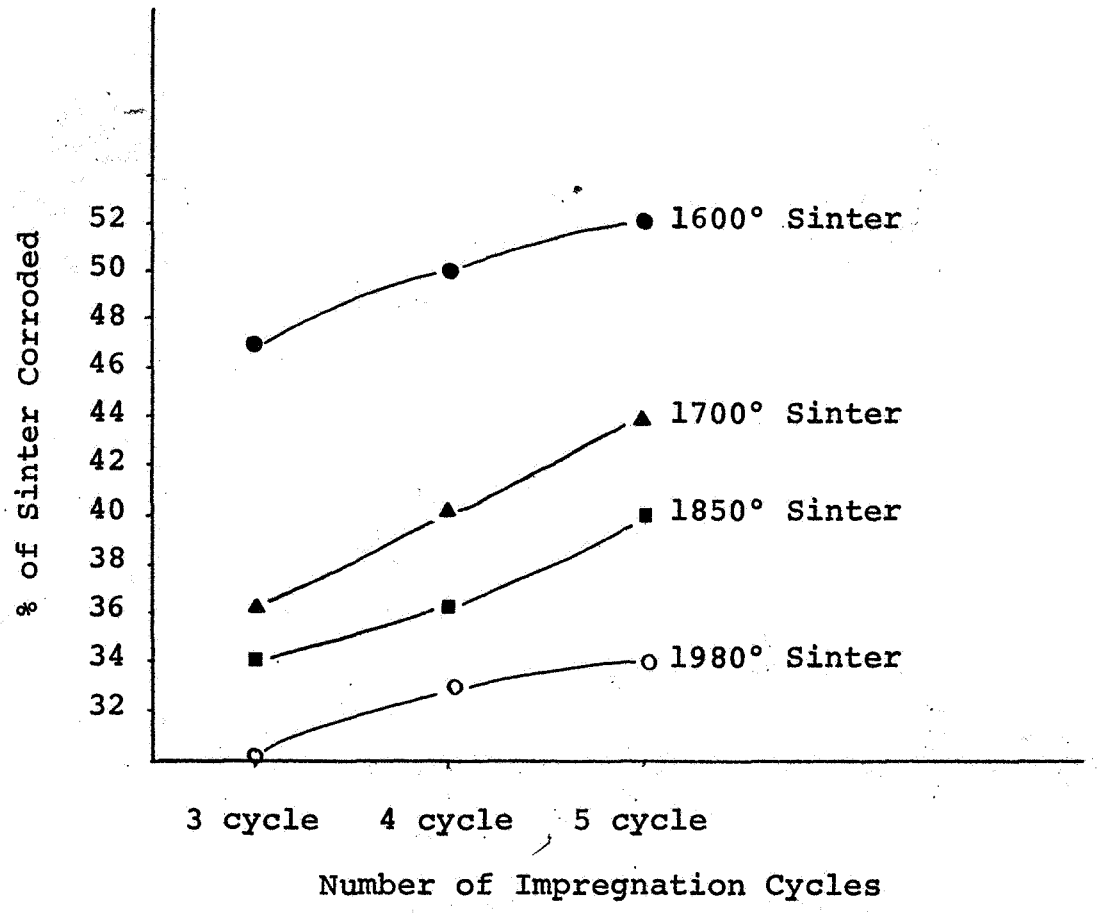

Typical Corrosion of Positive Impregnated Plaque

Produced at Various Sintering Temperatures

1. Higher gauge plates require more rinsing to effectively remove residual caustic from previous impregnation and conversion cycles.
2. Higher gauge plates require longer conversion time.
3. Higher gauge plates require more nitrate diffusion cycles to give efficient loading.

Work is planned to optimize impregnation parameters for high gauge negative impregnation.

SEVENTH QTR JPL REPORT

January - March 1969

III. IMPACT TESTING SECTION

J. Gondusky

A. Development of a High-Impact Test Facility (16 Figures)

B. Testing of Existing Ni-Cd Cells (No Figures)

C. Testing of Seals for Ni-Cd Cells (Flow Chart)

D. Testing of Battery Electrodes (3 Figures)

LIST OF FIGURES

DEVELOPMENT OF A HIGH-IMPACT TEST FACILITY

1. Introduction

In support of the unmanned exploration of the planets, the Jet Propulsion Laboratory has been actively interested in the development of electronic equipment capable of hard landing survival since 1959. Of immediate concern, is the development of a battery power supply required for a proposed hard landing on Mars in 1973. Based upon entry conditions calculated from information about the gravitational and atmospheric conditions on Mars, a design goal has been selected by JPL for all equipment aboard this hard landing capsule. At present, a shock level of approximately 4000 g (square pulse for 1 msec) from an impact velocity of 120 ft/sec is anticipated as the kind of environment to which capsule components will be subjected. Texas Instruments, as a major supplier of heat-sterilizable Ni-Cd space batteries, has long been interested in the cell's resistance to shock and vibration environments. During 1969, nearly 200 high-capacity cells (25AH) capable of impact resistance will be manufactured for evaluation. Under the same contract with JPL, development work concerned with prime cell components will be continued to further extend the knowledge required for high-impact cell design. In order to carry out this development work and the evaluation of complete cells, it is necessary to simulate the anticipated shock environment. The scope of this report is to describe in detail the existing impact facility at Texas Instruments. We wish to describe the development and resultant capabilities at our disposal.

2. Mechanical Design of Testing Equipment

a. General Description:

In the design of the test facility, prime concern was given to the means of achievement of the specified shock pulse (the desired shape, magnitude and length).

Secondary concerns were the great number of cell configurations (shapes and sizes) that must be accommodated. Finally, a

facility with enough versatility to permit the variation of the shock pulse was needed for a complete study of the dynamic response of components. The testing method selected to meet these demands consists of the following arrangement: The specimen is mounted within a sliding carriage by means of adjustable fixturing. Carriage and specimen are then accelerated to the desired velocity. The sliding carriage is finally impacted against an expendable target and massive anvil to produce the desired shock pulse. The overall system is shown in Figure 1.

b. HYGE Gun:

The accelerating "gun" is shown at the extreme left of Figure 1 along with its pressure supply and control module. The accelerator is a commercial unit produced by the Consolidated Electro-dynamics Corp. and called a HYGE gun. It is essentially a pneumatic cylinder with the piston operated by a pressure differential. The unit is shown diagrammatically in Figure 2. The gun used at present has a 6" dia. bore with a piston area ratio of 5.2:1 and compressed N_2 is the operating fluid. Because of the difference in available area of the top and bottom of the piston, it is possible to pressurize the lower load chamber up to 5.2 times as high as the upper set chamber. Thus with approximately 2000 psi N_2 supply this unit is rated at 40,000# thrust and capable of accelerating a 40# mass to a velocity of 125 ft/sec. in order to gain more complete firing control than provided by automatic unbalance of equilibrium, we have added an auxiliary firing valve. In operation, the desired set pressure is first placed in the upper chamber and the desired load pressure is placed in the lower chamber. The actuation is then manually accomplished by pressurizing the small volume between the acceleration orifice seal and the piston seal, thus lifting the piston slightly and the acceleration seal is opened. At this moment, the load pressure can act over the entire area of the piston overcoming the set pressure on the opposite side of the piston.

It is this pressure differential (ΔP) that produces the desired thrust and the resultant carriage velocity of interest. A preliminary calibration curve was constructed during system development runs and is shown in Figure 3. Repeatability of $\pm$ 1 ft/sec is attainable on a given sequence of testing using the manual firing valve. Larger initial variations ($\pm$ 5 ft/sec) from the desired value will occur if carriage mass or rail lubrication is changed by a considerable amount.

c. Carriage & Specimen:

The sliding carriage mass is approximately 32.5# as shown complete in Figure 4. The structural detail of the carriage is more clearly illustrated in Figure 5. All structural members were machined from 7075-T651 aluminum alloy plate. The carriage itself sustains repeated central impacts during acceleration and more importantly at impact. Of prime interest is the versatile fixture arrangement shown. We are thus able to accommodate various cell configurations and sizes in any orientation. Changes between tests involve very little time and insure a more rapid evaluation of particular cells or components. Potting material has been unnecessary with the obvious exception of impact at the terminal end of a cell. This insures a true evaluation of the cell in the absence of most shock attenuating material. A typical fixturing arrangement is included in Figure 5 and indicates the lack of external reinforcement and attenuating material afforded by this adjustable fixturing. The impact end of the carriage is fitted with a hardened steel (M2) impact tool. This tool is shown in detail in Figure 6. Several penetrater diameters have been ground and this design has proved quite satisfactory in resisting the repeated impact energy of over 7000 ft-lbs. As will be shown, the tool diameter is the prime variable affecting the g-Level attained at impact and the ability to change this tool readily is of great convenience.

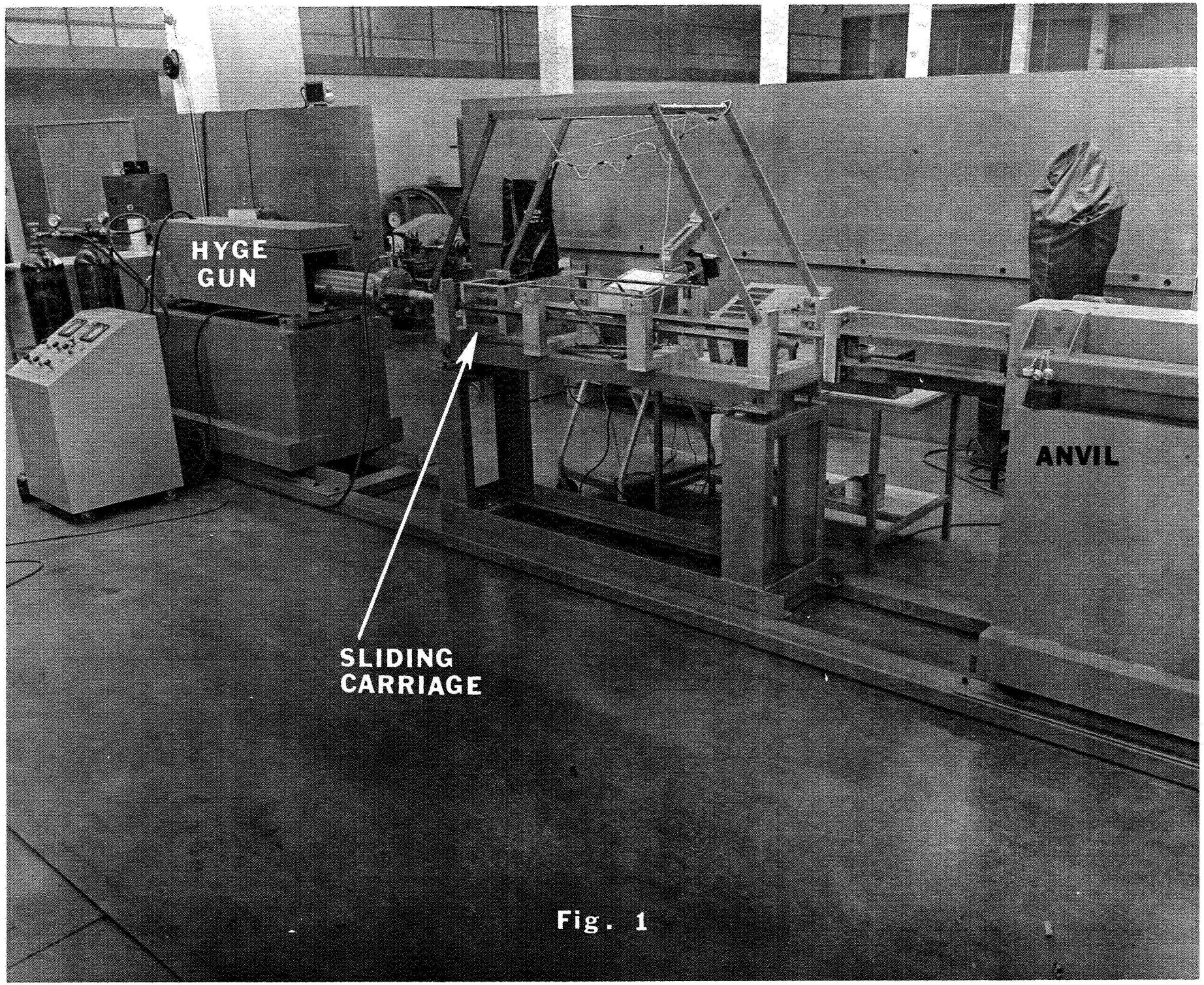

Fig. 1

Fig. 2

ACCELERATION GUN

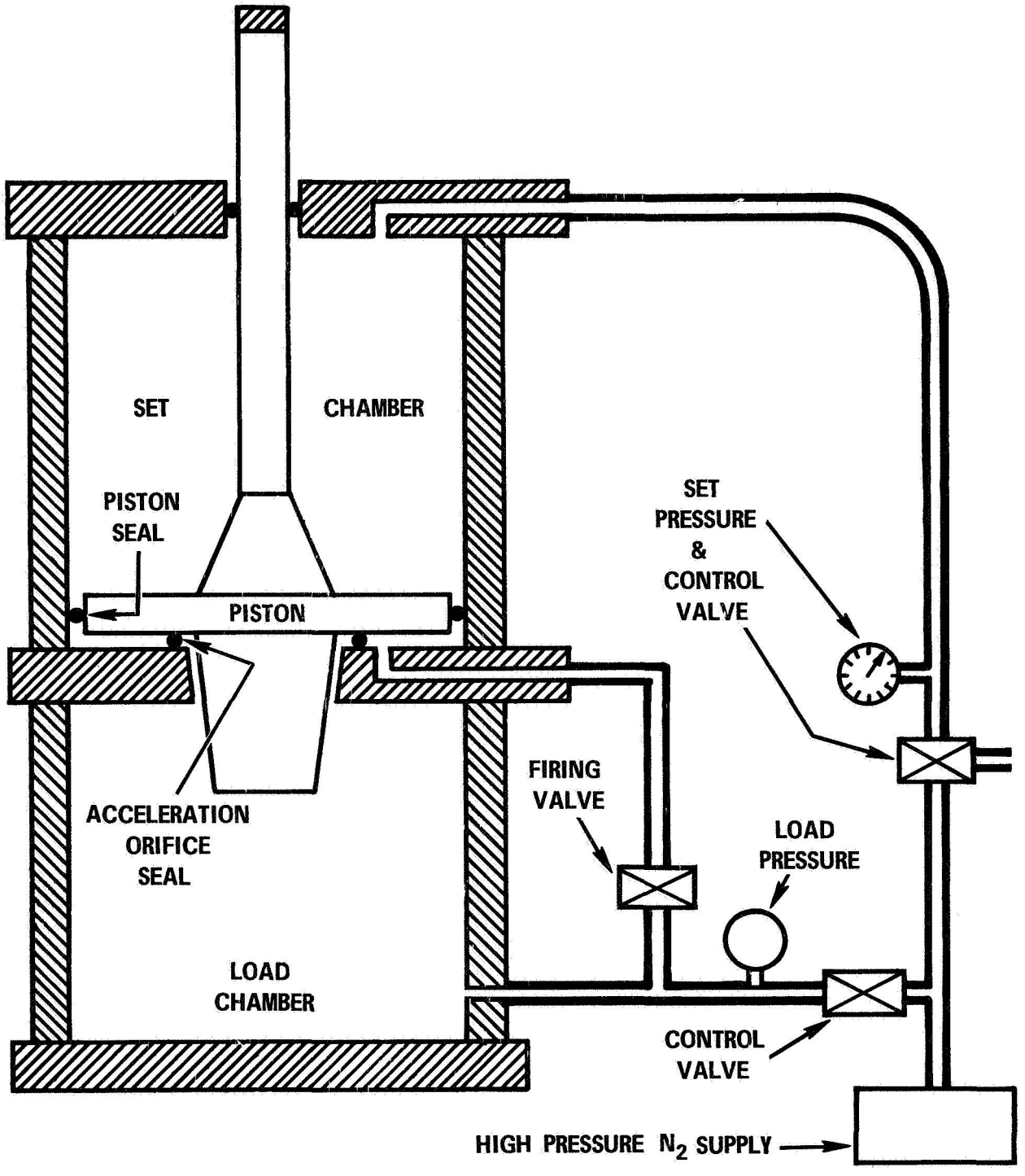

d. Anvil:

The anvil, against which the sliding carriage impacts, is shown on the extreme right of Figure 1. It is basically a 2000# block of steel mounted on a steel framework that is free to roll on tracks. At full impact conditions, the entire mass (approx. 2500#) will move 2-3 inches while shock absorbers arrest its motion and return it to the original position. A structural steel extension is fastened to the main anvil block and serves to position the main copper target block. Figure 7 shows a copper block in position at the impact end of the rail system. This copper block is our means of achieving the desired uniform deceleration of the carriage mass as we plastically deform the copper. Typically, the target is annealed copper (#110) 3" x 3" x 1-1/2" thick. The block is positioned by a single machine screw and lead insert thus permitting a flush mount against the steel backing plate yet very little reinforcement. The material flow is illustrated in Figure 8 which shows the deformation pattern created by the 1" dia. tool during an impact of 4670 g from 123 ft/sec.

3. Instrumentation System

a. General Description:

In order to fully evaluate a cell during shock environments, it is desirable to monitor the cell's voltage during impact along with the velocity at impact and an acceleration-time history for a full description of the event. The overall instrumentation system is shown in Figure 9. The carriage is shown in firing position and is accelerated to the desired velocity in approximately 2 feet. After approximately 4 feet of free travel, impact occurs and the carriage is stopped in approximately 5/8 inch. If rebound occurs, the carriage is arrested by the mechanical brake shown in the center section to prevent damage to the extended hyge ram. The aquisition

FIG. 3

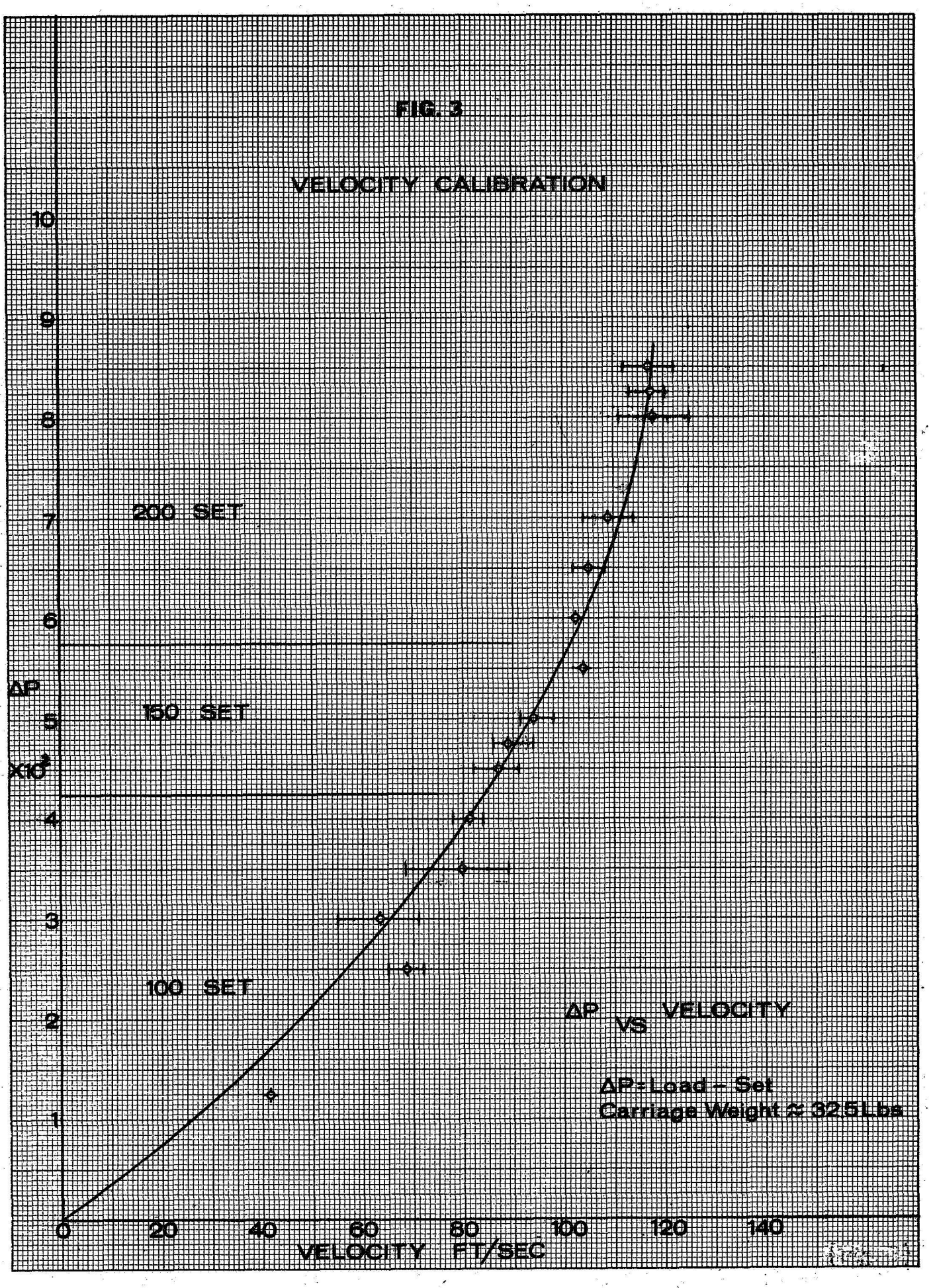
VELOCITY CALIBRATION
10
9
8
7
6
5
4
3
2
1
0
ΔP
X10²
200 SET
150 SET
100 SET
20
40
60
80
100
120
140
VELOCITY FT/SEC
ΔP VS VELOCITY
ΔP=Load - Set
Carriage Weight ≈ 325Lbs

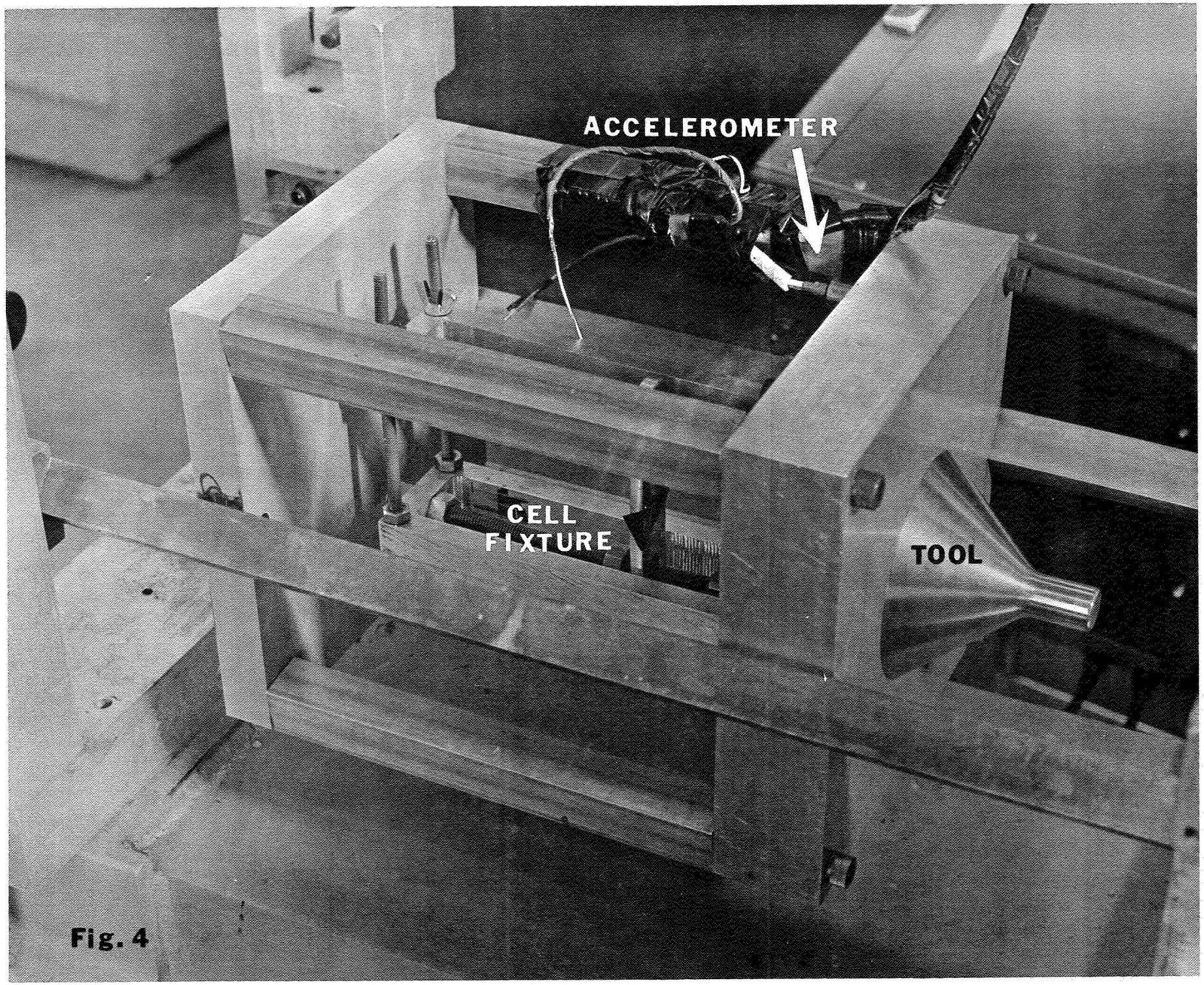

Fig. 4

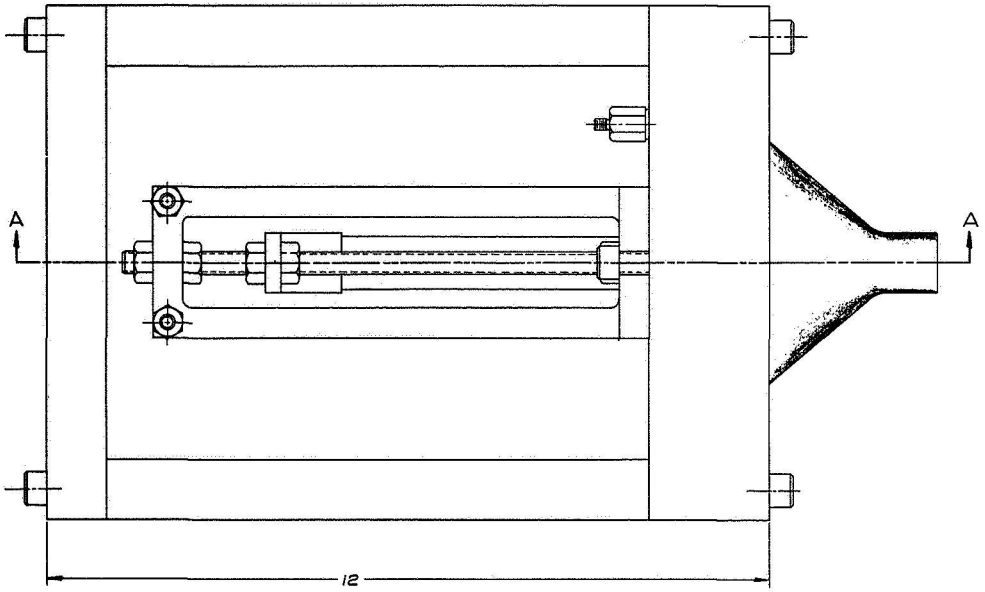

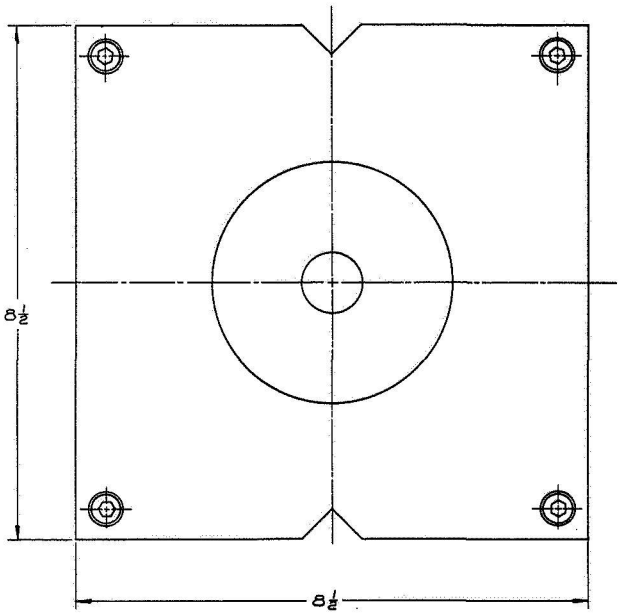

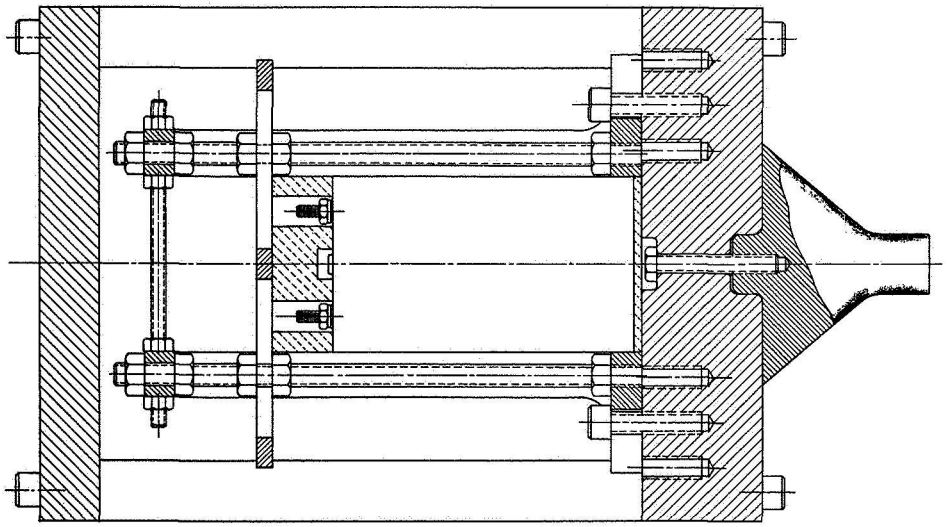

SECTION THRU A-A

Fig. 5

PART NO.	NO. REQD	DESCRIPTION	
TITLE: HIGH IMPACT TEST FIXTURE REF: J.P.L.		METALS & CONTROLS INC. 34 FOREST ST., ATTLEBORO, MASSACHUSETTS 02703 A CORPORATE DIVISION OF TEXAS INSTRUMENTS INCORPORATED	
		DRAWN: W.WALAS 2-6-69	CHKD: DATE:
APPD. DATE	APPD. DATE	SCALE: FULL	DWG. NO.: D SK0008 00 SHEET

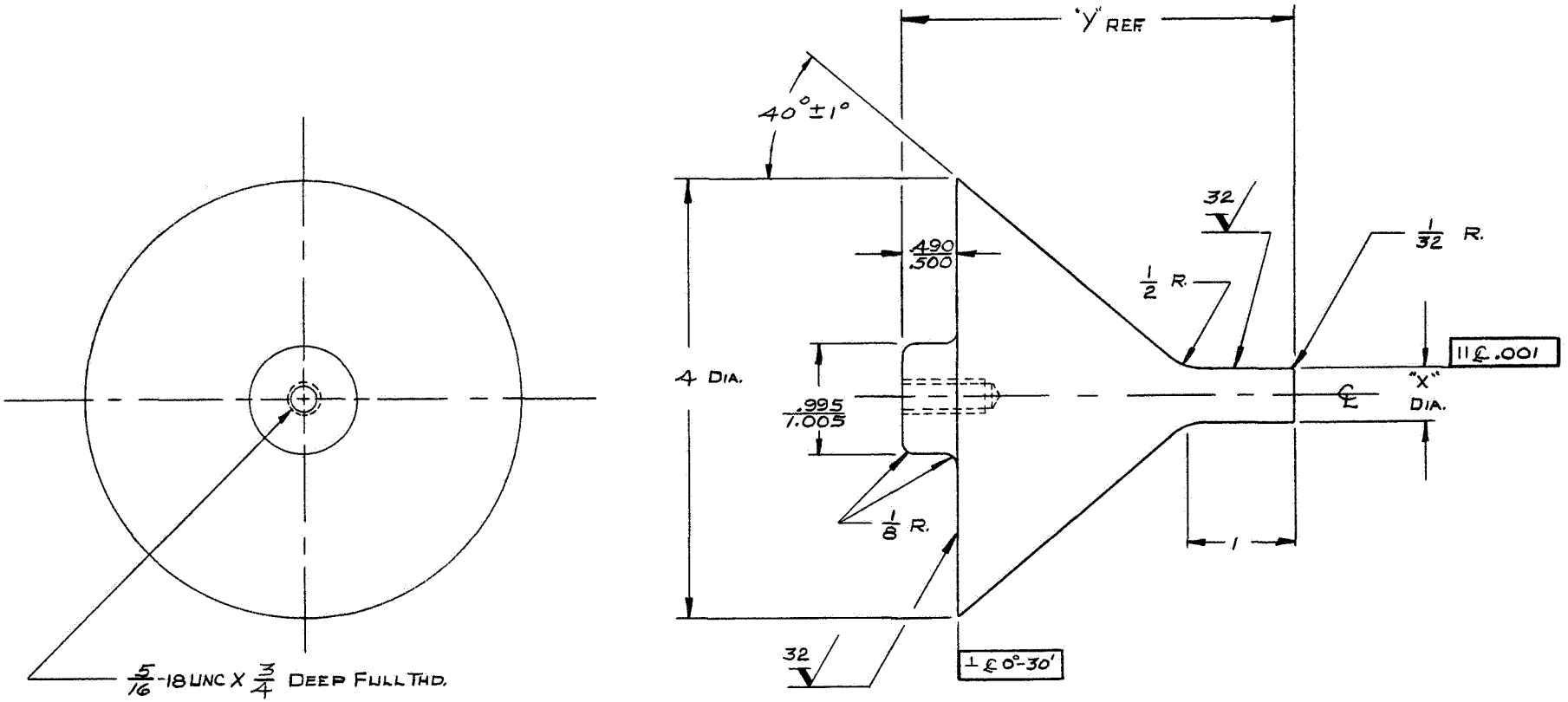

NO.	"X" DIA.	"Y" LENGTH (REF.)
	1.000	3 9/32
	.875	3 3/8
	.750	3 7/16
	.625	3 1/2
	.500	3 9/16
	.375	3 5/8

NOTES:

1. MATERIAL IS M2 STEEL
2. TOLERANCES UNLESS OTHERWISE SPECIFIED ±.010

Fig. 6

PART NO.	NO. REQD	DESCRIPTION

TITLE: IMPACT TOOL

METALS & CONTROLS INC.
34 FOREST ST. • ATTLEBORO, MASSACHUSETTS 02703
A CORPORATE DIVISION OF
TEXAS INSTRUMENTS
INCORPORATED

DRAWN	DATE	CH'KD	DATE
R.J.B.	1-30-69		

APPD.	DATE	APPD.	DATE	SCALE		DWG. NO.	SHEET
				FULL	B	SK 0008 01	

S-G-10116 8/67

of data from a projectile experiencing this kind of motion is not straightforward. The lead wire arrangement shown is the culmination of several unsuccessful attempts to compensate the inertia loads involved. Most satisfactory is this combination of high strength steel slide-wire and the two-point suspension loop of 1/4 inch dia. elastic shock cord (bungee). Combined with an abrasion resistant harness, this system provides adequate progressive restraint to control the lead wire motion. This umbilical cord contains the cables associated with the three measurements of interest.

b. Cell Voltage:

Ni-Cd cells present a nominal 1.3 volt open circuit signal. A signal of this magnitude presents no particular measurements problem once the lead wire motion has been controlled. Thus we are able to display this dc voltage level directly on the upper beam of the oscilloscope. Hence a cell which is truly impact resistant will exhibit a constant potential (straight line at dc level) throughout the impact period. Complete failure at impact (plates and tab fracture or complete shorting) will exhibit a drop to a lower dc level line. In addition we are able to observe any momentary shorts that may occur within the cell only during the period of impact. Should it be desirable, an external load is easily placed across the cell and thus discharge voltage (or charge voltage) can be measured during the actual impact.

c. Velocity:

The velocity of the carriage at impact is accomplished essentially by measuring the actual time of travel between two points of known distance apart. The two contact points of interest are best shown in Figure 7 mounted on the left hand rail support post. Each consists of an expendable brittle steel wire (.020" dia) inserted in a tubular holder. The distance between the holders is fixed (4.000" ± .020") and electrical connections are made to these insulated

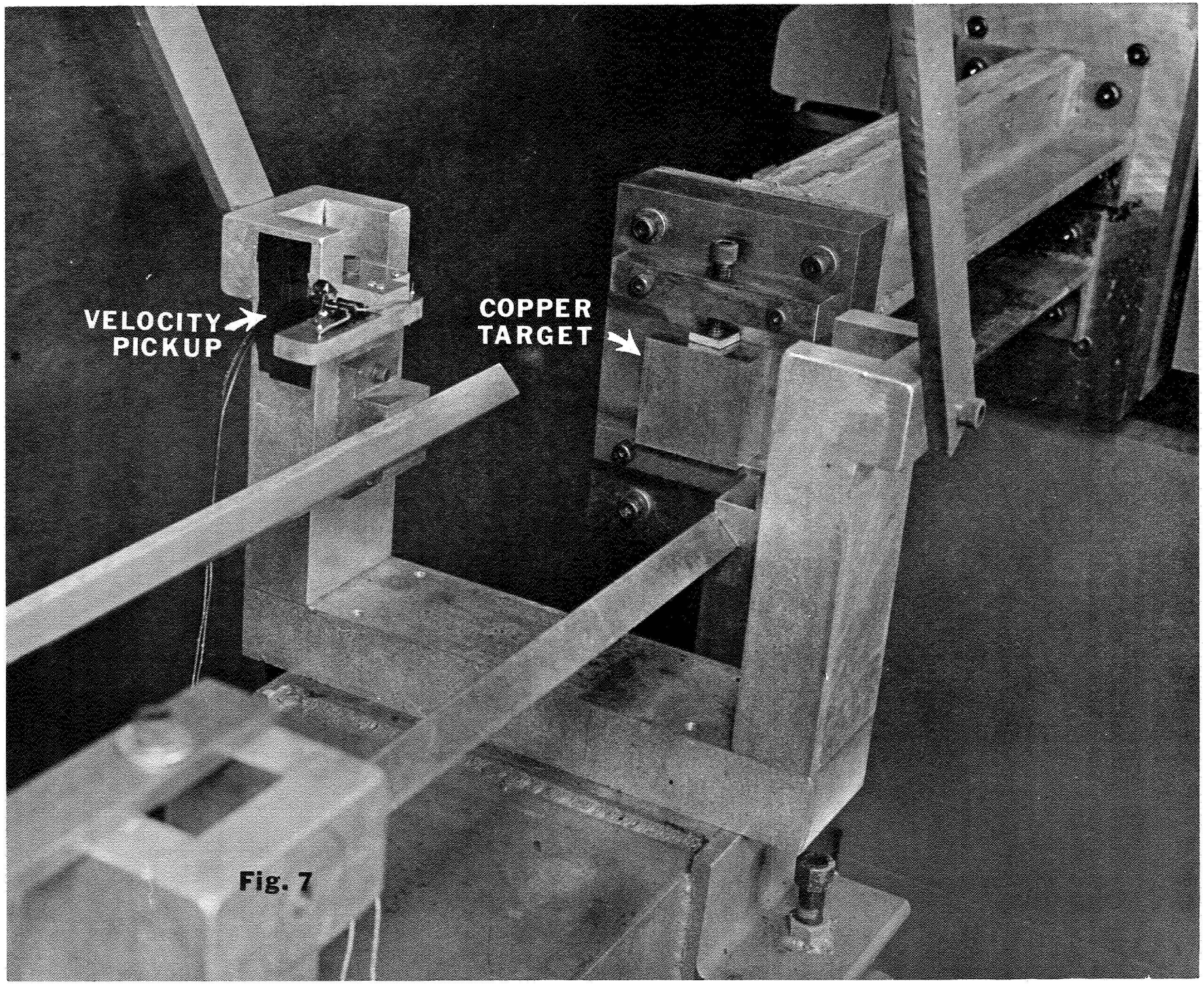

Fig. 7

Fig. 8

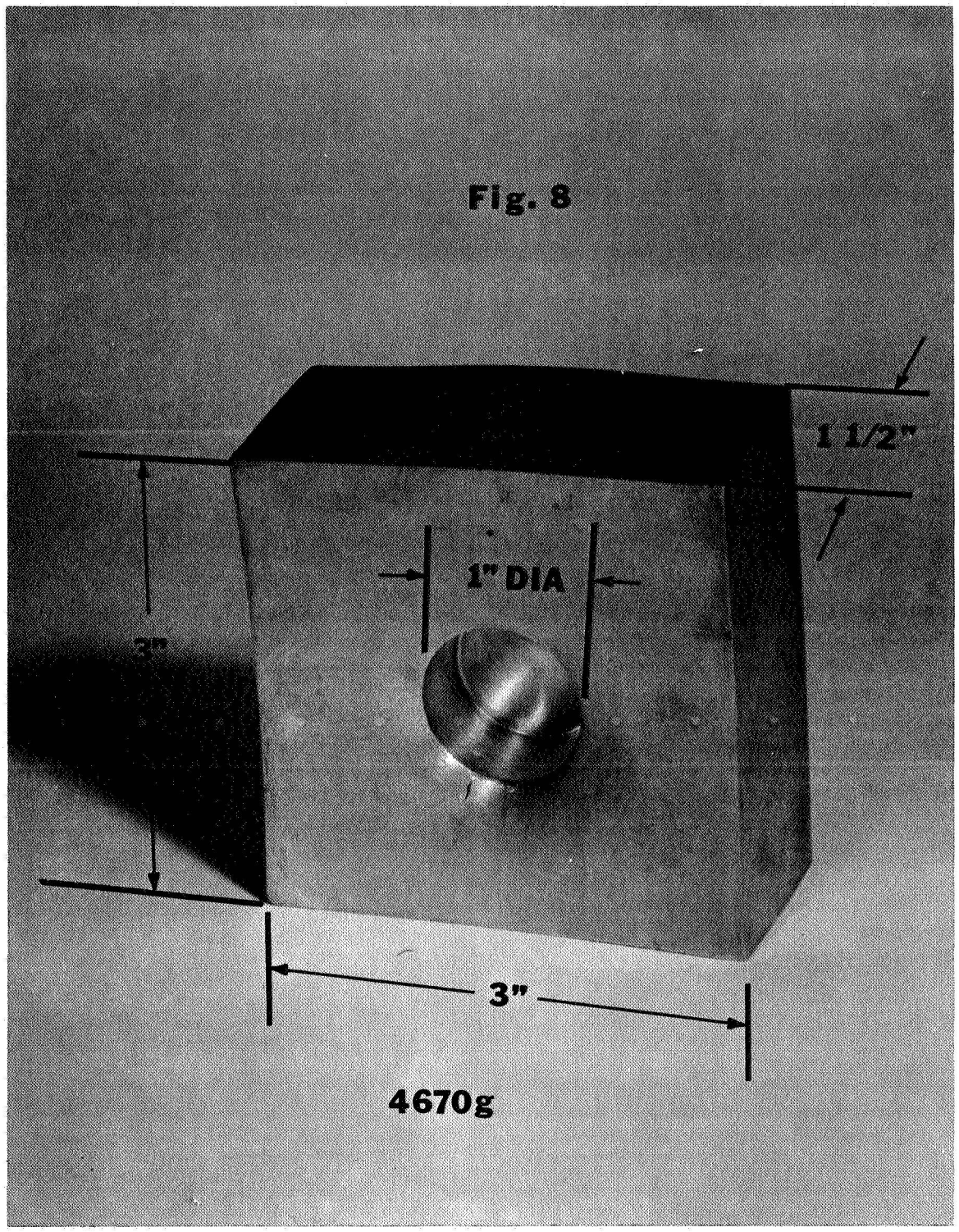

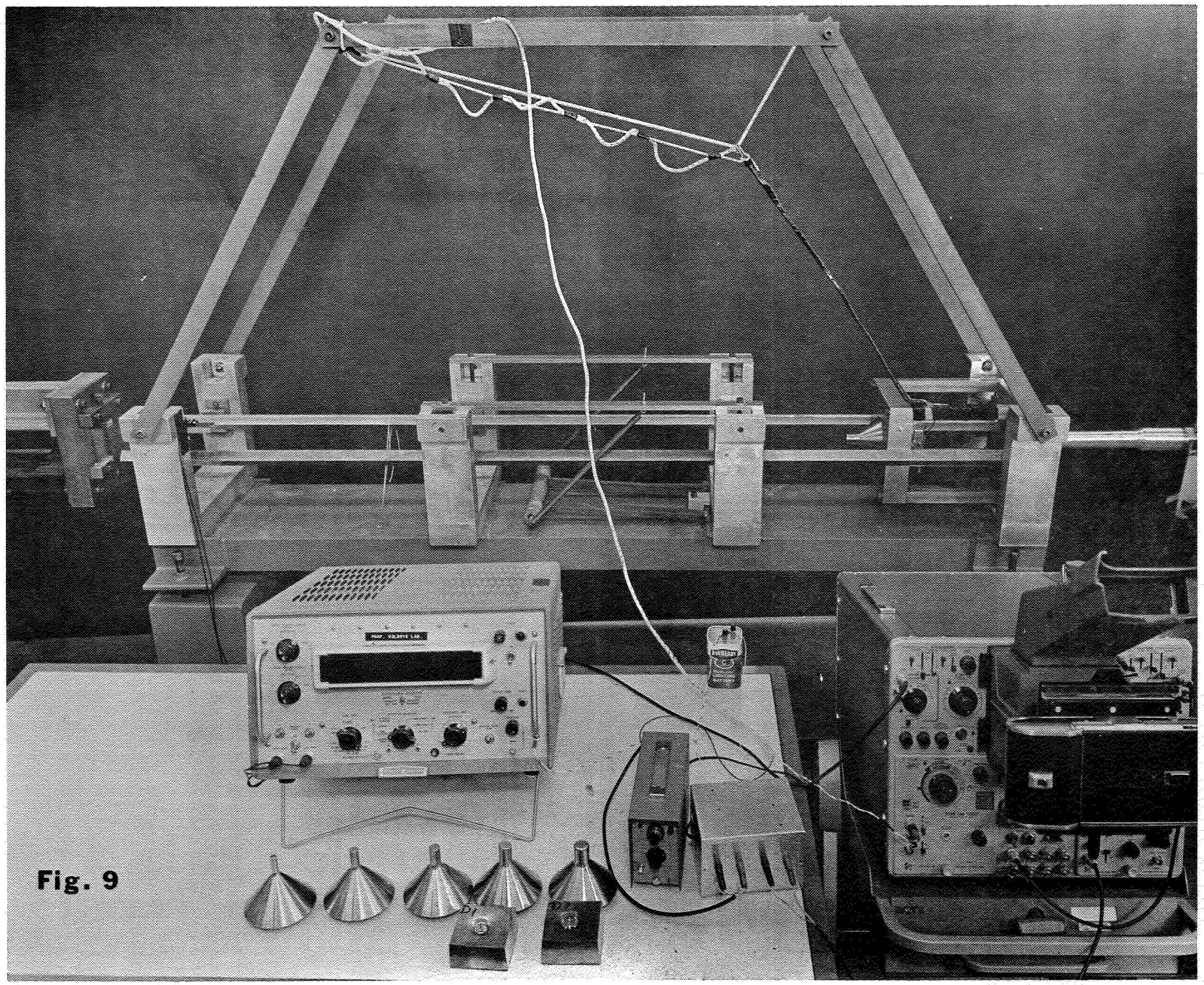

Fig. 9

holders. The carriage itself contains a permanent stud connected to the positive side of a 6 volt battery and electrically isolated from the carriage mass. Thus the moving carriage momentarily completes two circuits during its travel and the two voltage pulses are used to start and stop an electronic counter which records the time interval (μsec) between the known distance. Although basically very simple, this technique is highly reliable and possesses several advantages over other methods. Accuracy is better than 0.5 ft/sec. The 6 volt signal available permits high trigger gate levels to be set thus eliminating false triggers from the extraneous transients frequently encountered in this type of work. Isolation of the carriage stud insures a continuing ground base, desirable for the acceleration measurement described below.

The velocity measurement itself is made only one inch before the point of impact. This system readily supplies an equally reliable trigger pulse for the oscilloscope as shown in Figure 10.

d. Acceleration:

1. Instrumentation:

The measurement of the shock pulse associated with the **deceleration** of the carriage and specimen is obtained by a piezoelectric accelerometer mounted on the main carriage plate (Fig 4). The high impedance charge output of the transducer (Kistler 808A or 805A) is converted by an electrostatic charge amplifier (Kistler 504A) to the low impedance voltage signal desired for display on an oscilloscope (Tektronix 555). Initially, operation with conventional high impedance voltage amplifiers was found unsatisfactory. The addition of a charge amplifier seems to measure more directly the basic signal from the accelerometer, an electrical charge pCb/g, and produces

to provide the desired time constant. With the present instrument settings we have a time constant of 5.0 seconds ($<$0.1HZ) which is nearly 100 times better than the requirement for 2% accuracy. This is more than adequate response as is clearly shown in Figure 12b.

3. High-Frequency Response:

A fourier spectrum analysis of a rectangular pulse shows that most of the energy of that pulse is contained in the frequency band from zero to 1/T (T=pulse length). Hence, the system must have a minimum upper frequency response $f_H \geq 1/T$. It has also been shown that in order to prevent excessive rounding of corners, $f_H \geq 10/T$. In the present case (T=.001 sec) it was felt that f_H=10KHZ would be quite adequate to accomodate the rectangular pulse and rapid rise time. The high frequency response of the instrumentation system is practically limited by the first mechanical resonance of the accelerometer (mass-spring) itself. This implies the need for a high f_N device (with zero damping) to insure an amplitude and phase response that is invariant with frequency at least up to the 10KHZ presently desired. Three accelerometers have been evaluated (f_N=41.5 KHZ, 43KHZ, 62.5KHZ) and most work has been done with the higher output Kistler 808A with f_N=41.5KHZ. Manufacturers generally trust approximately $f_N/5$ as the useable ($\pm$ 5%) frequency range and this implies approx 8KHZ for our system. The charge amplifier itself is good to approximately 100KHZ and the passive resonance filter matched to this accelerometer is flat to 5KHZ and 3Db down at 17KHZ. Therefore we have set the 1A7 variable bandpass plug-in at flat to 10KHZ and have a net system $f_H \approx$ 8KHZ limited by the accelerometer itself. This value approached the desired 10KHZ and we expected fairly good performance.

Fig. 10

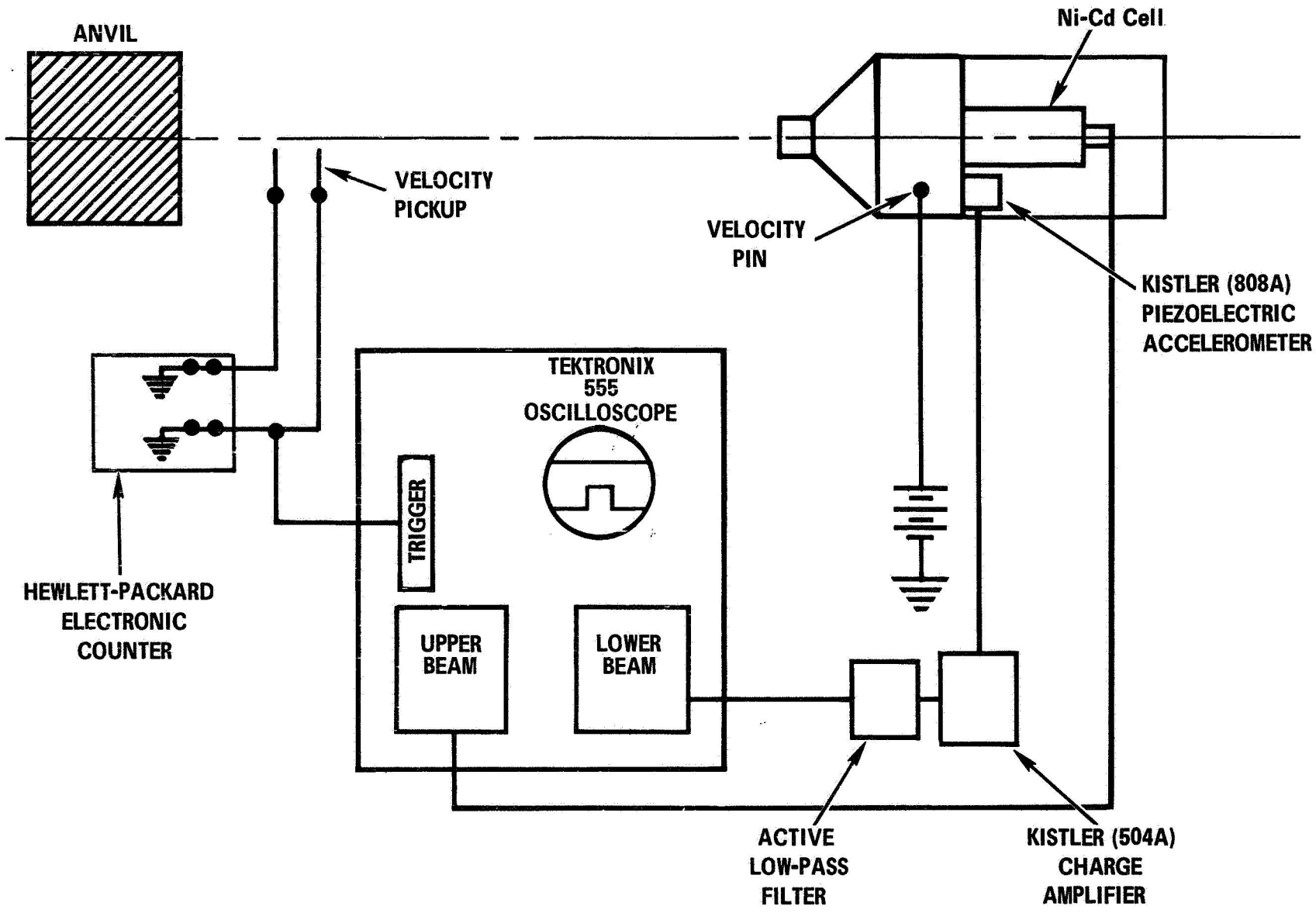
ANVIL
Ni-Cd Cell
VELOCITY PICKUP
VELOCITY PIN
KISTLER (808A) PIEZOELECTRIC ACCELEROMETER
TEKTRONIX 555 OSCILLOSCOPE
TRIGGER
UPPER BEAM
LOWER BEAM
HEWLETT-PACKARD ELECTRONIC COUNTER
ACTIVE LOW-PASS FILTER
KISTLER (504A) CHARGE AMPLIFIER

an output voltage signal precisely proportional to the input acceleration. Differing from a cathode follower (where the resistive component is very large), the capacitive component of the charge amplifier input impedance is very large. Normally, this characteristic results in most benefit to an application where long cable lengths (additional capacitive loading) are required. Although the present arrangement does not necessitate long cable lengths, the capacitance changes during severe dynamic motion are less likely to effect the output voltage of the transducer with the present system. In addition, the use of this amplifier permits accurate calibration of the overall system (Fig 12b) by insertion of a calibrated voltage signal at the transducer input. A passive transducer resonance filter is also provided at the amplifier. With this conditioning, the signal is connected to a Tektronix 1A7 plug-in at the scope. This preamp is a variable bandpass unit that can be used to further condition the signal if required. Because of the signal magnitude (8 volts @ 4000 g), noise is not a problem and high gain is unnecessary. The signal is a.c. coupled to this plug-in to eliminate any undesired d.c. component from disturbing the baseline at zero acceleration.

2. Low Frequency Response:

Good low-frequency response of the system is a necessity in order to follow the long duration of the rectangular pulse created. It has been shown that for a 2% error, an RC time constant approximately 50 times the duration of the pulse (.001 sec) is required. In the present instrumentation system, the dominant time constant is determined by the product of the feedback capacitor and resistor within the charge amplifier. The value of C_F is chosen to provide the desired system sensitivity and then R_F is chosen

4. Description of Output:

Figure 11 represents the kind of acceleration pulses we observed with the instrumentation as described above. Note that the rise time of our pulse is approximately 30 μ sec and the system seems to have more than adequate high frequency response to follow this pulse. However, the reason for showing this particular set of photographs is that they exhibit three distinct values of high frequency disturbance that seemed to persist throughout the system development (Runs #1-79). We remained interested in this so-called "ringing" and carried out some work to identify the cause.

(a) Stress Wave Sensitivity:

Firstly, the disturbing frequencies seemed far too low to be associated with the transducer resonant frequency. We spent some time investigating the accelerometer's response to elastic stress waves within the mounting specimen. An aluminum rod (1/2" dia x 12" long) with the accelerometer attached to one end was used for this purpose. A vertical drop of this rod, with the free end striking absorbing material backed by a rigid surface, produced a main deceleration pulse followed by predictable elastic wave propagation within the bar. The results shown in Figure 12a were obtained with the same instrumentation system response as used for impact testing. The main deceleration pulse is shown followed by the decaying elastic wave propagation at an experimentally determined frequency of 7KHZ which agreed very well with the calculated 7.7 KHZ considering the complication of connecting the accelerometer to the end of the bar. Additional confirmations were obtained by: a.) changing the length of the bar (observing the change in frequency)

b.) merely striking the end of the bar (elastic wave propagation only without initial deceleration pulse) and c.) insertion of absorbing material between accelerometer and bar (no reduction of deceleration pulse magnitude but near elimination of elastic phenomena because of mismatched acoustic impedance at the interface). Thus we demonstrated that the accelerometer is indeed quite capable of displaying output when excited by elastic waves. Important also was the fact that we were unable to excite transducer resonant frequency. However in transferring our study from the predictable behavior of the cylindrical aluminum bar to the carriage itself, we were unable to observe the calculated frequencies associated with elastic wave propagation (60KHZ). More importantly we were unable to shift the disturbing frequencies by techniques aimed solely at modification of elastic wave propagation.

(b) Effect of Vibrations:

Hence it was felt that lower frequency vibration might be the prime disturbing influence and we calculated the natural frequencies of key structural elements within the carriage for several modes of vibration. 5.3,13,21 KHZ were calculated as the first three modes for the main carriage plate. The recurring disturbances we had previously observed (Fig. 11) matched this calculation quite well. A further study of the carriage involved movement of the accelerometer to various mounting locations and striking the carriage by hand to induce only vibration (no main deceleration pulse). This study confirmed the description of the three modes of vibration and has provided us with a very

VERTICAL SENSITIVITY:

1000 g /CM.

Fig. 11

HORIZONTAL SENSITIVITY:

0.5 msec/CM.

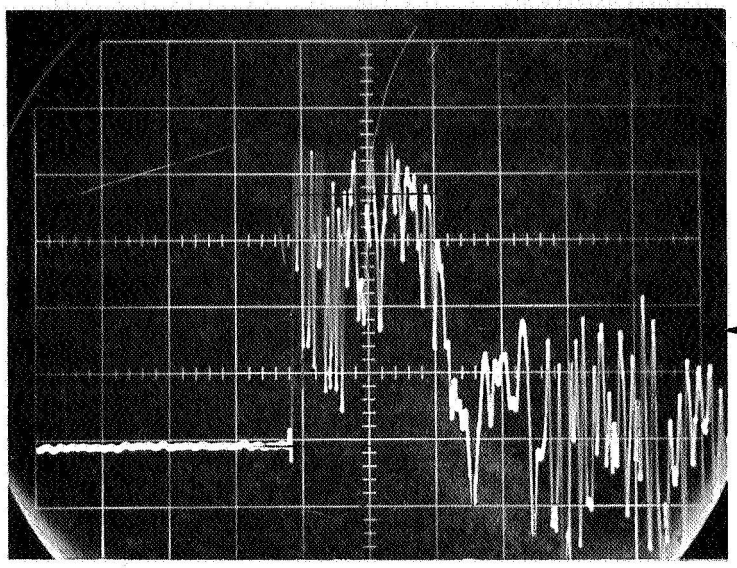

23 K HZ DISTURBANCE

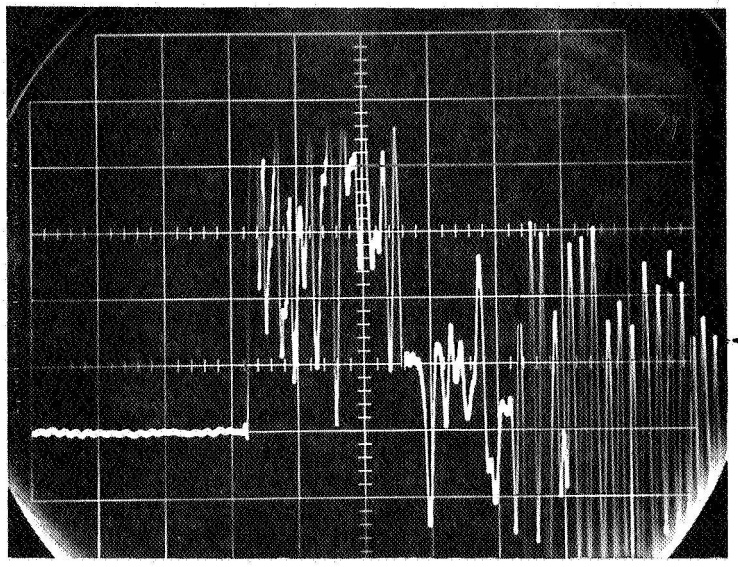

11.5 K HZ DISTURBANCE

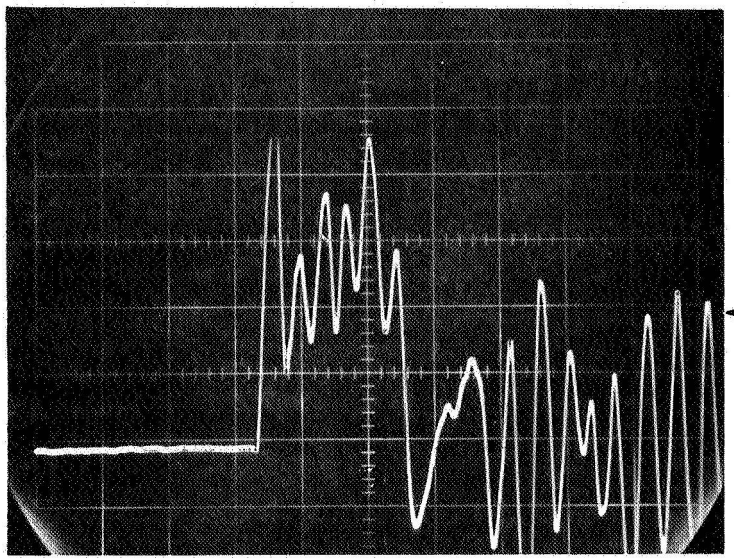

5.5 K HZ DISTURBANCE

Fig. 12(a) ELASTIC WAVE RESPONSE

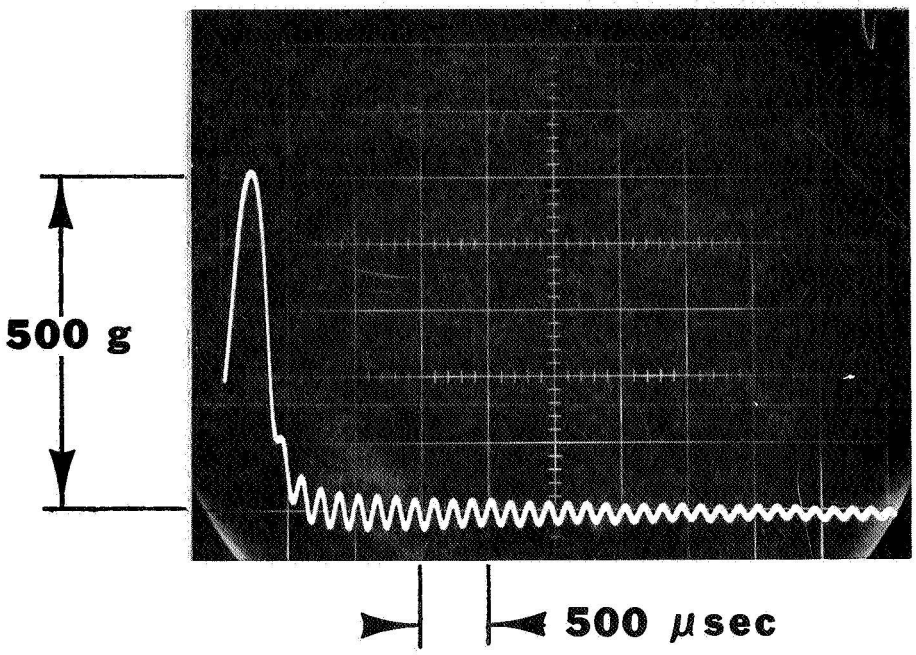

Fig. 12(b) SYSTEM CALIBRATION

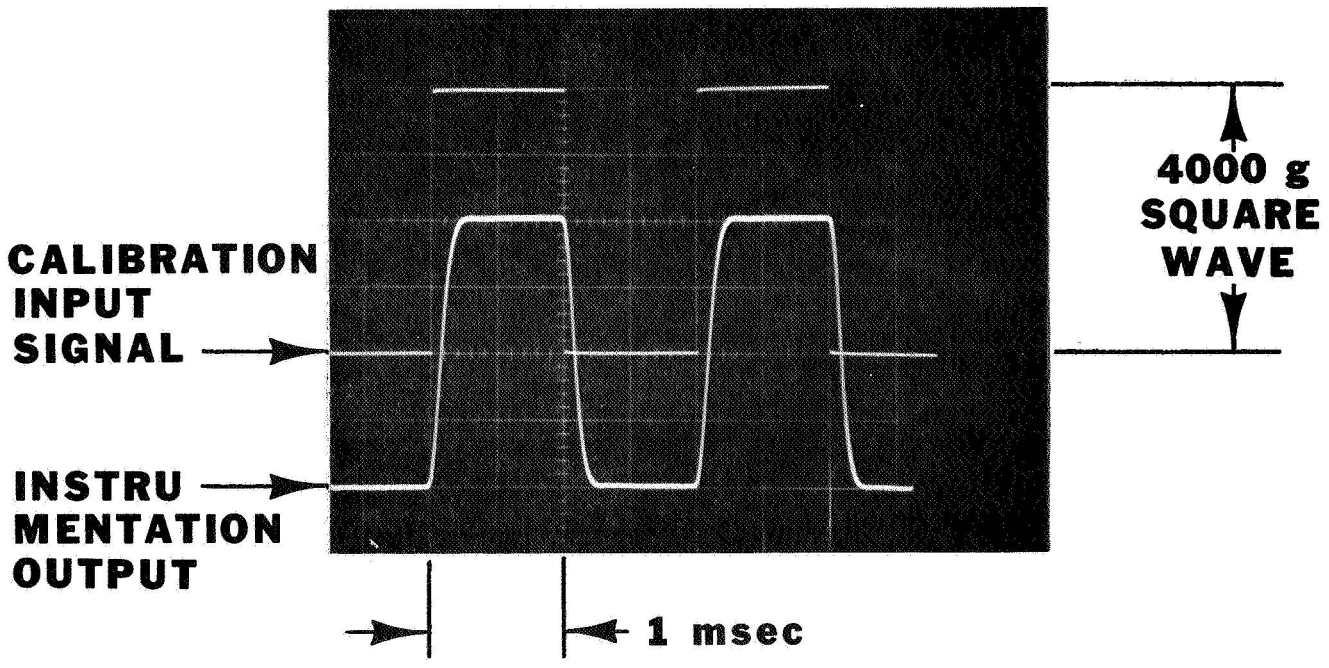

thorough understanding of both our mechanical and electronic system response. In order to obtain the precise waveforms desired latter in the testing program, this main plate will be redesigned to eliminate this low frequency vibration.

5. Filtration & Calibration:

Alternatively, such vibration and the frequencies involved were best eliminated from the system by electronic filtration. Thus an active low-pass filter network was designed and employed to attenuate all but the fundamental vibration frequency. Figure 12b best illustrates the characteristics of the final instrumentation system. The upper beam was used to trace the calibrated input square wave and the lower beam exhibits the overall system response to this simulated input. All system components (charge amplifier, passive filter, active filter, oscilliscope plug-in) were held at exactly the settings used for impact testing. One can see that the amplitude of the shock pulse (4000 g input simulated) is exactly reproduced. The effect of excellent low-frequency response as discussed is exhibited by the perfectly flat peak plateau. The system's inability to follow the input step exactly is also shown by the 200 μsec rise time. However the actual test pulse appears to have a real rise time on the order of 50 μ sec and thus we felt the final system's high frequency response was adequate to begin the initial testing program. This picture also directs the test engineer to the exact manner in which true pulse duration is to be measured.

4. Overall System Analysis

The benefit of employing the final instrumentation system as described is apparent from the quality of the acceleration traces shown in Figure 13. The photographs were taken at the end of the development phase and indicate the g-levels and pulse lengths typically achieved. They

were used as the basis for calculations to check the overall system accuracy. It is first appropriate to compare the two classes of mechanical collision:

Perfectly Elastic	Perfectly Plastic
$\varepsilon = 1$	$\varepsilon = 0$
Two bodies fully rebound	Two bodies move together
momentum conserved	momentum conserved
kinetic energy conserved	total energy conserved

We can see that our present collision into copper more closely approximates the perfectly plastic collision yet we experience some rebound. Considering the applicable relations:
Impulse = Δ Momentum:

$$\int_{t_o}^{t} F\,dt = m\,(V_{m2} - V_{m1}) \qquad (1)$$

Conservation of Momentum:

$$m\,V_{m1} + \cancel{M\,V_{M1}} = m\,V_{m2} + M\,V_{M2} \qquad (2)$$

Conservation of Total System Energy:

$$KE_{m1} + KE_{M1} = KE_{m2} + KE_{M2} + \text{E Absorbed in Deforming Copper} + \cancel{\text{E Heat Light Sound}} \qquad (3)$$

Equation (1) may be solved for V_{m2} by using the measured V_{m1} and the area of the acceleration-time trace. This would permit the solution of equation (2) for V_{M2} directly assuming m & M were known. Finally equation (3) could be solved for the force required to deform the copper since the depth of penetration is measured. This analysis involves only the assumptions of neglecting small energy losses from the system (although the noise during a test makes me question this!) However the force required to deform

1" DIA — 115 ft/sec
3650 g — 1.15 msec

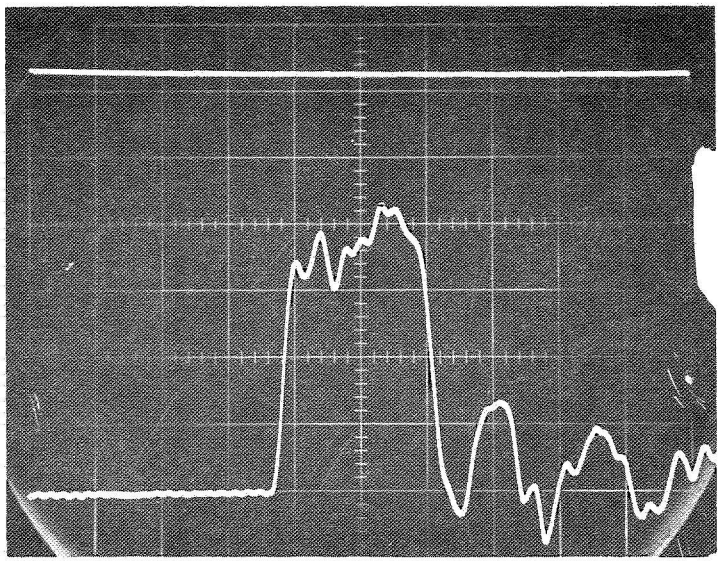

3/4" DIA — 91 ft/sec
2300 g — 1.2 msec

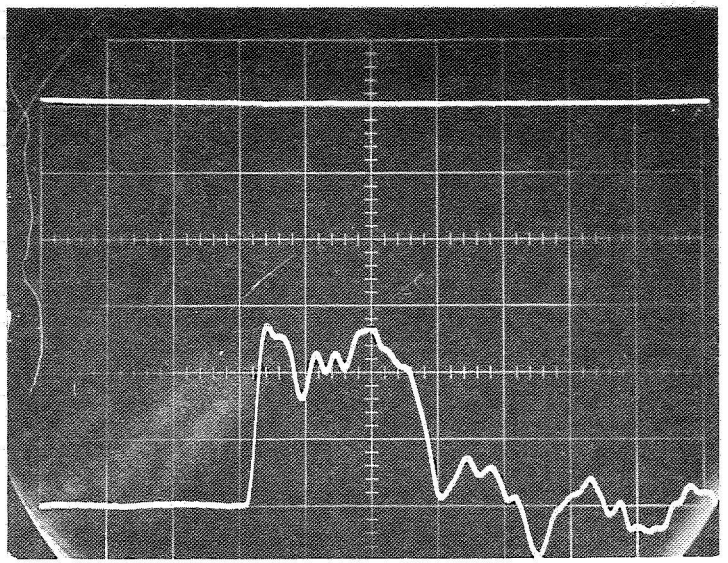

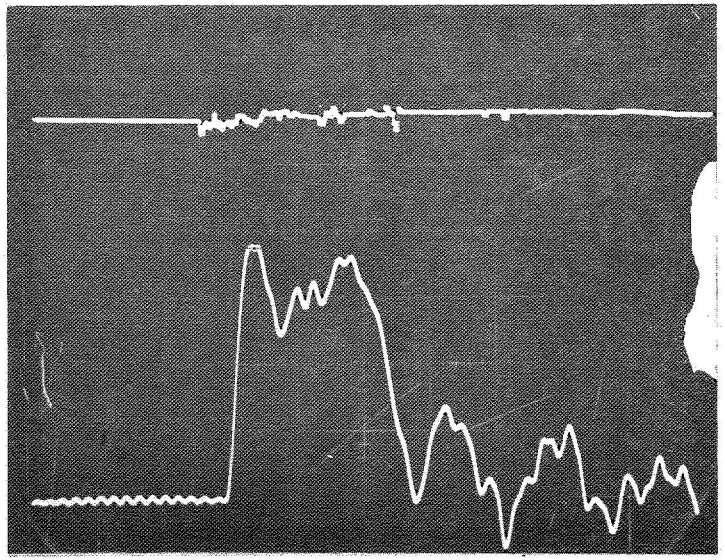

7/8" DIA — 108 ft/sec
3250 g — 1.1 msec

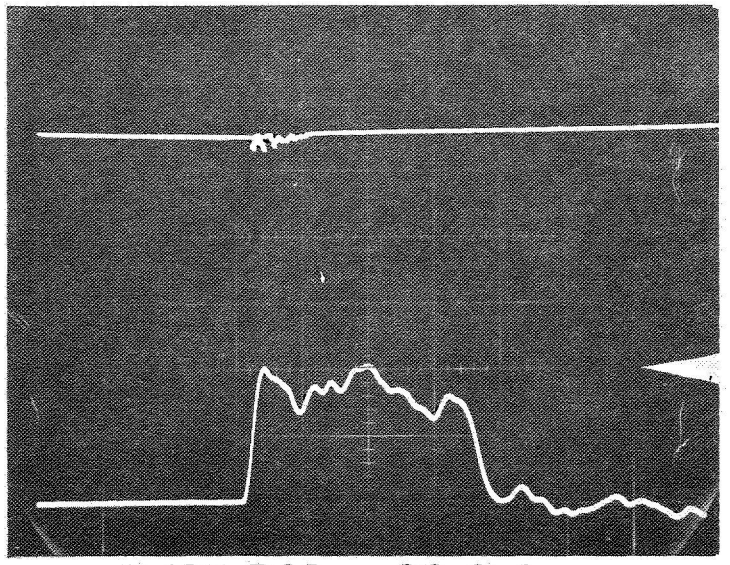

5/8" DIA — 82 ft/sec
1600 g — 1.5 msec

Fig. 13

copper at this strain rate and 3-dimensional state of stress is far from handbook knowledge and in truth would require extensive research to establish experimental data more reliable than the system measurements used in our calculations. Thus we can only compare this calculated force to that force associated with the test's mean g-Level. This has been done for the traces shown in Fig. 13 and the results are tabulated below:

TABLE III A-1

Tool Dia. (in)	Meas. Impact Velocity V_{m1} (ft/sec)	Calc. Rebound Velocity V_{m2} (ft/sec)	Calc. Velocity V_{M2} (ft/sec)	(1) F_{mean} Calc. From Full System Analysis As described above	(2) $F_{mean} = ma_{mean}$ a_{mean} Meas. from Photo	(3) $F_{mean} = ma_{mean}$ from uniform Decelleration $a_{mean} = \frac{(V_{m1})^2}{2S}$	(4) F_{mean} Impulse/ Time %	(5) $F_{pk} = ma_{pk}$ a_{pk} Measured From Photo
5/8	82	4.5	1.1	56,800#	55,200#	57,800#	51,400#	65,000#
3/4	91	0	1.1	78,700#	74,800#	79,700#	68,800#	87,700#
7/8	108.5	3.8	1.5	104,000#	104,000#	105,000#	103,000#	122,000#
1	115.5	10.8	1.6	135,000#	119,000#	138,000#	110,000#	140,000#

In the tabulated calculations we have noted the very small anvil velocity that is implied (ref. col. V_{M2}) and the fairly low carriage rebound velocity (ref. col V_{m2}) that follows the collision and thereby established the system's proximity to the classical plastic case. There are five approaches shown for the evaluation of the dynamic force (equivalent to real g-Level). We can note that the peak levels (ref. col. 5) as shown in the photos are not the real levels of test interest and are merely a result of the accelerometer's mounting location experiencing the superimposed vibration as described earlier. However they indicate a good upper bound especially in the case of strong rebound. The most important observation is the excellent agreement of the real force (g-Level) from uniform decelleration calculations and that calculated when total system energy is accounted for as discussed in detail (ref. col. 1 vs col. 3). This is true for each test shown regardless of rebound etc. which is not the case for the measured mean (ref. col. 2) which seems to have good agreement so long as rebound is not severe and near plastic collision is achieved. However this agreement is quite good under normal testing conditions and the comparison (ref. col. 2 vs col. 3) is made routinely in a practical testing program to insure reliable generation of data.

5. System Calibration

During the development phase and the initial testing program, a large amount of data was generated by this testing facility. Many separate studies were employed to extend the typical range of values and the total of this information constitutes the overall system calibration. It has been seen that the blunt end cylindrical tools are responsible for achieving a square deceleration pulse with excellent rise times. The actual g-Level and pulse length however, remain flexible and are under the control of the operator within certain bounds. It is this capability (calibration) that is best shown in the following figures which illustrate the

effects of changing the main system variables.

a. g-level vs Tool Diameter

As indicated earlier, tool diameter or the area of the penetrator is the prime variable affecting g-level. Assuming a fairly constant state of 3-dimensional stress during copper deformation, the total force (g-level) would be directly proportional to the area. Figure 14 shows this linear relationship as exhibited over many impact tests. The "calculated ave." points represent the average mean g-level attained with a given tool taken over all tests run with this tool. "Calculated" here, means using velocity and depth of penetration $\left(\frac{V^2}{2S}\right)$ assuming uniform decelleration. The "measured ave." points again represent the average mean g-level attained with a given tool taken over all tests run with this tool. "Measured" here, means reading the mean g-level directly from the oscillograph of acceleration vs time. Agreement between calculated and measured is quite good except at the highest level. This discrepancy was discussed in the previous section on overall system analysis. If measured peak g-level is plotted, the values will lie above the calculated values and as discussed previously, are not as meaningful as the measured mean levels. Accompanying each average value is a span line to indicate the acceleration limits obtained with each tool as various parameters were changed throughout the development testing.

b. g-level vs Velocity

The carriage mass, equipped with any given tool diameter may be fired at any desired velocity as regulated by the selection of differential pressure (Fig. 3). The practical limits are: 1) low velocity provides a short (time) pulse length which is usually not of interest, 2) high velocity provides a very deep penetration (tool may be embedded in the copper) and if a very long (time) pulse length is not required, it is avoided as a matter of convenience. The point is that in saying the g-level

is primarily a function of tool diameter, we would expect to see a g-level (for any given tool) that is invarient with respect to velocity. Figure 15 presents the mean g-level obtained (both calculated and measured) for each test performed at its respective velocity. We have varied the test velocity for each tool to illustrate the relative invariance of g-level. Thus the lines drawn in Figure 15 illustrate the rather constant g-level associated with each tool regardless of test velocity.

c. Pulse Length vs Velocity

With a constant carriage mass we would expect that, as a consequence of the result illustrated in Figure 15, the pulse length would be linearly related to the test velocity ($\int F dt = M \Delta V$). Figure 16 illustrates this result. Again, we are showing the pulse length obtained (both measured and calculated $\frac{2S}{V}$) for each test performed at its respective velocity. The lines drawn in Figure 16 indicate the degree of sensitivity (pulse length as a function of velocity) for each tool. Each tool has a different sensitivity as we have shown it in Figure 16 but this is simply a result of including an actual area function (d^2) within our third parameter tool diameter (d).

d. Additional System Variables

Figures 3, 14, 15, 16 provide adequate calibration data for the test engineer to select variables and achieve the type of impact test he desires. Although they contain the prime variables of interest, there are many other considerations which may change the character of this machine if desired.

(1) The actual impact (acceleration vs time) is a function of a great number of interrelated variables:

FIG. 14

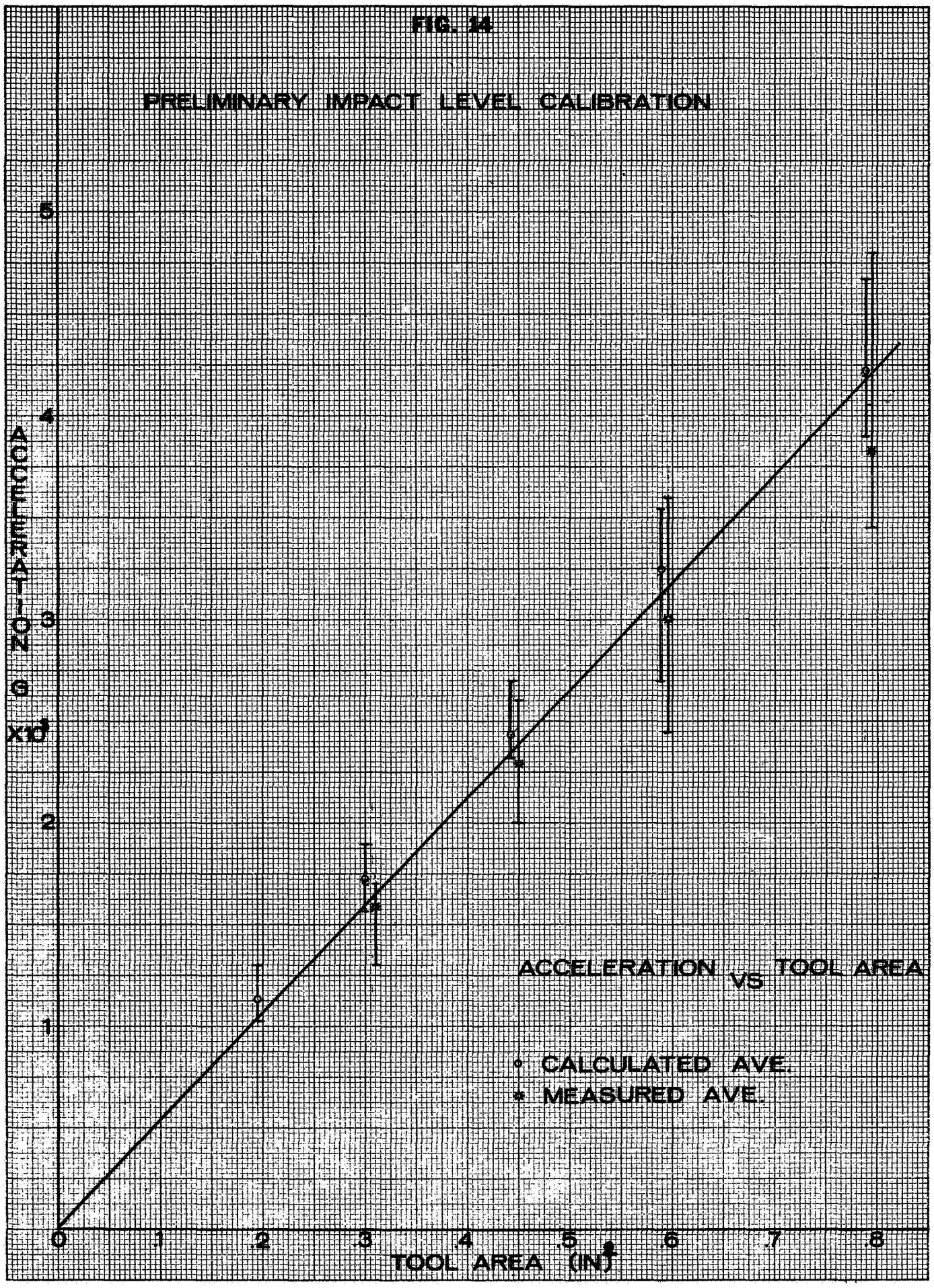
PRELIMINARY IMPACT LEVEL CALIBRATION
ACCELERATION G x10³
5
4
3
2
1
0
.1
.2
.3
.4
.5
.6
.7
.8
TOOL AREA (IN²)
ACCELERATION VS TOOL AREA
CALCULATED AVE.
MEASURED AVE.

$$a,t = f(V,\ m,\ d,\ Mat.,\ \dot{\varepsilon}\ M,\ Anvil\ Fixity,\ \ldots)$$

where: V - carriage velocity
m - carriage mass
d - penetrator diameter
Mat. - type or hardness of target material
$\dot{\varepsilon}$ - strain rate sensitivity ($\sigma_y = f(\dot{\varepsilon})$) target material
M - mass of anvil

(2.) (a) Even though our calibration Figures 14, 15 and 16 study only two of these variables (V & d), there are subltes contained in even this data. Considering the span lines at each data point on Figure 14, we cannot assume that this is solely an indication of experimental scatter. Contained within a given span line are experimental errors associated with the measurement of velocity and depth of penetration or the electronic calibration and measurements of the oscillograph. However the data within a span line was generated over a considerable time period and three lots of target material were used with slightly varying hardness values. More importantly, within the same lot of copper we must note that we are dealing with a material which is strain-rate sensitive ($\sigma_y = f(\dot{\varepsilon})$). It is, therefore, reasonable to assume that velocity may affect the force or g-level to some degree. Referring also to Figure 15 we have noted that g-level is primarily invarient with velocity and this remains true for our immediate testing requirements. Yet a few low velocity points can be seen on this figure and

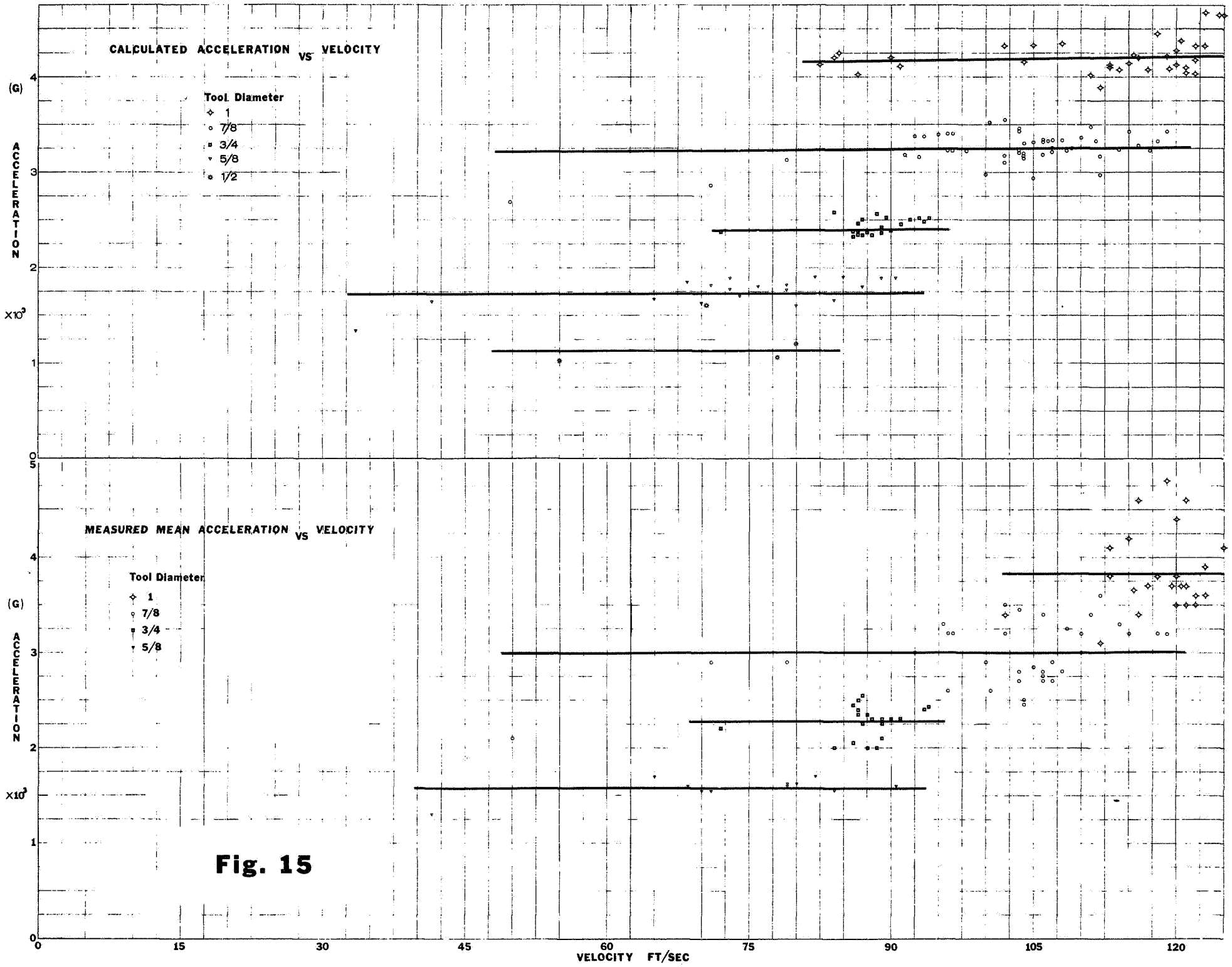
CALCULATED ACCELERATION VS VELOCITY
Tool Diameter
1
7/8
3/4
5/8
1/2
(G)
ACCELERATION
X10³
0
1
2
3
4
MEASURED MEAN ACCELERATION VS VELOCITY
Tool Diameter
1
7/8
3/4
5/8
(G)
ACCELERATION
X10³
0
1
2
3
4
5
0
15
30
45
60
75
90
105
120
VELOCITY FT/SEC

Fig. 15

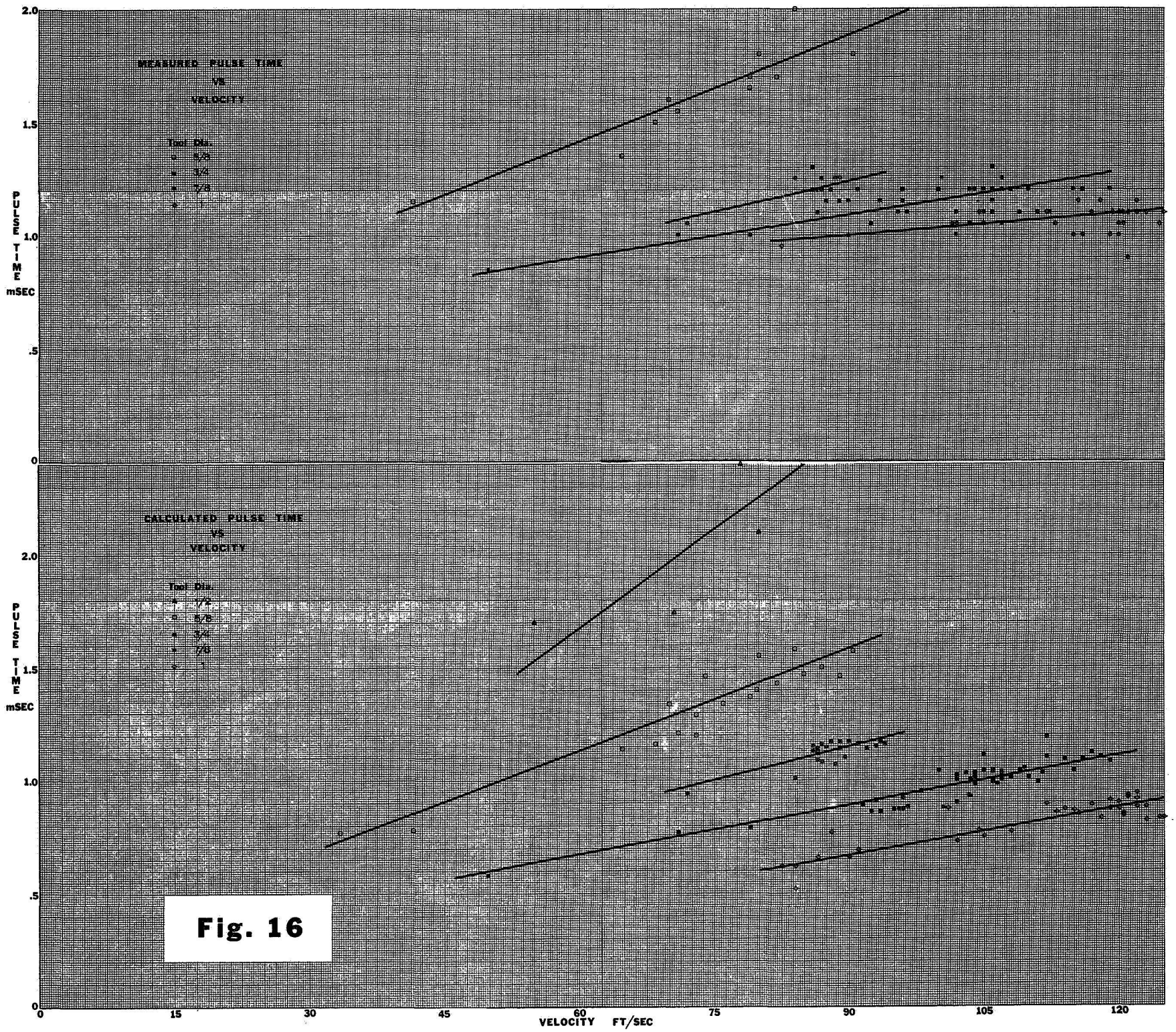
MEASURED PULSE TIME
VS
VELOCITY
Tool Dia.
5/8
3/4
7/8
PULSE TIME mSEC
2.0
1.5
1.0
.5
0
CALCULATED PULSE TIME
VS
VELOCITY
Tool Dia.
1/2
5/8
3/4
7/8
PULSE TIME mSEC
2.0
1.5
1.0
.5
0
0
15
30
45
60
75
90
105
120
VELOCITY FT/SEC

Fig. 16

indicate the g-level is reduced below the normal level for that tool. Hence, there is some experimental confirmation for this type of strain rate thinking and it may be more important for other target materials. The use of lead target blocks, for example, would obviously change the character of this testing machine.

(2.) (b) We have also changed the shape of the target block in order to evaluate its effect on the acceleration time trace for a given tool and test velocity. Three configurations were studied: 3" x 3" x 1 1/2" TK., 3" x 3" x 2" TK., 3" dia. x 2" TK. We were unable to observe any significant variation in the shape, magnitude or duration of the traces and have concluded that the plastic cold flow (Figure 8) within the present material is adequate to assure uniform behavior during testing.

(3.) In discussing the significance of Figure 16, we have demonstrated the effect predicted from impulse - momentum considerations. Stated in the discussion was the fact that the carriage mass was essentially constant. Many of the data points contained however, were taken from tests of various cells and their associated fixtures. Hence, some of the experimental scatter is attributed to this tacit variable (wt.) which is hidden when we make velocity alone the independent variable. In other words, the variation of momentum (not merely velocity) is the basic parameter under our control. For our immediate testing programs we find it very convenient (for calibration purposes) not to vary significantly the carriage mass. What we wish to point out, however, is the additional testing flexibility which can be easily attained by manipulation of this very important mass variable.

(4.) In summary, we have developed an impact testing machine capable of evaluating most cell configurations within the range of 1000g - 4800g and 0.8 - 2.0 msec. This has been accomplished by changing only two variables - tool diameter and carriage velocity. The ability to cover such a range this easily is of great convenience during a given testing program. However, this in no way represents the limit range for this machine. Two other prime variables (carriage mass and target materials) have been held constant throughout the system development described in this report. If necessary to study the dynamic response of components to pulses of broader length range, the additional capabilities of this machine can be employed later in the program.

References:

1. "High-impact survival", J.O. Lonborg, JPL technical report #32-647, Sept. 1964.

2. "Designing for high-impact technology" ASME bulletin 1967

3. "HYGE shock test facility at 6571ST Aeromedical Research Laboratory" USAF technical report #ARL-TOR-62-22, Sept. 1962

4. Shock & Vibration Handbook Harris & Crede, McGraw-Hill, 1961

5. "Specification of shock tests," Crede, SAE technical paper #585B, 1962

6. "Shock spectrum as a criterion of severity of shock impulses," Morrow, JASA 29 #5 May 1957 pg. 596

7. Bruel & Kjaer Technical Review #3, "Shock Measurement" 1966

B. TESTING OF EXISTING Ni-Cd CELLS

The programmed testing began during the last week in January to characterize existing cells and identify failure modes and levels. Cell configurations undergoing evaluation include:

(1) Short Sub-C Cyl. with Spindle
(2) Short Sub-C Cyl. w/o Spindle
(3) Long Sub-C Cyl. w/o Spindle
(4) 4 AH Prismatic

These cells will be tested on each non-redundant axis at three distinct impact levels:

(1) 4300 g - 1.1 msec from 117 ft/sec
(2) 3400 g - 1.1 msec from 104 ft/sec
(3) 2700 g - 1.3 msec from 90 ft/sec

Each cell has been fully characterized physically and electrochemically before impact testing. The cell is in the charged state and voltage is monitored during impact. Following post-impact discharge, each cell is further examined physically and electrochemically (post-characterization) before complete failure analyses.

During March the impact testing facility was used primarily to complete the scheduled evaluation of existing Ni-Cd cells. The complete results of this characterization are being summarized by E. Rubin for a subsequent quarterly report.

C. TESTING OF SEALS FOR Ni-Cd CELLS

As a portion of the impact testing of cell components for impact resistant cells, the initial seal evaluation program has been outlined. The overall evaluation is best depicted in the flow chart presented. We are primarily concerned with their hermeticity, ability to survive heat sterilization (as demonstrated by lack of physical degradation and maintenance of hermeticity), and impact resistance. Therefore, we have included a great variety of testing, as shown in the flow chart, in order to gain maximum data.

For each distinct seal configuration, information will be gained concerning:

1. Hermeticity
   Vacuum checks will be taken before and after heat sterilization.
2. Heat Sterilization Effects
   a. Visual determination of degradation.
   b. Static load values will be taken on each seal configuration both before and after heat sterilization.
   c. Vacuum checks will be taken after heat sterilization.
3. Comparative Impact Resistance
   Relative impact load levels will be obtained both statically and dynamically for each seal configuration.
4. Dynamic Force Amplification Factors (Rate of Loading Effects)
   a. Comparison of load values for each seal configuration exhibited at two quasi-static loading rates (0.002 in./min and 2.0 in./min)
   b. Static load values (0.002 in/min and 2.0 in/min) will be compared to dynamic load values ($> 3 \times 10^4$ in/min)

as obtained from measured g-level and weight of the failure - mass component.

c. Use of static load values to predict similar dynamic load level and compare results at this level with results at higher and/or lower levels.

5. Direction of Major Impact Susceptibility

a. Static testing will examine the axial loading capability in both tension and compression.

b. Dynamic testing will evaluate impact resistance for each configuration in both the axial and transverse direction at various levels.

We are presently concerned with the complete evaluation, as outlined, for nine (9) distinct seal configurations:

1. Ceramaseal - 200
2. Ceramaseal - 205
3. Ceramaseal - 208
4. Polymeric Crimp Seal - 01
5. Polymeric Crimp Seal - 02
6. Polymeric Crimp Seal - 03
7. Polymeric Crimp Seal - 04
8. Polymeric Crimp Seal - 05
9. Polymeric Crimp Seal - 06

As indicated in the flow chart, a minimum of 16 seals of each configuration will be required for complete evaluation. The polymeric crimp seals are now being fabricated. Loading fixtures for static and dynamic testing of all configurations have been built.

J P L SEAL EVALUATION PROGRAM

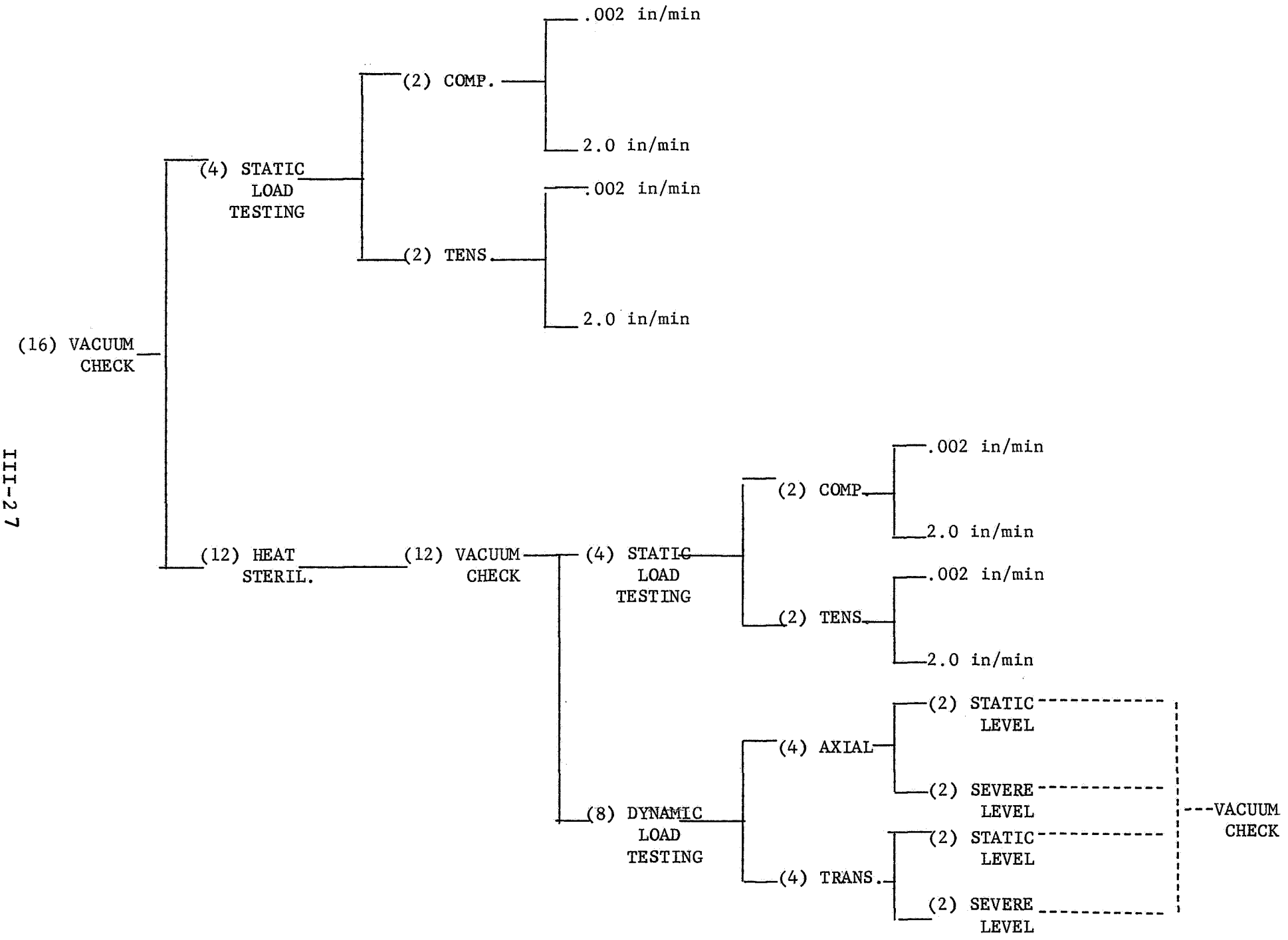

D. TESTING OF BATTERY ELECTRODES

The mechanical properties of battery electrodes must be known before the engineering design of an impact resistant cell can begin. At a minimum, static force data must be available to permit reasonable cell configuration design. A more refined design must be based on dynamic force data. An optimum cell design may indeed hinge on a complete knowledge of the mechanical properties of the fundamental structural elements of the battery. Of prime concern are the electrodes themselves. Their response to a dynamic force input must be determined from a knowledge of their stress-strain-time relation. A major effort under the current Jet Propulsion Laboratory contract will be expended in gathering the experimental data needed to describe the mechanical properties of these elements. At the beginning of this experimental work, it might be valuable to propose a model for the structural element we will be investigating. It is not uncommon to modify the first model selected as experimental results attenuate the predicted behavior. However, the value of an accurate model lies in its ability to promote a more complete understanding of the physical behavior observed. Hopefully, the development of the model will progress throughout the experimental phase. A point is always reached when the difficulty associated with making a further experimental measurement is sufficient, either to obviate a test or make the results of questionable validity. At that point the availability of an accurate model may be of great value. With this in mind we have made some assumptions about our battery plate material, formulated a model and made some preliminary predictions from that model.

If we neglect the electrochemical differences between the positive and negative plates, we can think about their basic structure

alone. Both positive and negative plates begin as a sintered nickel structure called plaque. Depicted in Figure 17 this structure is basically a 20 mesh screen of .007" diameter nickel wire to which particles of nickel powder have been sintered. Applied primary to one side of the screen, this sintered structure consists of particles of nickel powder sintered (fused) to each other and, of course, sintered to the screen. A first impression might be to observe the similarity of this plate to a slab of reinforced concrete. Indeed, it might seem valid to associate the screen with reinforcing rods and the sintered particles with the cemented aggregate. However, unlike steel in a concrete matrix, we have nickel in a nickel matrix. The difference between the two systems seems very great if only a solid structure is considered:

Steel Rods ∉ Concrete Matrix		Nickel Wire ∉ Sintered Nickel Matrix
30×10^6 psi	Modulus of reinforcing element	29×10^6 psi
3.2×10^6 psi	Modulus of matrix material	29×10^6 psi
170:1	Tensile ratio: $\left(\frac{\sigma \text{ult reinforcing element}}{\sigma \text{ult matrix material}}\right)$	1:1
14:1	Compression ratio: $\left(\frac{\sigma \text{ult reinforcing element}}{\sigma \text{ult matrix material}}\right)$	1:1

This comparison is not totally valid as will be seen later, since the sintered matrix of our plates is a highly porous structure.

Although electrochemically very desirable, the porosity of these plates makes structural analysis most difficult! We have shown (2nd JPL QTR Report 1967) that depending on positive or negative,

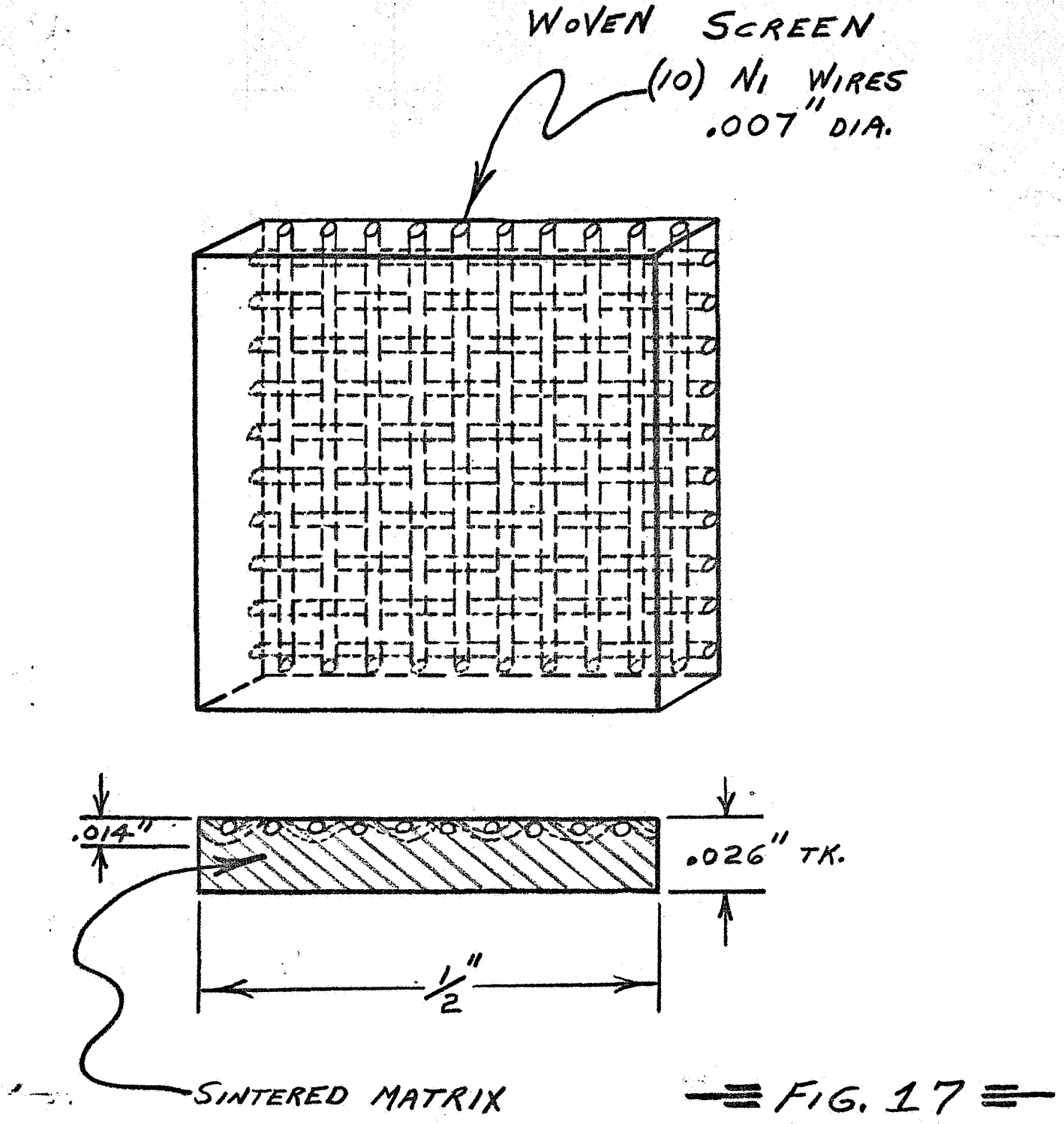
WOVEN SCREEN
(10) Ni WIRES
.007" DIA.
.014"
.026" TK.
1/2"
SINTERED MATRIX

FIG. 17

cycled or sterilized, the total porosity may range from 27% to 59%. Profiles of this final porous plate exhibit even broader ranges:

		2-50% of pores	<	0.1 micron dia.
0.1 micron dia.	<	8-22% of pores	<	0.5 micron dia.
0.5 micron dia.	<	3-31% of pores	<	1.0 micron dia
1.0 micron dia.	<	25-38% of pores	<	5.0 micron dia.
5.0 micron dia.	<	5-6% of pores	<	10.0 micron dia.
10.0 micron dia.	<	4-9% of pores		

It is apparent that we are dealing with a highly complex structure having a random distribution of various size openings. Some recent pictures obtained by scanning electron microscopy have illustrated the complexity and randomness of this matrix or at least the surface characteristics.

Fortunately, for the development of our structural model, these properties of the final plate are probably of little consequence. We are assuming that only the original sinter structure (plaque, common to all plates) is of load carrying concern. In other words, we are assuming that it matters little from strength considerations that we fill this basic sintered porous structure to various degrees with active chemical material which has little reinforcement capability (especially in tension). Accepting this assumption, we need to be primarily concerned with only the description of the sinter matrix itself. The total porosity of plaque is 78-80%. This porosity is also the net result of a random distribution of various pore sizes.

It is this more highly porous structure that we wish to describe via a structural model. This model should allow us to calculate the actual load carrying area within this structure. Then, using the mechanical properties of nickel metal, we may calculate the strength and modulus associated with our model. The model initially serves to predict mechanical properties and can be altered as experimental data is generated. We have considered various cubic crystals as representative of the nickel matrix. The "atoms" (of radius "a") normally placed in the basic crystal, are considered to be hollow spheres; normal void space within the crystal is considered to be solid nickel metal. The three cubic crystal structures investigated, are shown in Figure 18 These three were considered because they offer models of a matrix having 74% (FCC), 68% (BCC) and 52% (simple) porosity. Thus, we nearly span the range of plaque/plate values. As previously described, the sinter alone is of prime concern structurally and, therefore, most emphasis will be placed on the face centered cubic model.

The value of these porous models lies in our ability to look at various cross sections and calculate the load bearing areas that are available. This has been done for the three principle planes of each cubic structure. The values are shown in Figure 18 along with the apparent modulus of elasticity that the true area of these 9 planes would imply.

Table III D-1 presents the predicted values describing a plates mechanical behavior when each matrix model is considered with the wire screen. It is interesting to note that values2.3 to 4.0 times the lowest exist within the same crystal structure. More interesting than the range of values within a crystal, is the overlapping of modulus values for crystal structures representing widely different porosities.

FIGURE 18

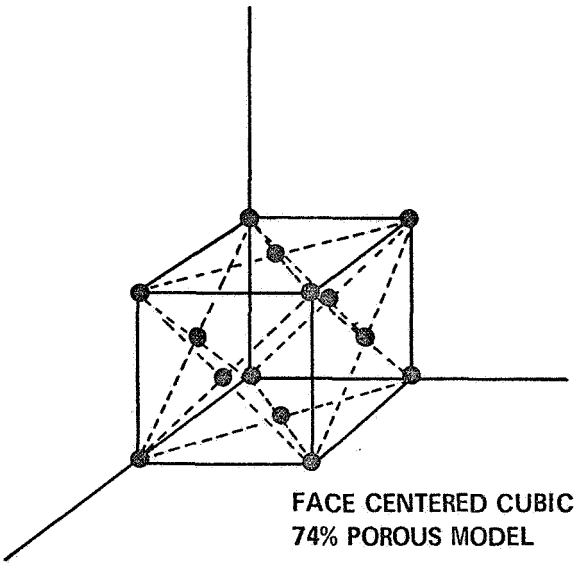

FACE CENTERED CUBIC
74% POROUS MODEL

(111)

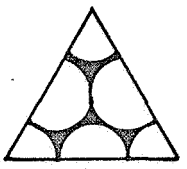

9.25% solid area
E = 2.74 x 10^6 psi

(100)

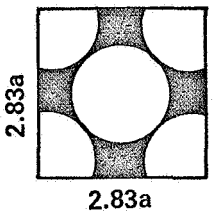

21.5% solid area
E = 6.37 x 10^6 psi

(110)

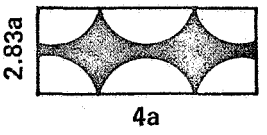

44.5% solid area
E = 13.2 x 10^6 psi

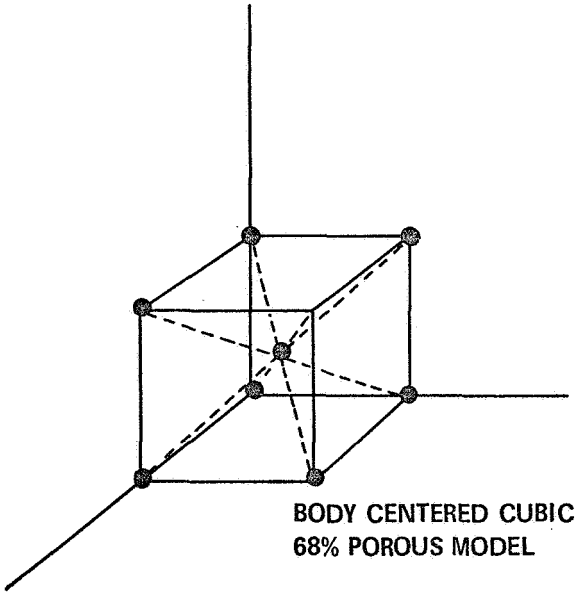

BODY CENTERED CUBIC
68% POROUS MODEL

(110)

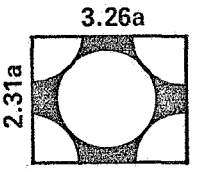

16.7% solid area
E = 4.95 x 10^6 psi

(100)

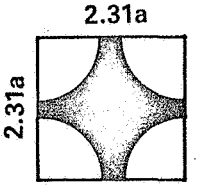

41.2% solid area
E = 12.2 x 10^6 psi

(111)

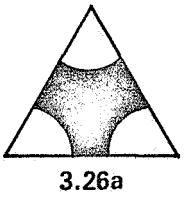

65.8% solid area
E = 19.5 x 10^6 psi

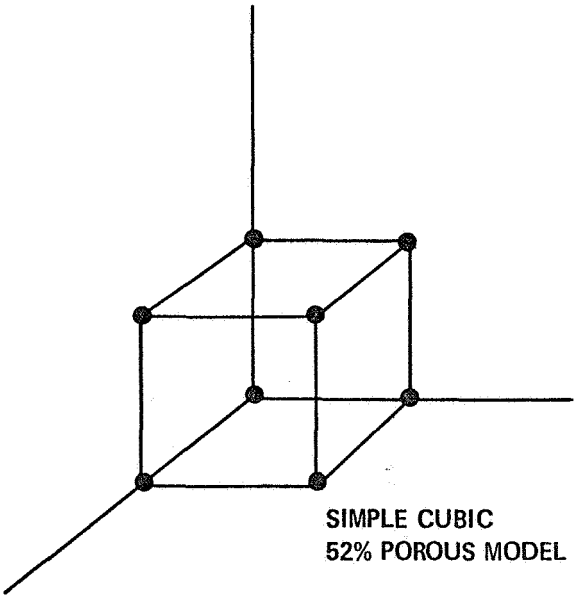

SIMPLE CUBIC
52% POROUS MODEL

(100)

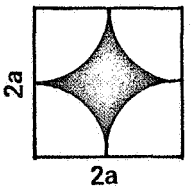

21.5% solid area
E = 6.37 x 10^6 psi

(110)

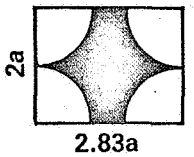

44.5% solid area
E = 13.2 x 10^6 psi

(111)

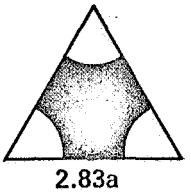

54.8% solid area
E = 16.2 x 10^6 psi

This is best shown below:

Ni Wires Alone	0.88×10^6 psi	absolute lower bound	
FCC (111)	3.5×10^6 psi	probable lower bound	
BCC (110)	5.7×10^6 psi	probable mean for random crossection	
Simple (100)	7.1×10^6 psi	"	
FCC (100)	7.4×10^6 psi	probable mean for random crossection	
BCC (100)	12.7×10^6 psi		
Simple (110)	13.7×10^6 psi		
FCC (110)	13.7×10^6 psi	probable upper bound	
Simple (111)	16.6×10^6 psi		
BCC (111)	19.8×10^6 psi	maximum upper bound	
Solid Nickel	29.6×10^6 psi	trivial absolute upper bound	

This overlapping of values obtained from such divergent models (of porosity) indicates something about the random distribution. Our real structure has been shown to contain a random number of various size pores. An actual cross section of load bearing area will certainly not be a replica of a given crystal plane as investigated. Therefore, one would expect to see a mean value between the extremes of any crystal. This seems strengthened by the fact that the least dense (100) plane of a 52% porous model has a modulus lower than the mean plane (100) of a 74% porous model. On this basis one might feel that $E = 7 \times 10^6$ psi is the best value that could be predicted from the calculations of T. III D-1. However, we may modify this prediction further by three considerations: a) the real sinter structure (plaque) is 78-80% porous and is thus higher than the 74% porosity of the FCC Model, b) the "necks" carrying load between pores in the structure are essentially areas of infinitesimal gage length. Thus, elongation is impossible and considerable tension load bearing area can be expected to be lost very readily, c) plate material has many small cracks initially due to manufacturing

processes. These considerations would tend to lower the apparent modulus and I would think that $E = 3.5 \times 10^6$ as predicted by the FCC (111) analysis would be more valid. This should be true especially in tension. In compression, however, we might suspect an increase toward the 7×10^6 value.

TABLE III D-1

del of latrix ructure	Porosity of Matrix Model %	Apparent Solid Area of Matrix Model %	Total Load Area (Wire & Matrix Model) $(in.^2)$	% of Apparent Area (0.013 $in.^2$)	P_{Y} Yield σ_Y = (15,000) #	E App. (psi)	P_{ult} (σ_{ult}= 55,000) (#)
ire lone	97	0	0.385×10^{-3}	3	5.8	0.88×10^6	21
CC (111)	74	9.25	1.56×10^{-3}	12	23	3.5×10^6	85
FCC (100)	74	21.5	3.10×10^{-3}	24	47	7.1×10^6	170
FCC (110)	74	44.5	6.01×10^{-3}	46	90	13.7×10^6	330
BCC (110)	68	16.7	2.50×10^{-3}	19	38	5.7×10^6	138
CC (100)	68	41.2	5.59×10^{-3}	43	84	12.7×10^6	310
CC (111)	68	65.8	8.69×10^{-3}	67	130	19.8×10^6	480
imple (100)	52	21.5	3.10×10^{-3}	24	47	7.1×10^6	170
Simple (110)	52	44.5	6.01×10^{-3}	46	90	13.7×10^6	330
Simple (111)	52	54.8	7.31×10^{-3}	56	110	16.6×10^6	400
Solid ickel	0	100	13.0×10^{-3}	100	195	29.6×10^6	715
esultant rediction					14	3.5×10^6 7×10^6	21

The model approach can also be used to predict values of plate strength. Using handbook values for nickel metal these calculations are also shown in T. III D-1. The previous consideration of

premature yielding of infinitesimal "necks" indicates that some of these calculated quantities are of little value. Once yielding occurs, the matrix will be ineffective and total load should be carried by the nickel wires.

This behavior and the mechanical properties predicted by this model analysis are best illustrated in Figure 19. The two curves shown actually present upper and lower bounds of the real behavior. The curve for screen alone is completely valid as the lower bound since it assumes no strength associated with a matrix. The curve for FCC (111) is somewhat of an intuitive selection as the possible upper bound (primarily for tension). I would expect then, to see experimental tensile data generate a curve between the two shown in Figure 19 and compression data may generate a curve very close to the upper bound.

A model for the sintered nickel structure has been presented. Predicted values have been calculated from the model. Experimental testing is now underway to modify the assumptions made in using the present model. A study of the final model shows that our first comparison to reinforced concrete is no longer true. Considering apparent modulus we have come closer. However, strength dissimilarities still exist. Experimental data must now be generated before further development of the model and the reinforced approach can continue.

EXPERIMENTAL PROGRAM OUTLINE

The data required in support of the model for plate material covers a rather broad experimental program. We are immediately interested in obtaining a stress-strain curve in both tension and compression that will enable us to examine this model more closely and check the assumptions that have been made. During the following months Ni-Cd electrodes will be fully characterized with respect to their mechanical properties. What is essentially involved is a determination of the

FIG. 19

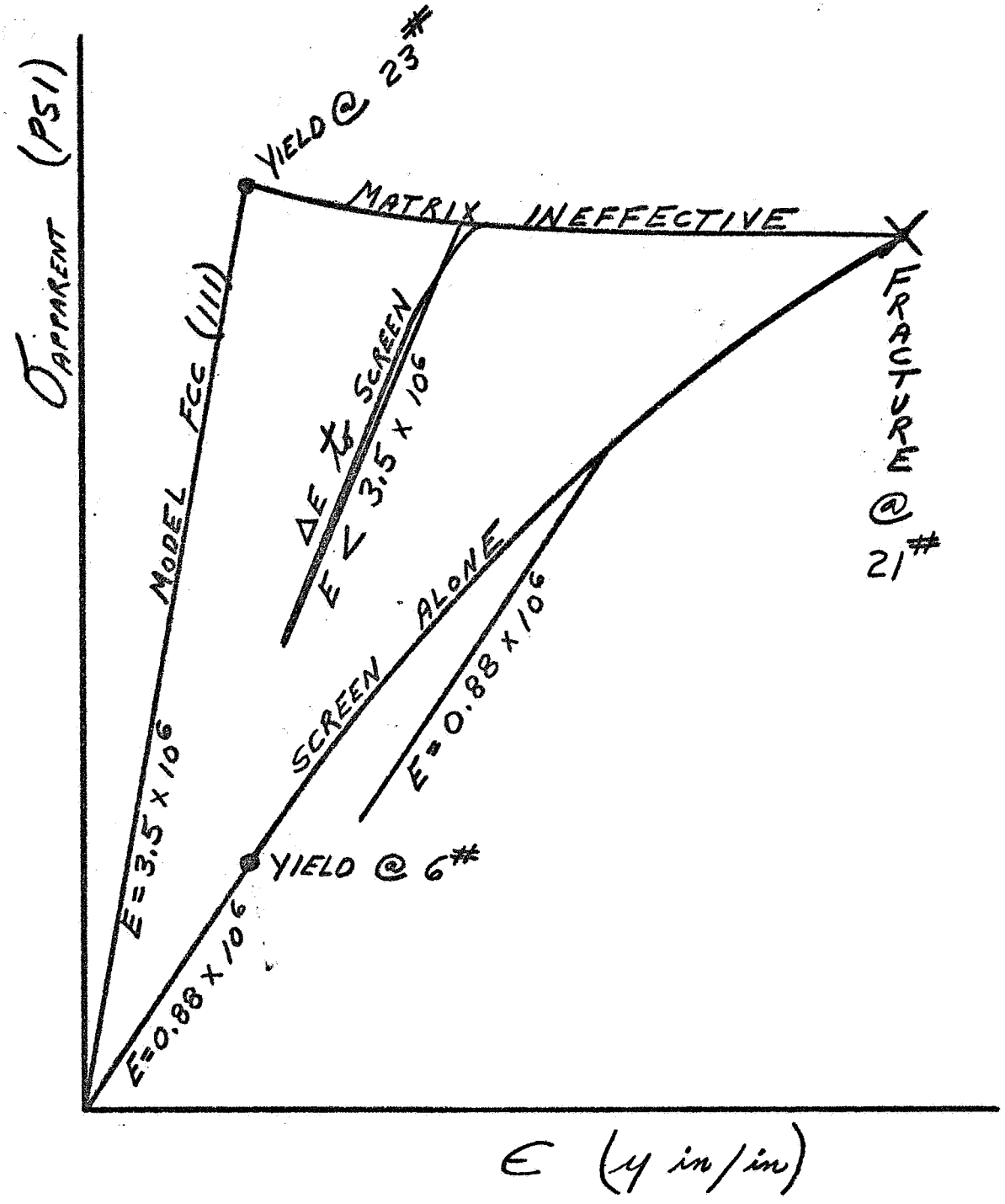
σ APPARENT (PSI)
YIELD @ 23#
MATRIX INEFFECTIVE
FRACTURE @ 21#
MODEL FCC (III)
E = 3.5 x 10^6
ΔE % SCREEN
E = 3.5 x 10^6
SCREEN ALONE
E = 0.88 x 10^6
YIELD @ 6#
E = 0.88 x 10^6
ε (μ in/in)

applicable stress-strain relation. However, there are a great many areas and tests required to fully explore this relation and obtain the kind of information required to permit the analytical prediction of their ability to withstand a shock environment. The scope of the desired information is best shown as outlined below:

STRESS STRAIN BEHAVIOR:

- A. Tensile
- B. Compressive
  - 1) Static
    - a) complete "shape" of curve
    - b) modulus of elasticity
      - (1) Δ E vs ε-level
      - (2) checked by wave propagation velocity within bulk material
    - c) yield strength
    - d) ultimate strength
    - e) poisson's ratio
    - f) damping capacity
      - (1) hysteresis
    - g) elongation
  - 2) Dynamic
    - a) strain-rate effects
      - (1) yield strength
      - (2) ultimate strength
    - b) stress amplification
    - d) $\sigma_y = f(\omega_n)$
- C. Bearing Strength (Edge Crushing)
- D. Thickness Compression of Pack
- E. Coef of Friction at Various Pressures
- F. Buckling at Various Spacing & Pressures

This investigation has now begun. First in the TENSILE area, a constant load machine is being used for the static testing (as opposed to constant deformation). A linearly increasing force (with time) is obtained at low rate by means of a water loading arrangement. Force

(stress) data is generated by a strain-gage loading ring and elongation (strain) is monitored over a 1" gage length by a commercial strain-gage extensometer. The two outputs allow the complete stress-strain curve to be plotted directly on an x-y recorder. For the dynamic tensile testing, a fixture has been built to hold several electrodes fixed within the carriage of the impact testing machine. All electrodes are fixed at one end, but each has a different free length. Knowing the mass density, free length, and the acceleration-time history, we are able to calculate the tensile forces associated with each plate during impact. Thus, we are able to determine ultimate and yield strengths under this loading condition. In addition, other strain-rate effects can be investigated.

The relationship of these material properties to the prediction of component response under transient accelerations has been previously discussed. This portion of the work is of high importance and will continue over an extensive period of time. At present only a preliminary study of the applicable literature and initial strain measurements have been made. It is considered important to expend considerable effort in employing foil strain gages as well as extensometers for measurements under static conditions. If we envision the measurements of dynamic forces and deformations on such materials, the development of a suitable strain gage technique is mandatory during the static determination of elastic-plastic properties. This technique will be developed as we begin the static determination of mechanical properties for our plate material.

TEXAS INSTRUMENTS
INCORPORATED
METALLURGICAL MATERIALS DIVISION
ATTLEBORO, MASSACHUSETTS U.S.A.

5-MMD-19528 2/69